



**UNIVERSITÀ
DI PARMA**

Department of Chemistry, Life Sciences and Environmental Sustainability

PhD program in Biotechnology and Life Sciences

XXX cycle

**ANTIBIOTIC COMPOUNDS TARGETING BACTERIAL RNA
POLYMERASE HOLOENZYME ASSEMBLY AND OTHER
PROTEIN-PROTEIN INTERACTION INHIBITORS IDENTIFIED
WITH AN *IN VIVO*-BRET DRUG DISCOVERY PLATFORM**

Coordinator:

Prof. Simone Ottonello

Tutor:

Prof. Barbara Montanini

PhD student:

Sara Sartini

2014-2017

Index

OUTLINE AND AIM OF THE PROJECT	I
Chapter 1	II
1.1 DRUG DISCOVERY	3
1.2 PROTEIN-PROTEIN INTERACTIONS	7
1.3 FÖRSTER RESONANCE ENERGY TRANSFER (FRET)	11
1.4 BIOLUMINESCENCE RESONANCE ENERGY TRANSFER (BRET)	14
ABBREVIATIONS.....	18
REFERENCES.....	20
Chapter 2	II
2.1 INTRODUCTION	31
2.2 RESULTS AND DISCUSSION	33
2.2.1 CLONING STRATEGIES	33
2.2.2 FEASIBILITY STUDY AND ASSAY OPTIMIZATION.....	35
2.2.3 MONITORING THE INHIBITION OF THE p53-HDM2 INTERACTION BY NUTLIN-3 USING A BRET BASED ASSAY IN YEAST AS PROOF OF CONCEPT	38
2.2.4 SCREENING	41
2.2.5 DISCUSSION.....	42
2.3 MATERIALS AND METHODS	44
ABBREVIATIONS	47
REFERENCES.....	48
Chapter 3	51
3.1 INTRODUCTION	53
3.2 RESULTS AND DISCUSSION	63
3.2.1 OPTIMIZATION AND VALIDATION OF THE β^1 - σ^{70} INTERACTION IN THE YEAST BRET PLATFORM.....	63
3.2.2 VALIDATION OF γ BRET RESULTS USING AN ELISA ASSAY	68
3.2.3. <i>IN SILICO</i> SELECTION AND SCREENING OF SMALL-MOLECULE LIBRARIES	71
3.2.4 RNAP-INHIBITORY AND ANTIBACTERIAL ACTIVITY OF MOLECULES IDENTIFIED IN γ BRET SCREENING AND VALIDATED IN ELISA	80

3.2.5 MOLECULAR MODELLING	85
3.2.6 DISCUSSION.....	86
3.3 MATERIALS AND METHODS	88
3.4 SUPPLEMENTARY.....	93
ABBREVIATIONS	107
REFERENCES.....	108
Chapter 4	113
4.1 INTRODUCTION	114
4.2 EXHAUSTION	119
4.3 2B4-CD48 INTERACTION	121
4.4 RESULTS	123
4.4.1 CHIMERIC PROTEIN CONSTRUCTION FOR BRET ANALYSIS AND VALIDATION OF SIGNAL SPECIFICITY	123
4.4.2 SCREENING	126
4.4.3 CYSTEINE-REACTIVE MOLECULES	128
4.4.4 P300-1755 AND STRUCTURAL ANALOGUE MOLECULES	130
4.5 CD40-CD40L INTERACTION.....	136
4.6 RESULTS	138
4.6.1 STRUCTURAL ANALYSIS AND MODEL CONSTRUCTION IN YBRET	138
4.6.2 OPTIMIZATION OF CLASSICAL-CYTOSOLIC YBRET	139
4.6.3 OPTIMIZATION OF SURFACE YBRET.....	142
4.6.4 SCREENING	146
4.7 DISCUSSION	147
4.8 MATERIALS AND METHODS	149
4.9 SUPPLEMENTARY	153
ABBREVIATIONS.....	156
REFERENCES.....	158

OUTLINE AND AIM OF THE PROJECT

The research and development of a new drug is a lengthy and costly process, which requires considerable investment by the pharmaceutical industries, with a very low success rate and a constant need for innovative approaches. The so-called “reverse approach” (or target-based drug discovery) is based on the screening of small molecule libraries, to identify "hit compounds" capable of interacting and modulating the biological activity of the target of interest. In recent years, protein-protein interactions (PPI) have emerged as promising new targets, especially considering their key role in most cellular processes, under both physiological and pathological conditions.

The aim of this thesis work is the development of an *in vivo* high-throughput platform based on the BRET (Bioluminescence Resonance Energy Transfer) technology as a tool to monitor PPI and to screen compound libraries for the identification of new potential PPI inhibitors.

This PhD dissertation is comprised of four main chapters.

Chapter 1 describes the state-of-the-art of drug discovery and presents PPI as new potential therapeutic targets, exposing the principal techniques used to analyse protein interactions and the approaches employed to find novel inhibitors; among these techniques, I have chosen the BRET assay, based on Förster Resonance Energy Transfer, for which the principal fundamentals are supplied, to reproduce interactions of biomedical interest.

Chapter 2 presents the set-up and validation of yeast BRET (yBRET) as a high-throughput platform (up to 800 compounds/day) for monitoring PPI *in vivo* and for screening new potential PPI inhibitors. p53-HDM2 interaction, involved in the cell-cycle control, was used to assess the utilization of a hyper-permeable *Saccharomyces cerevisiae* strain, rather than mammalian cells, exploiting the inhibitors Nutlin-3 and Nutlin-3a to validate this platform. The efficiency of different yeast growth conditions, type of donor (NLuc or RLuc) and donor/acceptor ratios were compared to identify the optimal conditions to perform a screening. This part of my work is published as a technical note on SLAS Discov. 2017;22(6) (Corbel C, Sartini S, Levati E, et al. Screening for Protein-Protein Interaction Inhibitors Using a Bioluminescence Resonance Energy Transfer (BRET)–Based Assay in Yeast).

Following up to the results obtained from the study of the p53-HDM2 interaction, I further optimized screening conditions for a bacterial interaction, described in the **chapter 3**. Bacterial resistance is a major health problem worldwide, which is actively being addressed through the discovery of novel

antibiotics acting on so far unexploited bacterial targets. Transcription is an essential process for pathogen propagation and represents an attractive, yet poorly exploited, drug target. In particular, I chose the interaction between the β' subunit of RNA polymerase (RNAP) and the house-keeping σ^{70} factor subunit, which is required for holoenzyme formation and transcription initiation. These proteins are highly conserved among bacteria, and thus inhibitors of the RNAP - σ^{70} interaction have a great potential for the discovery of broad-range antibiotics. A high-throughput platform that combines *in vivo* and *in vitro* assays has been developed. This strategy was applied to small molecule libraries of different origin, and led to the identification of new classes of potential antibiotics targeting β' - σ^{70} interaction, capable of inhibiting bacterial growth with higher efficiency in comparison to known inhibitors of this interaction.

In **chapter 4**, the yBRET method was translated to the immune-modulating 2B4-CD48 and CD40-CD40L interactions. The 2B4-CD48 interaction is involved in immune-inhibitory pathway and the disruption of this PPI can reverse the dysfunctional state of CD8+ T cells observed in various chronic diseases. No active small molecule has been reported so far that could overcome the drawbacks associated with immunotherapy. Compounds able to inhibit this PPI could thus represent a therapeutic alternative for the treatment of refractory viral infections. Screening of small molecule libraries has led to the identification of a class of hit compounds, capable of interfering with the interaction at micromolar concentrations both *in vivo* and *in vitro* assays. The CD40-CD40L is a co-stimulatory interaction associated to various autoimmune inflammatory pathologies of the central nervous system and in lymphomas. A number of antibodies that block this interaction have reached clinical trials against autoimmune diseases, but some of these give rise to thromboembolic complications. To find small molecule inhibitors able to disrupt this interaction, a surface exposed version of yBRET system was developed, in order to achieve expression of interacting partner proteins on the yeast cell wall, exploiting a protease-deficient yeast strain (EBY100). The surface-yeast BRET (syBRET) system was validated with the use of Suramin, a known inhibitor of this interaction. Both systems were employed for the screening of compounds from public libraries, but no active compounds were found for this interaction.

Chapter 1

Introduction

1.1 DRUG DISCOVERY

Drug research is a complex, long and very expensive interdisciplinary field intended to discover new compounds for the treatment of diseases. Historically, natural product extracts from botanical species have provided main sources of folk medicines, but no one of them fit a real chemical definition. At the end of the 18th century, chemistry began to take care of biological problems, opening the way to chemical characterization and analytical determination of active principles derived from plants: this allowed the isolation, for example, of morphine from opium^{1,2}, or salicin (the active principle of aspirin) from *Salix alba*³. In the 19th century pharmacology emerged as a new discipline, with the studies by Magendie and Bernard, which have highlighted the importance of experimental methods to understand chemical and physical principles at the basis of physiology: they tested some natural compounds (alkaloids) in animals to study the interactions between organism and drug^{4,5}. In the following century, Chain and Florey succeeded to purify penicillin, discovered by Fleming ten years before, giving a tremendous boost to the search of substances able to resolve infection diseases and to their production on large-scale^{1,6,7}. In the same period Paul Ehrlich suggested the idea that the biological effects of a compound depend on its chemical composition and on the cell on which it acts, proposing some years later the “magic bullet (*zauberkugel*)” concept: a compound that specifically kills the microorganisms that cause disease, without damage to the patient^{8,9}.

This also led to the beginning of the so called “forward approach” (also named phenotypic drug discovery, i.e. the research of biological active compounds) to identify molecules with a desirable effect on phenotype (e.g. arrest of cells growth) without any knowledge of the molecular basis of diseases^{10–13} (Fig.1). This method relies on single-cell organism or entire multicellular organism screening without a properly defined target, which has to be subsequently characterized. Several techniques can be used to capture the morphological changes caused by compounds, such as functional assay to measure cellular activity¹⁴, marker assay such as report-gene assay¹⁵, automated microscopy or imaging-based screening¹⁶. Once confirmed the active compounds, the target of interest has to be identified, for example by affinity matrix purification or phage display assay¹³. Over time, scientists began to suppose that it was possible to identify active compounds with a more rational method: in 1950, Elion and Hitchings, starting from the understanding of basic biochemical and physiological processes, developed the use of purine derivatives for the treatment of leukaemia, malaria, infectious diseases, gout and organ transplantations¹⁷. In 1960, Black developed beta-blockers to treat

cardiovascular diseases and cimetidine to prevent the formation of gastric acid in ulcers¹⁸. Together with the discovery of statins by Endo¹⁹, all these findings determined significant step forward for the pharmaceutical industry.

The greatest revolution in drug discovery comes with the genomics sciences, which completely transformed the point of view: with the sequencing of entire human genome it is now possible to identify the gene sequence of therapeutic targets²⁰. As an important consequence, the pharmacology could rely on a “reverse approach” (or target-based drug discovery). In this case, a High-Throughput Screening (HTS) is carried out on a target protein, to detect ligands binding the target, exploiting, for example, fluorescence-based methods and mass spectrometry. Subsequently the efficacy of the identified compound(s) is validated in cellular culture or on entire organisms¹³. It should be remembered that also hundreds of protein sequences from microbes and pathogen agents are available from sequenced genomic DNA, and that they could be used as targets to fight infections²¹ (Fig.1).

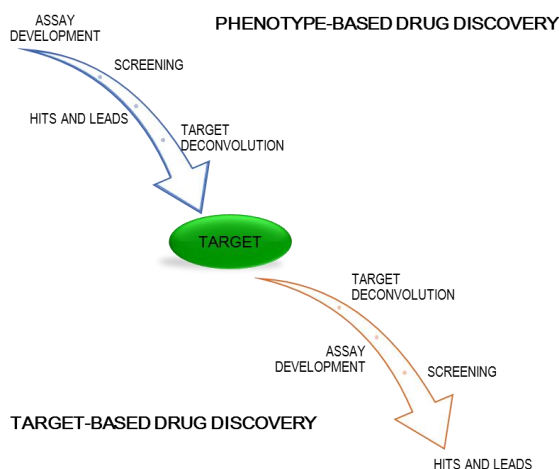
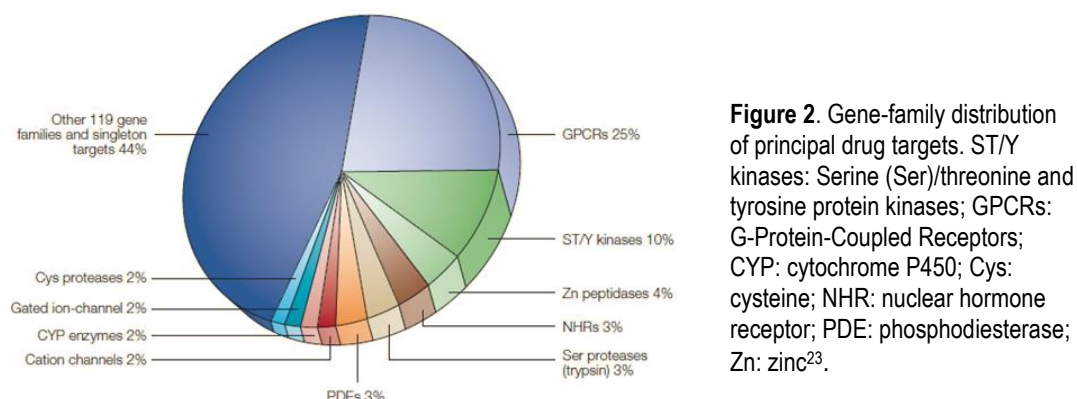


Figure 1. Schematic representation of phenotype-based and target-based drug discovery (modified by ²²).

Hopkins and Groom made a first effort to classify potential protein targets, starting from known drug-like ligands complying with the “rule of five” for oral bioavailability. They identified 399 molecular targets, of which 130 contained conserved domains (according to InterPro database) and could be classified in few families^{23,24}. The six most represented families were: G-Protein-Coupled Receptors (GPCRs), serine/threonine and tyrosine protein kinases, zinc metallopeptidases, serine proteases,

nuclear hormone receptors and phosphodiesterases^{25,26} (Fig.2). They also estimated that ~10% of all genes in the genome are druggable targets based on large-scale mouse-knockdown studies^{21,23}.



Small molecule compounds compose the majority of libraries employed in HTS and exhibit different advantages respect to biological agents: a low cost of production, simply to use on different cellular assays, no immune reaction and oral bioavailability²⁷. To accelerate drug discovery research in the past years libraries containing small molecules with well-annotated pharmacology were created to identify new targets of interest, reveal new uses for existing drugs, classify the toxic mechanism of new compounds, and characterize novel pharmacological mechanisms in the same gene family. Examples of this kind of libraries are: Pfizer chemogenomic library (2,984 compounds), Sigma Library of Pharmacologically Active Compounds (LOPAC, 1,280 compounds), Prestwick chemical library (1,280 compounds), Molecular Libraries Program Probes (NIH, 375 compounds)²⁸.

Because of the exponential costs of drugs research and development and of low rate drug approval on the market²⁹, the pharmaceutical industry started to use two new approaches: virtual screening and experimental fragment-based drug discovery. The first one exploits 3D protein structure to identify all possible binding sites on protein surface, for example using geometry-based algorithm (software like LIGSITE³⁰, SURFNET³¹, CAST³², etc.) or energy-based algorithm (software as GRID³³, vdwFFT³⁴, Drugsite³⁵, etc.). Subsequently, this information is used to screen very large numbers of compounds *in silico*, assessing all the electrostatic, van der Waals and hydrogen bonds involved with the target. Software like GOLD³⁶, AUTODOCK³⁷ and GLIDE³⁸ are used to this intent^{21,39}. An alternative method to conduct a virtual screening is based on the identification of the main features of the target and uses this motif as a pharmacophore, a three-dimensional representation of steric, electronic and hydrophobic interactions that guarantee an optimal ligand-target association⁴⁰. The second approach,

experimental fragment-based drug discovery, is useful to switch from hit compound to lead compound. Libraries of fragments, characterized by a reduced molecular mass (lower than 300 Da) and high number (thousands of chemicals), are screened against a target of interest. Typically fragments have high bonding-efficiency respect to the hit isolated by HTS, but show low binding-affinity (between μM and mM), so they require chemical modifications to improve affinity^{39,41}. In another approach, the rational drug design, the structure of an inhibitor is explored in relation to target's residues, to understand which amino acids are involved in the compound interaction, and which modifications can be introduced in the inhibitor to improve inhibition properties^{40,41}.

The path from a chemical compound to drug is still very slow, with high failure rates and very expensive investment for pharmaceutical industry and academics, and consist of different and long steps. A chemical with specific binding properties, called “hit”, is further validated to confirm its properties in secondary assays and to define chemical identity and purity. Afterward, in the lead-optimization step, hit affinity and selectivity to the target of interest is increased, also by the synthesis of chemical analogues. Cellular or biological models assays are used to validate lead-compound *in vitro* and *in vivo* to define the activity of the compound provided their ADME properties (Adsorption, Distribution, Metabolism and Elimination)¹³. Selected candidates enter in clinical trials, characterized by three phases, to analyse toxicity and efficiency profile for specific clinical use (Fig.3). Once a drug is approved by FDA (US Food and Drug Administration), an Anatomical Therapeutic Chemical Classification System code (ATC code) is assigned to each drug, attributed by WHO Collaborating Centre (WHOCC) for Drug Statistics Methodology, to classify drugs on five levels: level 1, the organ or anatomical system on which they act; level 2, the pharmacological action; levels 3 and 4, the chemical, pharmacological and therapeutic subgroups; and level 5, the specific single drug or drug combination²⁶.

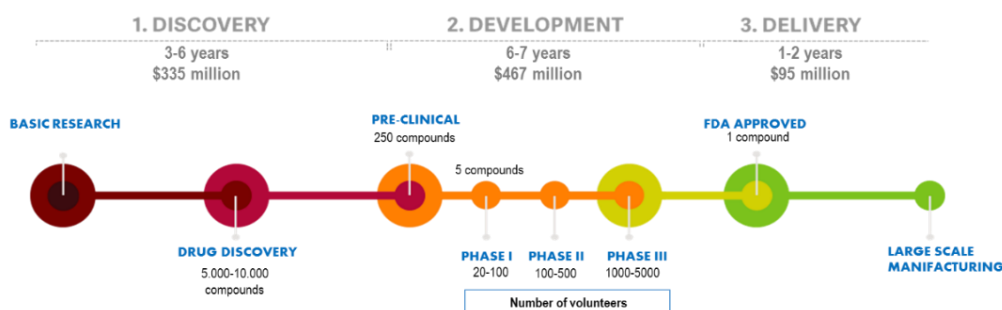


Figure 3. Infographic representation of drug discovery process (modified by ⁴²).

1.2 PROTEIN-PROTEIN INTERACTIONS

Proteins rarely work alone, their interactions are part of “molecular machines” that govern virtually all cellular processes, including metabolic cycles, DNA transcription and replication, enzyme activity, signaling cascades, apoptosis and other processes. The human ‘interactome’ (entire set of molecular interactions in an organism) is estimated to number between approximately 130,000 and 650,000 of protein-protein interactions (PPIs), which represents a potential source of therapeutic target, since a perturbation of the proteins dynamic equilibrium often leads to a dysfunction that, at a systemic level, means a pathology⁴³.

In addition, the contact surfaces of PPIs are larger (1500-3000 Å) compared to protein-small molecule interaction (300-1000 Å), are typically flat, lacking of pocket or grooves, and many amino acids residues not contiguous in polymer chain are involved in the contact surface, so are difficult to use as starting point in rational drug design⁴⁴. For these reasons, to target PPIs, biological agents (e.g. monoclonal antibodies and therapeutic proteins), such as Nivolumab (Opdivo, Bristol-Myers Squibb Company, New York, USA)⁴⁵, were preferentially approved in clinical trials, had high specificity and potency besides high stability in human serum. On the other side, biological agents tend to trigger an immune response before reaching the target, are not cell permeable, have difficulties in manufacture, high costs of production and lack of oral bioavailability^{27,46}.

X-ray crystallography and alanine-scanning mutagenesis studies (which investigate the contribution of individual residues to the binding energy, by mutating sequentially them to alanine) paved the way to a better understanding of protein-protein interfaces organization^{27,40}. The driving binding affinity is focalized on some residues, called “hot spots”, usually located in the centre of the proteins interface, on a surface area of ~ 600 Å², which therefore can be targeted by a small molecule⁴⁷. Site-direct mutagenesis indicates that tryptophan, tyrosine and arginine are often hot spot residues, while leucine, serine, threonine and valine are less representative, probably because do not allow the necessary adaptive conformational changes needed to interact with a small molecule⁴⁰. These finding gave a strong impetus to drug research, leading to the discover PPIs inhibitors, like Tirofiban, the first example of a clinical successful, that inhibits the glycoprotein IIb/IIIa fibrinogen interaction, mimicking the linear tripeptide Arg-Gly-Asp⁴⁸.

PPIs can be modulated by small molecules with three different mechanisms of action: i) in the orthosteric inhibition the compound directly competes with the interacting partner, hampering macromolecular complex formation (e.g. Ras-SOS¹⁴⁹); ii) in the allosteric inhibition, the small molecule binds a region different than protein interface, inducing conformational changes of the target, that obstacle the interaction (e.g. BRaf-CRaf⁵⁰); iii) in the interfacial inhibition a ternary complex is formed by the ligand and the proteins: in this case the inhibitor binds a pocket present in the interface and blocks the complex in a non-productive conformation (e.g. ARF-Sec7⁵¹). Some molecules can also act in a combination of multiple mechanisms of inhibitions⁵².

The analysis of PPIs can be performed with different experimental techniques, like “binary” method, that directly measure physical interactions between proteins, for example Yeast two Hybrid (2YH) methodology, or co-complex method, which measure direct and indirect physical interactions among groups of proteins, as the tandem affinity purification coupled to mass spectrometry⁵³. To clarify the binding mechanism and the effect of PPI modulators, it is possible to use biophysical methods that directly measure the interaction between drug and target, such as Analytical Ultracentrifugation (AUC)⁵⁴, Surface Plasmon Resonance (SPR)⁵⁵, Nuclear Magnetic Resonance (NMR)⁵⁶, Isothermal Titration Calorimetry (ITC)⁵⁷, Förster Resonance Energy Transfer (FRET)⁵⁸ and Bioluminescence Resonance Energy Transfer (BRET)⁵⁹.

A wide variety of strategies has been used in order to identify compounds capable of disrupting specific PPIs:

- **HTS (High Throughput Screening)**: allows the identification of a “hit” molecule, among a large number of initial compounds, with moderate potency that needs to be improved subsequently. In the last years, many improvements were made to increase the number of compounds that can be tested in an efficiently, reliably and relatively low cost manner. The results obtained from these screening showed that PPIs inhibitors tend to be larger and more lipophilic than molecules classically bind to druggable sites and this kind of compounds are poorly represented in the majority of libraries in use⁴⁷. Despite these disadvantages, inhibitors for several PPIs were found, for example for interaction between Human protein Double Minute 2 (HDM2) and p53. HDM2 is a negative regulator of p53, causing the ubiquitination

of the protein. Large scale HTS resulted in the identification of a class of compounds, called Nutlins, able to inhibit this PPI^{44,48,60}.

- **Fragment screening:** detection of libraries of low molecular weight organic compounds (fragments), screened for binding to a protein target, normally with low affinity ($K_D \sim 100 \mu\text{M}$). Active fragments are optimized to create a little set of molecules that are screened for improved function^{39,40,47}. The two principal methods to optimize fragments include SAR (Structure-Activity Relationship) by NMR and Tethering: the first one uses ^1H - ^{15}N Heteronuclear Single Quantum Correlation (HSQC) NMR to characterize the binding site of fragments in a protein of interest^{61,62}. Tethering relies on reversible covalent disulphide-bond formation between the fragment and the protein of interest; this effect amplifies the affinity of the fragment for the target, enabling detection at lower concentration. In this case, a residue within 5 to 10 Å of the small molecule binding site mutated into cysteine and the mutated protein is interrogated with a library of disulphide-containing fragments, under partially reducing conditions. At the equilibrium, the fragments that bind the target and form a thiol-disulphide will tie strongly with the protein⁶³. This method, applied to find and improve modulators against interleukin-2 (IL-2), allowed the identification of SP4026, which binds hot spot of the target and mimics the hot spot residues of the receptor IL-2R α , turning the protein conformation, resulting in a side-chain rotation and loop rearrangement^{66,64}.
- **Rational design:** the use of peptides and peptidomimetics began with the observation that a continuous epitope and well defined grooves or pockets were involved in many PPIs on the surface of interaction. The aim is to mimic the three principal motifs of recognition that modulate PPIs: α -helix, β -strand and reverse-turns⁴⁰. Binding energy comes from hydrophobic interactions and hydrogen bonds in the exposed side. For example, B-cell lymphoma-2 (Bcl-2) and Bcl-X_L are pivotal in the regulation of cell death by apoptosis, making them attractive targets for the treatment of cancer cells⁶⁵. These proteins interrupt the apoptotic process by binding a α -helix portion of pro-apoptotic molecule BAK (Bcl-2-Antagonist/Killer); several laboratories produced molecules that mimic the α -helix involved in this interaction, among which the most potent is ABT-737^{66,67}.

- **Virtual screening:** utilizes computational approaches to analyse chemical compound libraries (either available commercial compounds or virtual, not yet synthesized compounds) able to modulate the PPIs. *In silico* screening can be performed to implement HTS, before the screening to focus on potentially more active compounds, and after the screening to retrieve compounds lost during the screening. There are two principal methods: the ligand-based screening, that uses 2D or 3D chemical structure of active compounds (included inactive compounds as negative control), or common substructures to find similar compounds in databases; in the structure-based screening, instead, compounds are docked in the binding site, starting also from the similarity to pharmacophore model. At this purpose, *in silico* tools are available, e.g. FAF-Drugs online server, which helps in the chemical libraries preparation: it estimates physical-chemical proprieties, it considers the presence of PAINS (Pan Assay Interference Compounds) and the potential activity of a compound⁶⁸.

1.3 FÖRSTER RESONANCE ENERGY TRANSFER (FRET)

In 1948, Theodor Förster illustrated how quantum physics was fundamental for all photosynthetic organisms in the Earth, explaining physical processes of Resonance Energy Transfer (RET) that occurs between pigments like chlorophyll⁶⁹. The Förster theory (FRET) describes the non-radiative long-range dipole–dipole coupling between two chromophores sufficiently close: a donor chromophore (D), initially in its electronic excited state, may transfer energy to an acceptor chromophore (A)⁷⁰ (Fig.4). This mechanism of energy transfer is analogue to Near Field Communication (NFC): the interactions between radio antennas or chromophores occur at smaller distance than the wavelength of light emitted. In the near field region, the donor chromophore emits a photon that is immediately absorbed by the acceptor chromophore; this photon is not reliable because its existence infringed the conservation of energy and momentum, in this regard, FRET is defined non-radiative transfer⁷¹. This technique allows to obtain a careful spatial measure in a range of 10-100 Å and allows to detect cellular events such as protein folding⁷², substrate interactions⁷³, enzyme kinetics⁷⁴ and intercellular signalling⁷⁵.

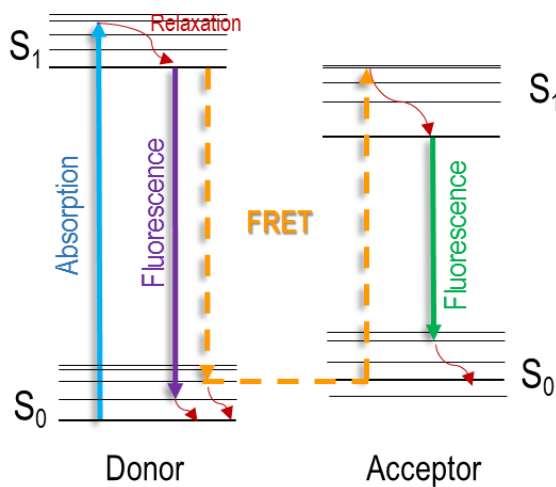


Figure 4. Jablonski diagram illustrating the coupled transitions involved between the donor emission and acceptor absorbance in fluorescence resonance energy transfer (modified by ⁷⁶).

The efficiency of the energy transfer (E) is a quantitative measure of number of quanta transferred from D to A on the number of donor excitation, that can be expressed as the ratio between k_T (rate of energy transfer) to the total sum of rates of all the processes where an excited D molecule transfers its energy state⁷⁰.

$$E = \frac{k_T}{k_f + k_T + \sum k_i}$$

Equation 1. Efficiency of FRET: k_T is the rate of energy transfer, k_f the radiative decay rate, and the k_i are the rate constants of any other de-excitation pathways⁷⁶.

The efficiency of FRET is strongly influenced by the donor-acceptor separation with an inverse sixth power law, caused by a mechanism of dipole-dipole coupling; this makes the FRET methodology extremely sensitive to small changes in distance⁷¹.

$$E = \frac{1}{[1 + (r/R_0)^6]}$$

Equation 2. Efficiency of FRET fall off with the sixth power of the distance between the donor and acceptor molecules. A distance lower than R_0 has an efficiency close to the maximum value, if instead is (much) higher than R_0 , the efficiency is close to zero⁷¹.

R_0 is characteristic for each interaction and represents the distance where the efficiency is 50%, depending both on the spectral overlap integral of the donor emission spectrum and the acceptor absorption spectrum and on the relative orientation of the donor emission dipole moment and the acceptor absorption dipole moment⁷¹ (Fig.5).

Different techniques can be adopted to quantify FRET, one of the most used is the Fluorescence Lifetime Imaging Microscopy (FLIM), where the lifetime of donor alone (t_D) or with the acceptor (t_{DA}) are measured. The donor fluorescence is defused by FRET and the intensity of quenching could be determined by measuring shortening of donor and acceptor fluorescence decrease in presence of FRET⁷⁷.

$$\tau = \frac{1}{f + k_{NR} + q + k_T}$$

Equation 3. Calculation of FLIM, considering the sum of rate constants of all the mechanisms leaving the excited state: f is the rate constant of emitting photon, k_{NR} is non radiative-decay, q is quenching and k_T is FRET⁷⁸.

$$E = 1 - \frac{\tau_{DA}}{\tau_D}$$

Equation 4. Efficiency of FLIM: the lifetime of donor with (τ_{DA}) and without (τ_D) an acceptor is measured by fluorescence decay time course⁷⁸.

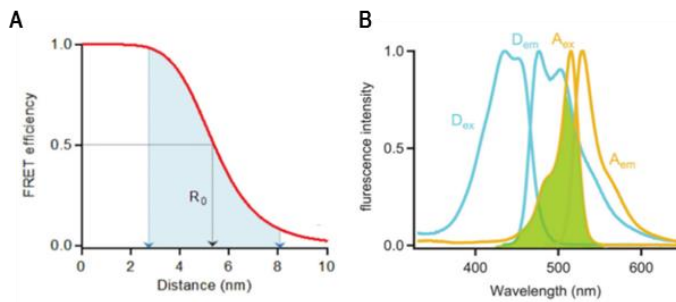


Figure 5. A) FRET efficiency as a function of the distance between the donor and the acceptor fluorophores; notice the linearity of the FRET efficiency values at distances near R_0 . B) Absorption and emission spectra of donor (cyan) and acceptor (green). The overlap between donor emission spectrum and acceptor absorption spectrum is highlighted by green shade⁷⁸.

FRET technology is also applied to analyse conformational changes⁷⁹ (static or in real time), membrane molecule interactions⁸⁰, protein structure⁸¹, PPIs⁸² and nucleic acid –proteins complexes⁸³. Green Fluorescent Protein (GFP) from the jellyfish *Aequorea victoria* is widely used to study interactions *in vivo*, as a non-invasive fluorescent marker for gene expression, protein localization and intracellular protein targeting⁸⁴;

Furthermore, mutations of GFP led to discover several fluorescent proteins with different spectral properties^{85,86}. Originally, the first couple of chromophores was the Blue Fluorescent Protein (BFP) as donor and the GFP as acceptor⁸⁷. BFP was a GFP mutant (Try66His) with an excitation peak in the ultraviolet (UV), with a drawback to cause strong noise by cellular autofluorescence and scattering⁸⁵. Therefore other fluorescent proteins were created starting from GFP: Cyan Fluorescent Protein (CFP) (Tyr66Trp), characterised by an excitation peak at 436 nm and an emission peak at 476 nm, and the Yellow Fluorescent Protein (YFP) (Thr203Tyr) characterized by spectra red shift, with an excitation peak at 516 nm and an emission peak at 529 nm^{85,88}. CFP-YFP pair allows monitoring very broad distances, and despite the cross talk in the excitation and emission spectra, was the most used FRET couple. Recently the Red Fluorescent Protein (RFP) was discovered from corals, with a long excitation tails, that forms another FRET pair with GFP⁸⁹.

The chromophores can also be fused to the same molecule (intramolecular FRET) to monitor, for example, cleavage of proteases, Ca^{2+} -calmodulin signal and phosphorylation of the transcription factor CREB (cAMP-responsive element binding protein)⁹⁰. Instead, when the chromophores are fused to different proteins (intermolecular FRET) it is possible to study PPIs (e.g. Bcl-2 Bax interaction)⁹⁰.

Unfortunately, FRET approaches present several limitations in the physical process and in the measurement of signal. The donor chromophore must be excited with an external source of illumination (lamps or laser) causing the raising of the background noise both through the direct excitation of the chromophore acceptor and through mechanisms of photobleaching, which result in loss of signal. In case of HTS, the photosensitive compounds could be damaged or they can reach an energetic level enough to react covalently with biological macromolecules, preventing any subsequent characterizations. Finally, cells' structures, especially the membranes, tend to absorb the external light inducing autofluorescence that annihilate the signal⁹¹. To overcome these drawbacks, the Bioluminescence Resonance Energy Transfer (BRET) has been developed⁹².

1.4 BIOLUMINESCENCE RESONANCE ENERGY TRANSFER (BRET)

Bioluminescence is a natural phenomenon defined as the emission of visible light by marine and some terrestrial organisms, because of a natural chemical reaction, typically produced by the oxidation of a light emitting molecule by an enzyme (luciferase or photoprotein)⁹³. The discovery and cloning of various components of bioluminescence allowed the development of the BRET, a highly versatile system that can be used to measure protein interactions *in vitro* (using purified proteins, crude cell membranes, or other cell fractions), in cultured cells, and *in vivo*⁹⁴. It has been used to study different PPIs in plant cells⁹⁵, bacteria⁹⁶, budding yeast⁹⁷ and mammalian cells⁹⁸: the first experiments detected the interaction of circadian clock proteins⁹⁶; subsequently it was used to monitoring dimerization or oligomerization of G-protein-coupled receptor⁹⁹ and to study membrane and cytosolic proteins¹⁰⁰.

The BRET method is based on the Förster Resonance Energy Transfer, which happens between a light-emitting donor enzyme and an energy acceptor fluorescent protein. In the presence of its substrate, bioluminescence from the luciferase occurs, and the transfer of energy leads to the

excitation of the acceptor fluorophore, which re-emits light at longer wavelength. To satisfy the requirement of energy transfer, the emission spectrum of the donor must overlap the excitation spectrum of the acceptor¹⁰¹ (Fig.6).

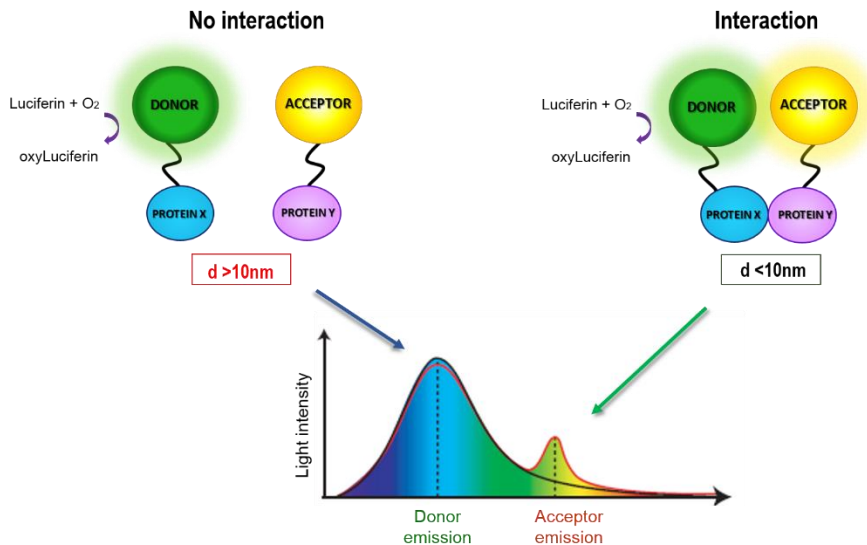


Figure 6. BRET-based assay: the energy transfer can occur only when the donor and the acceptor are sufficiently close (modified by ¹⁰²).

In BRET applications for the study of PPIs, the donor and the acceptor are genetically or chemically fused *in frame* to candidate targets. If two proteins interact, and the donor and acceptor are in close proximity ($<10\text{ nm}$) to allow energy transfer, it is possible to detect the light emitted by the acceptor to measure the BRET signal; if instead the proteins do not interact, only the signal derived from the donor emission is monitored¹⁰². An absence of BRET signal does not necessarily mean that the interaction does not occur: the distance between the donor and the acceptor is inversely proportional to intensity of signal, decreasing of energy transfer with the increase of distance, so the protein partners may interact, but the donor and the acceptor moieties can be too far to allow the energy transfer. Moreover, like the case of FRET, a non-optimal orientation of the BRET partners can prevent energy transfer (Fig.7). To circumvent these problems, it is crucial to test different combinations in which the proteins of interest are fused to donor and acceptor at the C- or N-terminal extremities and using several linker peptides characterized by high flexibility (for example, GS or GGS repetitions). Indeed, one of the orientations would be favourable over the others and lead to maximal BRET signal¹⁰².

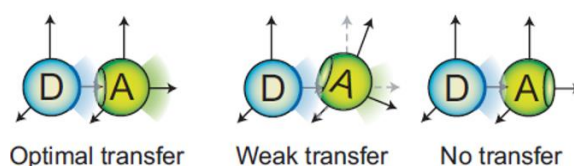


Figure 7. The relative orientation of BRET partners, due to the dipole-dipole nature of RET mechanism, is a parameter that could influenced the BRET signal¹⁰².

When the BRET technology is used as a tool to find PPI inhibitors, the sensitivity to signal variations (due for example to the interaction with an inhibitor) is an extremely important factor to be considered. PPIs take place in limited space such as membranes, cellular organelles, cytosol etc. Therefore, if the protein concentration is too high, the probability of casual contacts increases, leading to a non-specific BRET signal. The specificity of interactions is provided by saturation assay, where a fixed quantity of donor luciferase is co-expressed with increasing amount of acceptor fluorophore: specific BRET signal rises in a hyperbolic manner, achieving a plateau upon saturation; while a non-specific interaction is characterized by a BRET signal that is generally weak and grows in a quasi-linear manner according to the increased concentration of the acceptor^{103,104}. The 1:1 ratio (equimolar condition) occurs when all the donor molecules stably interact with the acceptor ones, leading to the most sensitive signal detection, while an excess of free donor or of acceptor may lead to compound titration. To prevent this situation and to obtain the highest BRET sensitivity, the acceptor-donor ratio would arise an ideal window of expression of the two proteins, located in the dynamic range of the saturation curve¹⁰⁵ (Fig.8).

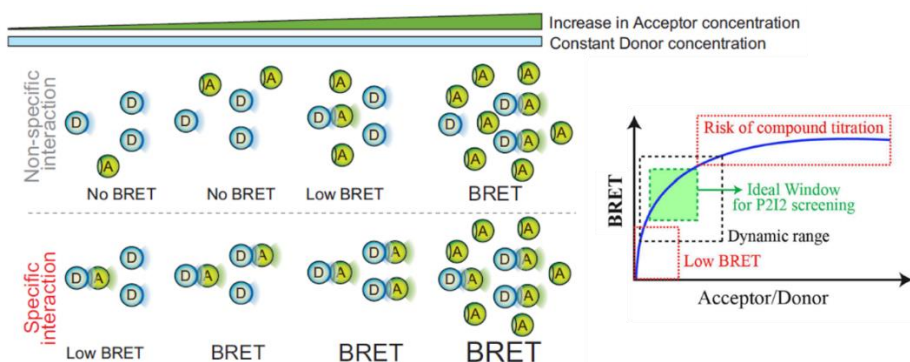


Figure 8. The donor/acceptor ratio described by the donor saturation assay, for the setup of PPI BRET-based screening assay. The donor concentration is kept constant, while raising acceptor concentrations is tested: a specific BRET signal augment in a hyperbolic manner, while a non-specific interaction in a quasi-linear manner. The ideal window of donor/acceptor is highlighted in green^{105,106}.

Since the birth of BRET in 1999, different type of donors, acceptors and substrates have been developed. The first version of BRET exploited the sea pansy *Renilla reniformis* luciferase (RLuc), a 36 kDa-monomeric, ATP-independent enzyme, which uses coelenterazine h as substrate. Light emitted by RLuc (480 nm) is appropriate for the excitation of the acceptor protein YFP. RLuc have a prolonged and intense signal, although the “bleed through” between the spectra is large^{96,107,108}. The BRET2 version is characterized by an increased separation of the donor and the acceptor spectra and was based on DeepBlueC or coelenterazine 400a as substrates of RLuc to shift emission peak at 395 nm, and exciting the acceptors GFP2 or GFP10. The disadvantage of this version was the necessity of the luciferase overexpression due to low light emission of DeepBlueC¹⁰⁹. The RLuc8 luciferase (RLuc mutant) was not even sufficiently powerful to improve performance compared to other BRET versions¹¹⁰. In the last few years, NanoLuc (NLuc) luciferase has been developed from *Oplophorus gracilirostris*, and it is characterized by small dimension (19 kDa) and a specific activity of about 150 times higher than the RLuc^{111–116}; NLuc can be matched with YFP or other mutated versions, such as YPF topaz, Citrine, Venus and YPet^{85,102,117}.

ABBREVIATIONS

2YH Yeast two Hybrid

ADME Adsorption, Distribution, Metabolism and Elimination

ARF ADP-Ribosylation Factor

Arg-Gly-Asp Arginine – Glycine - Aspartate

ATC code Anatomical Therapeutic Chemical Classification System code

AUC Analytical Ultracentrifugation

BAK Bcl-2-Antagonist/Killer

Bcl-2 B-cell lymphoma-2

Bcl-XL B-cell lymphoma-extra large

BFP Blue Fluorescent Protein

BRET Bioluminescence Resonance Energy Transfer

CFP Cyan Fluorescent Protein

CREB cyclic adenosine monophosphate (cAMP)-Responsive Element Binding protein

FDA US Food and Drug Administration

FLIM Fluorescence Lifetime Imaging Microscopy

FRET Förster Resonance Energy Transfer

GFP Green Fluorescent Protein

GPCRs G-Protein-Coupled Receptors

HDM2 Human protein Double Minute 2

HSQC Heteronuclear Single Quantum Correlation

HTS High-Throughput Screening

IL-2 Interleukin-2

IL-2R α Interleukin-2 Receptor α

ITC Isothermal Titration Calorimetry

LOPAC Library of Pharmacologically Active Compounds

NFC Near Field Communication

NIH National Institutes of Health

NLuc Nanoluc Luciferase

NMR Nuclear Magnetic Resonance

PAINS Pan Assay Interference Compounds

PPIs Protein-Protein Interactions

RET Resonance Energy Transfer

RFP Red Fluorescent Protein

RLuc Renilla reniformis luciferase

SAR Structure-Activity Relationship

SPR Surface Plasmon Resonance

UV Ultraviolet

YFP Yellow Fluorescent Protein

REFERENCES

1. Drews J. Drug Discovery : A Historical Perspective. *Science*. 2000;287:1960-1965.
2. Brook K, Bennett J, Desai SP. The Chemical History of Morphine: An 8000-year Journey, from Resin to de-novo Synthesis. *J Anesth Hist*. 2017;3(2):50-55.
3. Mahdi JG, Mahdi AJ, Mahdi AJ, Bowen ID. The historical analysis of aspirin discovery, its relation to the willow tree and antiproliferative and anticancer potential. *Cell Prolif*. 2006;39:147-155.
4. Conti F. Claude Bernard : primer of the second biomedical revolution. *Nat Rev Molcellbio*. 2001;2:3-8.
5. Bowman WC. Neuromuscular block. *Br J Pharmacol*. 2006;147:S277-86.
6. Kardos N, Demain AL. Ernst Chain: A great man of science. *Appl Microbiol Biotechnol*. 2013;97(15):6613-6622.
7. Ligon BL. Penicillin: Its Discovery and Early Development. *Semin Pediatr Infect Dis*. 2004;15(1):52-57.
8. Strebhardt K, Ullrich A. Paul Ehrlich ' s magic bullet concept : 100 years of progress. *Nat Rev cancer*. 2008;8(june):473-480.
9. Winau F, Westphal O, Winau R. Paul Ehrlich - In search of the magic bullet. *Microbes Infect*. 2004;6(8):786-789.
10. Szabo M, Akusjärvi SS, Saxena A, Liu J, Chandrasekar G, Kitambi SS. Cell and small animal models for phenotypic drug discovery. *Drug Des Devel Ther*. 2017;11:1957-1967.
11. Moffat JG, Vincent F, Lee JA, Eder J, Prunotto M. Opportunities and challenges in phenotypic drug discovery: an industry perspective. *Nat Rev Drug Discov*. 2017;16(8):531-543.
12. Moffat JG, Rudolph J, Bailey D. Phenotypic screening in cancer drug discovery — past, present and future. *Nat Rev Drug Discov*. 2014;13(8):588-602.
13. Bredel M, Jacoby E. Chemogenomics: an emerging strategy for rapid target and drug discovery. *Nat Rev Genet*. 2004;5(4):262-275.
14. Bedard J, May S, Barbeau D, Yuen L, Rando R BT. A high throughput colorimetric cell proliferation assay for the identification of human cytomegalovirus inhibitors. *Antivir Res*. 1999;41:35-43.
15. DeBasio R, Guiliano K, Zhou L DK. Quantification of G-protein coupled receptor internalization using G-protein coupled receptor–green fluorescent protein conjugates with the ArrayScan™ high-content screening system. *J Biomol Screen*. 1999;4:75-86.
16. Ellenberg J PR. High throughput fluorescence microscopy for systems biology. *Nat*

- Rev Molcellbio.* 2006;7.
17. Elion B. Gertrude. The quest for a Cure. *Annu Rev Pharmacol Toxicol.* 1993;33:1-23.
 18. Black J. Drugs from Emasculated Hormones : The Principle of Syntopic Antagonism. *Biosci Rep.* 2004;24.
 19. Endo Akira. A historical perspective on the discovery of statins. *Proc Jpn Acad, Ser.* 2010;86:484-493.
 20. Venter J, Adams M, Myers E, et al. The sequence of the human genome. *Science.* 2001;291(5507):1304-1351.
 21. Hajduk PJ, Huth JR, Tse C. Predicting protein druggability. *Drug Discov Today.* 2005;10(23).
 22. Terstappen G.C., Schlüpen C, Raggiaschi R GG. Target deconvolution strategies in drug discovery. *Nat Rev Drug Discov.* 2007;5:891-903.
 23. Hopkins AL, Groom CR. The druggable genome. *Nat Rev Drug Discov.* 2002;1(9):727-730.
 24. Lipinski CA, Lombardo F, Dominy BW, Feeney PJ. Experimental and computational approaches to estimate solubility and permeability in drug discovery and development settings. *Adv Drug Deliv Rev.* 2012;64:4-17.
 25. Imming P, Sinning C, Meyer A. Drugs, their targets and the nature and number of drug targets. *Nature.* 2007;5:821-835.
 26. Santos R, Ursu O, Gaulton A, et al. A comprehensive map of molecular drug targets. *Nat Rev Drug Discov.* 2016;16(1):19-34.
 27. Arkin MR, Wells JA. Small-molecule inhibitors of protein–protein interactions: progressing towards the dream. *Nat Rev Drug Discov.* 2004;3(4):301-317.
 28. Jones LH, Bunnage ME. Applications of chemogenomic library screening in drug discovery. *Nat Rev Drug Discov.* 2017;16(4):285-296.
 29. Rask-Andersen M, Almén MS, Schiöth HB. Trends in the exploitation of novel drug targets. *Nat Rev Drug Discov.* 2011;10(8):579-590.
 30. Hendlich M, Rippmann F BG. LIGSITE: automatic and efficient detection of potential small molecule-binding sites in proteins. *J Mol Graph Model.* 1997;15.
 31. Laskowski R. SURFNET: a program for visualizing molecular surfaces, cavities, and intermolecular interactions. *J Mol Graph.* 1995.
 32. Liang J, Edelsbrunner H, Woodward C. Anatomy of protein pockets and cavities: Measurement of binding site geometry and implications for ligand design. *Protein Sci.* 1998;7(9):1884-1897.
 33. Goodford P. A computational procedure for determining energetically favorable binding sites on biologically important macromolecules. *J Med Chem.* 1985.

34. Bliznyuk AA, Gready JE. Simple method for locating possible ligand binding sites on protein surfaces. *J Comput Chem*. 1999;20(9):983-988.
35. An J, Totrov M, Abagyan R. Comprehensive identification of “druggable” protein ligand binding sites. *Genome Inform*. 2004;15.
36. Verdonk ML, Cole JC, Hartshorn MJ, Murray CW, Taylor RD. Improved Protein – Ligand Docking Using GOLD. *Proteins Struct Funct Bioinforma*. 2003;52:609-623.
37. Goodsell DS, Morris GM, Olson AJ. Automated docking of flexible ligands: applications of AutoDock. *J Mol Recognit*. 1996;9(1):1-5.
38. Friesner RA, Banks JL, Murphy RB, et al. Glide: A New Approach for Rapid, Accurate Docking and Scoring. 1. Method and Assessment of Docking Accuracy. *J Med Chem*. 2004;47(7):1739-1749.
39. Pandurangan AP, Ascher DB, Sherine ET, Blundell TL. Genomes, structural biology and drug discovery: combating the impacts of mutations in genetic disease and antibiotic resistance. *Biochem Soc Trans*. 2017;45(2):303-311.
40. Scott DE, Bayly AR, Abell C, Skidmore J. Small molecules, big targets: drug discovery faces the protein–protein interaction challenge. *Nat Rev Drug Discov*. 2016;15(8):533-550.
41. Hoelder S, Clarke PA, Workman P. Discovery of small molecule cancer drugs: Successes, challenges and opportunities. *Mol Oncol*. 2012;6(2):155-176.
42. AmericaResearch. Bench to Bedside: Drug Development Pipeline.
43. Sevimoglu T, Arga KY. The role of protein interaction networks in systems biomedicine. *Comput Struct Biotechnol J*. 2014;11(18):22-27.
44. Wells JA, McClendon CL. Reaching for high-hanging fruit in drug discovery at protein–protein interfaces. *Nature*. 2007;450(7172):1001-1009.
45. Raedler LA. Opdivo (Nivolumab): Second PD-1 Inhibitor Receives FDA Approval for Unresectable or Metastatic Melanoma. *Am Heal drug benefits*. 2015;8:180-183.
46. Nero TL, Morton CJ, Holien JK, Wielens J, Parker MW. Oncogenic protein interfaces: small molecules, big challenges. *Nat Rev Cancer*. 2014;14(4):248-262.
47. Jubb H, Higuero AP, Winter A, Blundell TL. Structural biology and drug discovery for protein-protein interactions. *Trends Pharmacol Sci*. 2012;33(5):241-248.
48. Arkin MR, Tang Y, Wells JA. Small-molecule inhibitors of protein-protein interactions: progressing towards the reality. *Chem Biol*. 2014;21(9):1102-1114.
49. Patgiri A, Yadav K.K, Arora P.S and B-SD. An Orthosteric Inhibitor of the Ras-Sos Interaction. *Nat Chem Biol*. 2012;7:585-587.
50. Bollag G, Hirth P, Tsai J, et al. Clinical efficacy of a RAF inhibitor needs broad target blockade in BRAF-mutant melanoma. *Nature*. 2010;467(7315):596-599.

51. Pommier Y, Cherfilis J. Interfacial inhibition of macromolecular interactions: nature's paradigm for drug discovery. *Trends Pharmacol Sci.* 2005;26(3):138-145.
52. Mattmann ME, Stoops SL and LC. Inhibition of Akt with small molecules and biologics: historical perspective and current status of the patent landscape. *Expert Opin Ther Pat.* 2011;21(9):1309-1338.
53. De Las Rivas J, Fontanillo C. Protein-protein interactions essentials: Key concepts to building and analyzing interactome networks. *PLoS Comput Biol.* 2010;6(6):1-8.
54. Arkin M, Lear JD. A New Data Analysis Method to Determine Binding Constants of Small Molecules Using Equilibrium Analytical Ultracentrifugation with Absorption Optics. *Anal Biochem.* 2001;299:98-107.
55. Karlsson R, Kullman-Magnusson M, Hämäläinen MD, et al. Biosensor Analysis of Drug–Target Interactions: Direct and Competitive Binding Assays for Investigation of Interactions between Thrombin and Thrombin Inhibitors. *Anal Biochem.* 2000;278(1):1-13.
56. Emerson SD, Palermo R, Liu CM, et al. NMR characterization of interleukin-2 in complexes with the IL-2R alpha receptor component, and with low molecular weight compounds that inhibit the IL-2/IL-R alpha interaction. *Protein Sci.* 2003;12(4):811-822.
57. Sarver RW, Peevers J, Cody WL, et al. Binding thermodynamics of substituted diaminopyrimidine renin inhibitors. *Anal Biochem.* 2007;360(1):30-40.
58. Biazzo-Ashnault DE, Park Y-W, Cummings RT, et al. Detection of Insulin Receptor Tyrosine Kinase Activity Using Time-Resolved Fluorescence Energy Transfer Technology. *Anal Biochem.* 2001;291(1):155-158.
59. Namkung Y, Le Gouill C, Lukashova V, et al. Monitoring G protein-coupled receptor and β -arrestin trafficking in live cells using enhanced bystander BRET. *Nat Commun.* 2016;7.
60. Jin L, Wang W, Fang G. Targeting Protein-Protein Interaction by Small Molecules. *Annu Rev Pharmacol Toxicol.* 2014;54(1):435-456.
61. Rees DC, Congreve M, Murray CW CR. Fragment-Based Lead Discovery. *Annu Rep Med Chem.* 2017;3(August):660-672.
62. Harner MJ, Frank AO, Fesik SW. Fragment-Based Drug Discovery Using NMR Spectroscopy. *J Biomol NMR.* 2013;56(2):65-75.
63. Erlanson DA, Wells JA, Braisted AC. TETHERING: Fragment-Based Drug Discovery. *Annu Rev Biophys Biomol Struct.* 2004;33:199-223.
64. Braisted AC, Oslob JD, Delano WL, et al. Discovery of a potent small molecule IL-2 inhibitor through fragment assembly. *J Am Chem Soc.* 2003;125(13):3714-3715.
65. Adams JM, Cory S. The Bcl-2 Protein Family: Arbiters of Cell Survival. *Science.* 1998;281(5381):1322-1326.

66. Levoine N, Vo DD, Gautier F, et al. A combination of in silico and SAR studies to identify binding hot spots of Bcl-xL inhibitors. *Bioorganic Med Chem*. 2015;23(8):1747-1757.
67. Oltersdorf T, Elmore SW, Shoemaker AR, et al. An inhibitor of Bcl-2 family proteins induces regression of solid tumours. *Nature*. 2005;435(7042):677-681.
68. Villoutreix BO, Kuenemann MA, Poyet JL, et al. Drug-like protein-protein interaction modulators: Challenges and opportunities for drug discovery and chemical biology. *Mol Inform*. 2014;33(6-7):414-437.
69. Şener M, Strümpfer J, Hsin J, et al. Förster energy transfer theory as reflected in the structures of photosynthetic light harvesting systems. *Chemphyschem*. 2011;12(3):518-531.
70. Clegg RM. Fluorescence Resonance Energy Transfer. *Curr Opin Biotechnol*. 1995;6:103-110.
71. Piston DW, Kremers G-J. Fluorescent protein FRET: the good, the bad and the ugly. *Trends Biochem Sci*. 2007;32(9):407-414.
72. Jia YW, Talaga DS, Lau WL, Lu HSM, DeGrado WF, Hochstrasser RM. Folding dynamics of single GCN4 peptides by fluorescence resonant energy transfer confocal microscopy. *Chem Phys*. 1999;247(1):69-83.
73. Jabaiah AM, Getz JA, Witkowski WA, Hardy JA, Daugherty PS. Identification of protease exosite-interacting peptides that enhance substrate cleavage kinetics. *Biol Chem*. 2012;393(9).
74. Kettling U, Koltermann A, Schwille P, Eigen M. Real-time enzyme kinetics monitored by dual-color fluorescence cross-correlation spectroscopy. *Proc Natl Acad Sci U S A*. 1998;95(4):1416-1420.
75. Nagai Y, Miyazaki M, Aoki R, et al. A fluorescent indicator for visualizing cAMP-induced phosphorylation in vivo. *Nat Biotechnol*. 2000;18:313-316.
76. Szöllosi J, Damjanovich S, Mátyus L. Application of fluorescence resonance energy transfer in the clinical laboratory: Routine and research. *Cytometry*. 1998;34(4):159-179.
77. Sun Y, Hays NM, Periasamy A, Davidson MW, Day RN. Monitoring Protein Interactions in Living Cells with Fluorescence Lifetime Imaging Microscopy. *Methods Enzym*. 2012;504:371-391.
78. Ma L, Yang F, Zheng J. Application of fluorescence resonance energy transfer in protein studies. *J Mol Struct*. 2014;5:87-100.
79. Nakanishi J, Takarada T, Yunoki S, Kikuchi Y, Maeda M. FRET-based monitoring of conformational change of the β_2 adrenergic receptor in living cells. *Biochem Biophys Res Commun*. 2006;343(4):1191-1196.

80. Wang S, Vafabakhsh R, Borschel WF, Ha T, Nichols CG. Structural dynamics of potassium channel gating revealed by single molecule FRET. *Nat Struct Mol Biol.* 2016;23(1):31-36.
81. Kasprzak A. The Use of FRET in the Analysis of Motor Protein Structure. *Methods Mol Biol.* 2007;392.
82. Schaap M, Hancock R, Wilderspin A, Wells G. Development of a steady-state FRET-based assay to identify inhibitors of the Keap1-Nrf2 protein-protein interaction. *Protein Sci.* 2013;22(12):1812-1819.
83. Nougalli Tonaco IA, Borst JW, De Vries SC, Angenent GC, Immink RGH. In vivo imaging of MADS-box transcription factor interactions. *J Exp Bot.* 2006;57(1):33-42.
84. Tsien RY. The Green Fluorescent Protein. *Annu Rev Biochem.* 1998;67(1):509-544.
85. Olenych SG, Claxton NS, Ottenberg GK DM. The fluorescent protein color palette. *Curr Protoc Cell Biol.* 2007;21.
86. Shaner NC, Patterson GH, Davidson MW. Advances in fluorescent protein technology. *J Cell Sci.* 2007;120(24):4247-4260.
87. Xu X, Gerard AL, Huang BC, Anderson DC, Payan DG, Luo Y. Detection of programmed cell death using fluorescence energy transfer. *Nucleic Acids Res.* 1998;26(8):2034-2035.
88. Miyawaki A, Llopis J, Heim R, et al. Fluorescent indicators for Ca²⁺ based on green fluorescent proteins and calmodulin. *Nature.* 1997;388(6645):882-887.
89. Campbell RE, Tour O, Palmer AE, et al. A monomeric red fluorescent protein. *PNAS.* 2002;99(12):7877-7882.
90. Truong K, Ikura M. The use of FRET imaging microscopy to detect protein – protein interactions and protein conformational changes in vivo. *Curr Opin Struct Biol.* 2001;11:573-578.
91. Leavesley SJ, Rich TC. Overcoming limitations of FRET measurements. *Cytom Part A.* 2016;89(4):325-327.
92. Boute N, Jockers R, Issad T. The use of resonance energy transfer in high-throughput screening: BRET versus FRET. *Trends Pharmacol Sci.* 2002;23(8):351-354.
93. Haddock SHD, Moline MA, Case JF. Bioluminescence in the Sea. *Ann Rev Mar Sci.* 2010;2(1):443-493.
94. Pfleger KDG, Seeber RM, Eidne KA. Bioluminescence resonance energy transfer (BRET) for the real-time detection of protein-protein interactions. *Nat Protoc.* 2006;1(1):337-345.

95. Subramanian C, Kim B-H, Lyssenko NN, Xu X, Johnson CH, von Arnim AG. The Arabidopsis repressor of light signaling, COP1, is regulated by nuclear exclusion: Mutational analysis by bioluminescence resonance energy transfer. *PNAS*. 2004;101(17):6798-6802.
96. Xu Y, Piston DW, Johnson CH. A bioluminescence resonance energy transfer (BRET) system: Application to interacting circadian clock proteins. *Proc Natl Acad Sci*. 1999;96(1):151-156.
97. Gehret AU, Bajaj A, Naider F, Dumont ME. Oligomerization of the yeast α -factor receptor: Implications for dominant negative effects of mutant receptors. *J Biol Chem*. 2006;281(30):20698-20714.
98. Angers S, Salahpour A, Hilairet S, Chelsky D, Dennis M, Bouvier M. Detection of beta 2-adrenergic receptor dimerization in living cells using bioluminescence resonance energy transfer (BRET). *PNAS*. 2000;97(7):3684-3689.
99. Pflieger KDG, Eidne KA. Monitoring the formation of dynamic G-protein-coupled receptor-protein complexes in living cells. *Biochem J*. 2005;385:625-637.
100. Lan T-H, Liu Q, Li C, Wu G, Lambert NA. Sensitive and High Resolution Localization and Tracking of Membrane Proteins in Live Cells with BRET. *Traffic*. 2012;13(11):1450-1456.
101. Dimri S, Basu S, De A. Use of BRET to Study Protein-Protein Interactions In Vitro and In Vivo. *Nucl Recept Superfamily Methods Protoc Methods Mol Biol*. 2016;1443:57-78.
102. Bacart J, Corbel C, Jockers R, Bach S, Couturier C. The BRET technology and its application to screening assays. *Biotechnol J*. 2008;3(3):311-324.
103. Pflieger KDG, Eidne KA. Illuminating insights into protein-protein interactions using bioluminescence resonance energy transfer (BRET). *Nat Methods*. 2006;3(3):165-174.
104. Mercier JF, Salahpour A, Angers S, Breit A, Bouvier M. Quantitative assessment of beta1- and beta2-adrenergic receptor homo- and heterodimerization by bioluminescence resonance energy transfer. *J Biol Chem*. 2002;277(47):44925-44931.
105. Couturier C, Deprez B. Setting up a bioluminescence resonance energy transfer high throughput screening assay to search for protein/protein interaction inhibitors in mammalian cells. *Front Endocrinol (Lausanne)*. 2012;3:1-13.
106. Corbel C, Wang Q, Bousserouel H, et al. First BRET-based screening assay performed in budding yeast leads to the discovery of CDK5/p25 interaction inhibitors. *Biotechnol J*. 2011;6(7):860-870.

107. Woo J, Howell MH, von Arnim AG. Structure-function studies on the active site of the coelenterazine-dependent luciferase from Renilla. *Protein Sci.* 2008;17(4):725-735.
108. Matthews JC, Hori K, Cormier MJ. Purification and Properties of Renilla reniformis Luciferase. *Biochemistry.* 1977;16(1):85-91.
109. Bertrand L, Parent S, Caron M, et al. The BRET2/arrestin assay in stable recombinant cells: a platform to screen for compounds that interact with g protein-coupled receptors (GPCRS). *J Recept Signal Transduct.* 2002;22:533-541.
110. Loening AM, Fenn TD, Wu AM, Gambhir SS. Consensus guided mutagenesis of Renilla luciferase yields enhanced stability and light output. *Protein Eng Des Sel.* 2006;19(9):391-400.
111. Inouye S, Watanabe K, Nakamura H, Shimomura O. Secretional luciferase of the luminous shrimp Oplophorus gracilirostris: cDNA cloning of a novel imidazopyrazinone luciferase. *FEBS Lett.* 2000;481(1):19-25.
112. Kim J, Grailhe R. Nanoluciferase signal brightness using furimazine substrates opens bioluminescence resonance energy transfer to widefield microscopy. *Cytom Part A.* 2016;89(8):742-746.
113. Machleidt T, Woodroffe CC, Schwinn MK, et al. NanoBRET-A Novel BRET Platform for the Analysis of Protein-Protein Interactions. *ACS Chem Biol.* 2015;10(8):1797-1804.
114. Schaub FX, Reza MS, Flaveny CA, et al. Fluorophore-NanoLuc BRET reporters enable sensitive In Vivo optical imaging and flow cytometry for monitoring tumorigenesis. *Cancer Res.* 2015;75(23):5023-5033.
115. Boute N, Lowe P, Berger S, Malissard M, Robert A, Tesar M. NanoLuc Luciferase - A multifunctional tool for high throughput antibody screening. *Front Pharmacol.* 2016;7:1-11.
116. Hall MP, Unch J, Binkowski BF, et al. Engineered luciferase reporter from a deep sea shrimp utilizing a novel imidazopyrazinone substrate. *ACS Chem Biol.* 2012;7(11):1848-1857.
117. Nagai T, Ibata K, Park ES, Kubota M, Mikoshiba K, Miyawaki A. A variant of yellow fluorescent protein with fast and efficient maturation for cell-biological applications. *Nat Biotechnol.* 2002;20(1):87-90.

Chapter 2

Yeast BRET screening set-up

2.1 INTRODUCTION

Protein-protein interactions (PPIs) govern virtually all cellular processes and thus offer a tremendous panel of opportunities for therapeutic intervention. Targeting PPIs instead of single proteins provides a means to increase drug specificity and efficacy. Because the interface of a particular PPI is formed by the combination of interacting domains of two particular proteins, it will display a higher level of uniqueness in comparison to, for instance, the catalytic pocket of an enzyme, which is often well conserved throughout a whole enzyme class. As examples, all of the active human protein kinases use adenosine triphosphate (ATP) to phosphorylate their substrates. On the market since 2001, imatinib mesylate (Gleevec, Novartis, Basel, Switzerland), which targets the ATP-binding site of the tyrosine kinase Bcr-Abl, was the first targeted therapy developed for chronic myelogenous leukemia (CML). During cancer treatment, point mutations may arise on a single cavity to escape drugs targeting the catalytic pocket while keeping the enzymatic activity. Concerning CML treatment with imatinib mesylate, the main cause of therapy failure is related to mutations affecting principally the ATP-binding cleft and notably a key residue, termed the *gatekeeper*, located at the back of this pocket¹. To circumvent such resistance phenomenon, one potential therapeutic strategy can be the inhibition of PPIs required for the activation of signalling pathways downstream of Bcr-Abl². Indeed, eluding a PPI inhibitor (P212) while preserving the interaction would require a second compensatory mutation in the binding partner, which would be much less probable. The challenge is thus to discover small molecules that disrupt protein-protein complexes. To this end, robust, facile high-throughput methods, preferentially in a living cellular context, are needed³. The yeast-based Bioluminescence Resonance Energy Transfer (yBRET) assay described herein offers a powerful method to discover small-molecule inhibitors of PPIs. We used the p53-HDM2 interaction (of particular interest for cancer therapy⁴) and its small-molecule inhibitor Nutlin-3 to exemplify this scalable method.

BRET is a naturally occurring phenomenon that can be observed in the sea pansy *Renilla reniformis* and is similar to an existing method for assessing PPI, the Förster or more commonly called Fluorescence Resonance Energy Transfer (FRET). In FRET, one fluorophore (the “donor”) transfers its excited-state energy to another fluorophore (the “acceptor”), which emits fluorescence at a longer wavelength. In both methods, the donor and acceptor are genetically or chemically fused to candidate proteins or compounds. In BRET, a luciferase is used as the energy donor to avoid the consequences of donor excitation in FRET (for instance, the damage of tissues by the excitatory light, photobleaching,

and simultaneous excitation of the acceptor by the donor excitatory light). In the presence of its substrate, bioluminescence from the luciferase occurs, and the transfer of energy leads to the excitation of the acceptor fluorophore, if the donor and acceptor are close enough (<10 nm), which can occur upon a molecular interaction between the fused proteins. BRET is a highly versatile technique that can be used to measure protein interactions *in vitro* (using purified proteins, crude cell membranes, or other cell fractions) in cultured cells and *in vivo*⁵. Based on the BRET method, different screening assays have been designed⁶.

The unicellular baker's yeast *Saccharomyces cerevisiae* is a proven model for fundamental and applied research⁷. For example, basic cellular processes occurring in human cells are well conserved in yeast (e.g., the control of the cell division cycle). This safe organism is also genetically well defined, because its entire genome was sequenced in 1996⁸. Moreover, yeast growth and division can be precisely controlled, and different strategies can be adopted to maximize hit rates in yeast based assays: (1) Enhancing the limited cell permeability to small molecules by alteration of yeast membrane composition. Classically, *erg6* gene mutation (involved in the ergosterol biosynthesis, one of the components of fungal membranes) was found to increase permeability to a growing list of chemical compounds, in particular to small lipophilic drugs^{9,10}. (2) Screening molecules against nonpreformed complexes^{3,11}. It is now considered essential that small molecules have to be delivered to the cellular system before the synthesis of one of the two interacting proteins¹². The use of inducible promoters, such as the *GAL1* promoter, enables the small molecules to first interact with one of the two partners, prior to protein complex formation. Indeed, in a BRET study conducted in mammalian cell lines, in which cells were transiently transfected with fusion genes to monitor the p53-HDM2 interaction, the inhibitor Nutlin-3 was not able to completely disrupt a preformed complex¹³. In our experimental setup, the use of inducible protein expression allowed complete inhibition of the p53-HDM2 interaction. (3) The development and selection of stable strains in the interacting proteins can be expressed, which can be achieved in one to two weeks. This is in sharp contrast to mammalian cells, in which obtaining stable lines is classically time-consuming and sometimes arduous. (4) The possibility of expressing mammalian proteins involved in toxic or death response in mammalian cells. (5) The rapid expansion of yeast compared with mammalian cells, allowing for the acquisition of the proper amount of cells needed to perform High-Throughput Screening (HTS) experiments in less time. Besides all technical benefits described above, this is one of the main advantages of this model. Indeed, proteins implicated in the cell cycle or apoptosis control may impair the development of such screening assays in

mammalian cells. Nevertheless, some limitations exist when using yeast, such as (1) the reduced sensitivity to some classes of compounds due to efficient drug efflux pumps; (2) when overexpressed in yeast, some human proteins can be toxic (e.g., some tyrosine kinases); (3) some protein interactions depend on post-translational modifications that do not exist in yeast and cannot be screened (e.g., absence of tyrosine phosphorylations in yeast); and (4) some protein interactions might involve folding/conformations that depend on chaperones that may not exist or may not function in yeast. However, easier genetic manipulations of yeast allowed the development of strains expressing human genes counteracting cell death¹⁴. These models may thus represent a major advantage of yeast for such screening purpose. The study of cyclin-dependent kinase 5 (CDK5)/p25 interaction highlights this key advantage of yeast¹¹. Indeed, p25 is a 25 kDa pathological proteolytic fragment of p35, one of the physiological regulatory subunits of CDK5 kinase. A previous study has shown that even low basal level expression of p25 is toxic for mammalian cells, and thus, stable cell lines were obtained only if the tau protein is constitutively co expressed¹⁵. In yeast, we were able to establish a stable inducible p25 yeast strain that does not require tau co-expression as a suitable model to study the CDK5/p25 interaction¹¹. Here, it's detailed a robust and scalable BRET-based cellular screening assay developed in the budding yeast, which supports the discovery of inhibitors of PPIs.

2.2 RESULTS AND DISCUSSION

PPIs control many cellular processes, including metabolic cycles, DNA transcription and replication, enzyme activity, different signalling cascades, and other processes^{16,17}. The importance of PPIs justifies the development of new powerful methods to understand the role of such interactions and to discover inhibitors. The protocol described below is based on the BRET technology, a non-radiative energy transfer, which can be applied to monitor protein interactions and to identify potential inhibitors. The innovation of this HTS assay lies in the use of the budding yeast *S. cerevisiae* rather than mammalian cells, which facilitates, expedites, and reduces the cost of assay development.

2.2.1 CLONING STRATEGIES

Human HDM2 was amplified by PCR using oSB22 and oSB23 primers and a YFP-HDM2 containing plasmid as a template¹³. The PCR product was inserted in frame with RLuc in pcDNA3-RLuc vector¹⁸

using *NheI/AgeI* restriction enzyme digestion and DNA ligation. The vector obtained, pcDNA3-HDM2-RLuc, was then used as a template for the amplification of HDM2-RLuc cDNA using oSB22 and oSB34 primers. The PCR product was digested with *BamHI/XhoI* enzymes and subsequently cloned in p415-GAL vector to obtain the p415GAL-HDM2-RLuc vector¹⁹. A PCR overlap extension strategy was used to clone HDM2-NLuc in p415-GAL. NLuc (NanoLuc®, Promega) was amplified from pNL.3.2.NF-kB-RE vector (Promega) using NLuc Fw and NLuc Re primers; HDM2 was amplified from p415GAL-HDM2-RLuc vector using HDM2 Fw and HDM2 Re primers. These PCR products were then used as templates for a fusion PCR using NLuc Fw and HDM2 Re primers, *BamHI/XhoI* digested and cloned in p415-GAL to obtain p415GAL-HDM2-NLuc vector. Human CDK5 was amplified by RT-PCR using *NheI*-hCDK5_Sens and hCDK5-AgeI_AS primers and cloned in frame with YFP in the pcDNA3-YFP vector¹⁸, using *NheI/AgeI* restriction enzyme digestion and DNA ligation. *NheI*-CDK5-YFP-HindIII PCR product was generated using *NheI*-hCDK5_Sens and pcDNA3-HindIII_AS primers and vector pcDNA3-hCDK5-YFP as a template. This PCR product and p416-GPD vector¹⁹ were then digested with *NheI/HindIII* restriction enzymes and ligated together to gain the p416GPD-hCDK5-YFP expressing vector. Human p53 and a human p53 mutant (F19A) were amplified using oSB28 and oSB29 primers and with RLuc-p53 and RLuc-p53.F19A containing plasmids as templates¹³. PCR products were then digested by *BamHI/AgeI* and inserted in frame with YFP in p416GPD-CDK5-YFP digested with *BamHI/AgeI* (Fig.1).

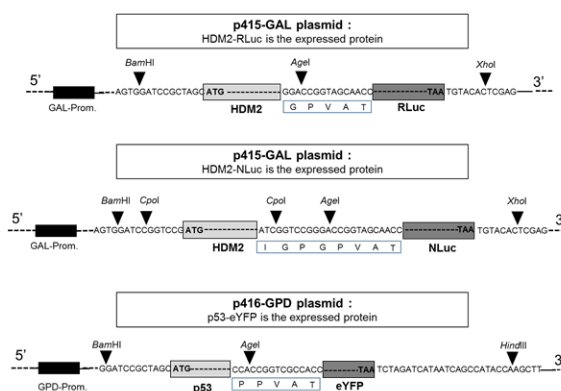


Figure 1. Simplified map of the different fusion proteins used in this study.

2.2.2 FEASIBILITY STUDY AND ASSAY OPTIMIZATION

A schematic representation of the BRET-based assay is provided in Figure 2A. As depicted, energy transfer occurs when the donor and the acceptor, respectively fused to the interacting proteins, are 1 to 10 nm apart. To monitor the BRET signal, two yeast strains are needed: one strain expressing the energy donor alone (for background detection, here HDM2-Luc) and the other expressing both the donor and the acceptor fusion proteins (here, HDM2-Luc and p53- YFP).

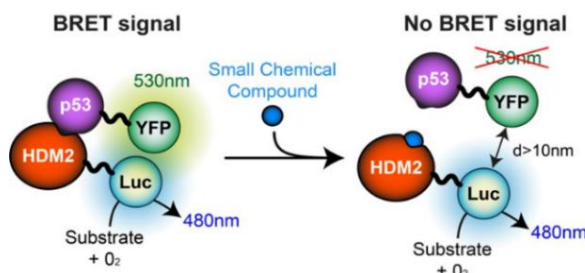


Figure 2A. Yeast Bioluminescence Resonance Energy Transfer (yBRET) technique validation and optimization. Schematic representation of the BRET-based assay, used to detect the interaction between two proteins (e.g., HDM2 and p53).

An advantage of working with yeast is the possibility of modifying membrane permeability to favor the penetration of small drug-like molecules inside the cell. An *erg6* strain is thus chosen for the development of the BRET based screening assay in order to increase the hit rate. Moreover, to screen against a nonpreformed complex, the protein expression of the energy donor is placed under the control of an inducible *GAL1* (galactose-regulated) promoter. Once the yeast is transformed, expression of both chimeric proteins should be verified by sodium dodecyl sulfate polyacrylamide gel electrophoresis followed by immunoblotting (Fig. 2B).

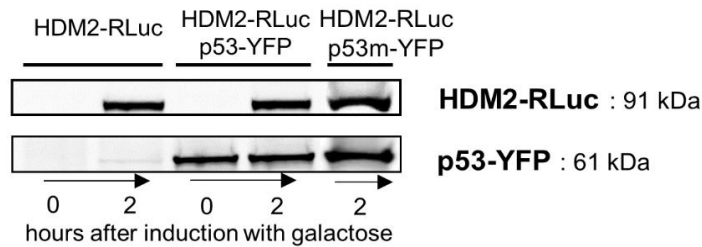


Figure 2B. Protein expressions are analysed by sodium dodecyl sulfate polyacrylamide gel electrophoresis followed by Western blotting using antibodies directed against YFP and RLuc, from 25 μ g of crude extracts produced from the control strain expressing HDM2-RLuc only and from the test strain expressing HDM2-RLuc and p53-YFP or p53m-YFP. p53m: F19A p53 mutant (F19 residue is involved in the interaction).

Induction using galactose is an effective way to control gene expression, as shown for HDM2-RLuc. To obtain a significant BRET signal, donor and acceptor groups should be in closed proximity, but an absence of the BRET signal does not necessarily mean that there is no interaction; it could be due to a non optimal orientation of the BRET partners. To circumvent this problem, it is crucial to test different combinations in which the proteins of interest are fused to donor and acceptor at the C- or N-terminal extremities and using several linker peptides with flexibility (for example, GS or GGS repetitions). Indeed, one of the orientations would be favorable over the others and lead to maximal BRET signal. In our case, donor and acceptor groups fused at the C-terminal extremities are considered for screening. The optimal expression level of donor fusion protein should be evaluated by measuring the BRET signal in response to increasing galactose concentration (from 0.001% to 2%) and time of induction (up to 6 h). This evolution of the BRET signal is protein interaction dependent and must be monitored for each new PPI. The conditions to choose for the screening are those that produce the highest measured BRET signal. The use of other donor proteins can be envisaged. NLuc (NanoLuc, Promega) is a smaller and brighter luciferase (19.1 kDa) than RLuc. It presents a high thermal stability and a strong activity over a broad pH range, and its emission peak (465 nm) is suitable for BRET assay²⁰. Moreover, NLuc signal is stable for long time (up to 1 h). Therefore, NLuc was tested in the same way as RLuc. In the case of p53-HDM2, the highest BRET signal was measured after 2 h, in the presence of 2% galactose (Fig. 2C, D).

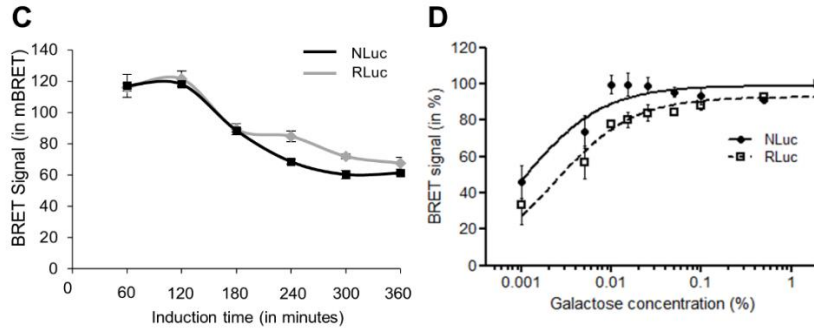


Figure 2. C) Evolution of the BRET signal following induction time. The yeast strains observed express p53-YFP and HDM2-RLuc or HDM2-NLuc (mean \pm SD; error bars represent SD, $n = 3$). **D)** Comparison between RLuc and NLuc signals, measured after 2 h of induction, with various galactose concentrations. MilliBRET signals are expressed in percentages with respect to RLuc signal at 2% of galactose (error bars represent %RSD, $n = 3$).

As expected, the NLuc signal intensity is higher compared with RLuc (almost 20-fold in our hands) at all inducer concentrations assayed (not shown). The BRET signal was 20 to 50 mBRET higher with NLuc versus RLuc at low inducer concentration ($\leq 0.05\%$), whereas it was comparable when the donor saturated the acceptor (galactose concentration $> 0.1\%$; Fig. 2D). NLuc can thus be employed usefully to overcome problems of low expression levels of some heterologous proteins. Another requirement to validate a screening assay is to demonstrate the specificity of the BRET signal, which can be done either by using a mutation that destroys the interaction or by performing a donor saturation assay. For this purpose, the F19A mutation, involving a key residue for the interaction with HDM2²¹, was introduced in p53. It caused a complete loss of the BRET signal, thus confirming the specificity of the signal obtained using wild-type proteins (Fig. 2E).

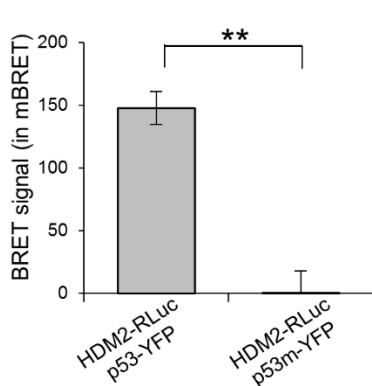


Figure 2E. Validation of BRET signal specificity. Note the total absence of BRET signal when HDM2-RLuc and p53m-YFP are co-expressed (mean \pm SD; error bars represent SD, $n = 3$; **values are significantly different, $p < 0.01$).

Otherwise, when information about a point mutation abolishing PPI is lacking, non-specific BRET signal, due to random collisions between donor and acceptor, can be measured by co-transforming yeast with YFP alone (cloned in the same vector of the acceptor fusion protein) and donor fusion protein.

In the classical donor saturation assay, the BRET signal is measured in response to increasing amounts of acceptor (achieved by increasing inducer concentration), whereas the donor is kept constant. The expected result for a specific BRET signal is a hyperbolic curve²². Nevertheless, inducible donor fusion protein is preferred for HTS, as besides the possibility of directly verifying that the expression of the protein is well induced, another advantage of inducing the donor instead of the acceptor is the ability to reach the maximal BRET signal upon induction. Indeed, donor saturation by the acceptor occurs quite instantly, as a huge amount of the acceptor is already present because of its constitutive expression.

2.2.3 MONITORING THE INHIBITION OF THE p53-HDM2 INTERACTION BY NUTLIN-3 USING A BRET BASED ASSAY IN YEAST AS PROOF OF CONCEPT

p53, also called the guardian of the genome, is negatively modulated by HDM2. Disrupting the p53-HDM2 interaction may thus offer a new strategy for cancer therapy. To this end, in 2004, the chemical compound Nutlin-3 was discovered using Surface Plasmon Resonance²³. We have examined the effect of Nutlin-3 on the p53-HDM2 BRET signal in our assay. The BRET signal decreased in a dose-dependent manner (Fig. 3A). As shown in Figure 3B, the inhibitory effect of Nutlin-3 and its enantiomer Nutlin-3a²³ has also been verified using NLuc as donor. As expected, Nutlin-3a, known to be more potent on the p53-HDM2 inhibition than Nutlin-3, showed a higher inhibitory effect (Nutlin-3 $IC_{50} = 28.6 \mu M$, Nutlin-3a $IC_{50} = 8.8 \mu M$) on the p53-HDM2 interaction.

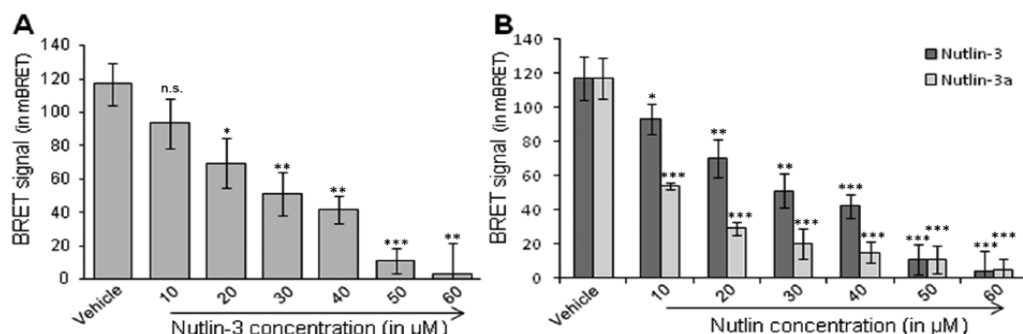


Figure 3. Monitoring the effect of a P212 using Bioluminescence Resonance Energy Transfer (BRET) in yeast. **A)** Verification of the dose-dependent inhibition of BRET signal by Nutlin-3, a known inhibitor of the p53-HDM2 interaction. RLuc was used as donor protein (mean \pm SD, error bars represent SD, $n = 3$). Statistical analyses were done using a Student t test. Significance levels are * $p < 0.05$, ** $p < 0.01$, *** $p < 0.001$, and n.s. = not significant. **B)** Comparison of dose-dependent inhibition of Nutlin-3 and its enantiomer Nutlin-3a using NLuc as donor protein (mean \pm SD, error bars represent SD, $n = 3$). Significance levels are * $p < 0.05$, ** $p < 0.01$, and *** $p < 0.001$.

The effect of other known PPI inhibitors was also evaluated on the p53-HDM2 interaction using this BRET-based assay. As shown in Figure 3C, no effect was observed on the BRET signal using FK506, T3, or tamoxifen, which inhibit the FKBP12/TGF β R²⁴, NCoR/TR α ²⁵, and CDK5/p2513 interactions, respectively. Prior to starting a large screening campaign, pilot screenings are used to predict if it would be feasible in a high throughput setting.

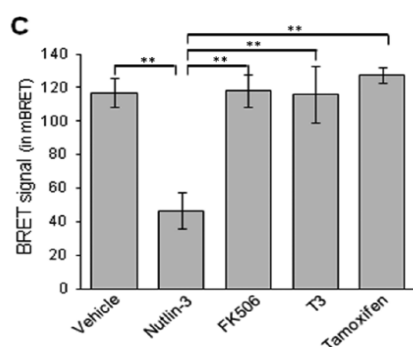


Figure 3C. Specific inhibition of the BRET signal with Nutlin-3 (40 μM) compared with unrelated compounds without activity on the p53-HDM2 interaction (mean \pm SD, error bars represent SD, $n = 3$; **values are significantly different, $p < 0.01$).

For this purpose, the calculation of a coefficient called the Z'-factor is recommended²⁶. This statistical dimensionless parameter is essential to evaluate and validate the quality of HTS assays. The Z'-factor is defined in terms of four parameters: the means and standard deviations of both the positive (p) and

negative (n) controls (μ_p , σ_p and μ_n , σ_n). Usually, the negative control is determined without the tested enzyme or using non induced conditions. Considering this yeast-based screening assay, it is experimentally inconceivable to use the same yeast strain to obtain a “non induced” negative control. Indeed, in the non induced condition (yeast growing in raffinose-based media without galactose), no reliable BRET signals can be achieved. We therefore decided to adapt the calculation using a known inhibitor, Nutlin-3. To characterize this estimated coefficient (named Z-yBRET factor in Fig. 3D), we prepared a 96-well plate and measured the BRET signal obtained with the compound vehicle (DMSO; p, positive controls) or 20 μ M of Nutlin-3 (n, negative controls) on the p53-HDM2 interaction. The formula used for the calculation is reported in Figure 3D and is similar to the one of the Z'-factor²⁶. According to the scatterplot obtained, we observed a significant difference between the two sets of samples (separation band), confirming that this method is adapted for screening, with a calculated factor coefficient of 0.67 (Fig. 3D).

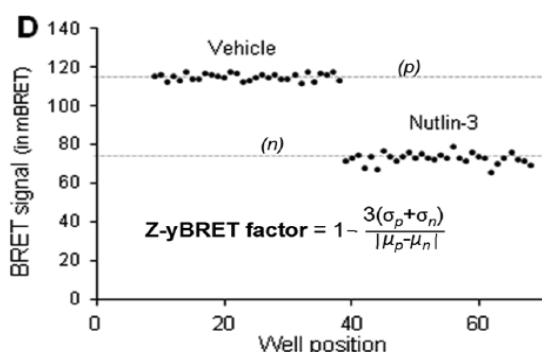


Figure 3D. Measurements of the BRET signal in a 96-well plate: 30 wells are filled with the vehicle and 30 others wells are filled with Nutlin-3 (at 20 μ M). The formula reported in the figure was used to calculate a Z-yBRET factor of 0.67.

This value indicates a suitable difference between maximal signal and inhibited values (or background) together with low variability. Moreover, when the more efficient inhibitor Nutlin-3a was used, the calculated factor coefficients were 0.70 and 0.85 using RLuc or NLuc as donor, respectively (not shown). Nevertheless, if any P2I2s are already described for the targeted PPI, values obtained for strains transformed with Luc-fusion protein and YFP alone can be also used as negative control. For our model interaction, p53-HDM2, we obtained a factor coefficient of 0.80 (using RLuc as donor protein) and 0.94 (when using NLuc; not shown). These results indicate that this yeast-based screening method is suitable for use in a full-scale HTS.

2.2.4 SCREENING

On day 1, 10 to 20 yeast colonies were picked from selection plates (SD-Ura-Leu media, SD: synthetic dextrose medium) and inoculated in liquid media. The two yeast strains, transformed by the donor and acceptor expression vectors or the donor alone and the empty acceptor plasmid p416GPD, were grown overnight (12 h) at 29 °C in 5 mL of liquid SR-Ura-Leu (SR: synthetic raffinose medium). Raffinose 2% (final concentration) is a carbon source that neither represses nor induces the *GAL* promoter and that allows prompt donor expression upon galactose (inducer) addition. On day 2, the cultures were diluted to an optimal optical density of 1 ($A_{600nm} = 1$) suitable for screening in fresh SR-Ura-Leu. Then, the 96-well plates were filled with 36 μ L of yeast culture (according to the plate map, see Fig. 4). As depicted, the first and 12th columns of the 96-well plate were dedicated to controls, and eight wells were filled by the control strain expressing the BRET donor only (used for the background BRET ratio calculation). Then, 0.4 μ L of the tested molecules, at the appropriate concentration, was added. Alternatively, and depending on liquid-handling systems available in the lab, yeasts can be added to the 96-well plate already containing the tested compounds. We experimentally observed that yeast tolerates up to 3% of DMSO (solvent for chemical compounds). Eighty different compounds can be analysed per 96-well plate. Finally, to induce the *GAL1* promoter, 3.6 μ L of galactose was added from a 10x stock solution (20% or otherwise optimized), and the plate was placed in a shaking platform for 2 h at 29 °C. We used here the induction time optimized as described previously and reported on Figure 2C. A few minutes before the end of the incubation, a fresh dilution of luciferase substrate was prepared. For RLuc donor substrate, coelenterazine h was solubilized in ethanol and diluted in Phosphate-Buffered Saline (PBS) to 5 μ M final concentration in the wells. The Nano-Glo Luciferase Assay Substrate was first diluted in PBS and used as 5000x final dilution in the wells. The multi well plate was then loaded in the BRET reader, and BRET values were determined as described in section “BRET Calculation.” The analysis of a 96-well plate is represented in Figure 4. A positive hit was defined as a chemical compound producing a significant inhibition of the BRET signal. To avoid false-positives, standard deviation obtained on 96 wells can be used to set a threshold; for example, in our experiments, a decrease of 25% of the BRET value was considered as an inhibited signal: this value was willingly higher than 3x the standard deviation of control samples. Special attention should be paid to those molecules that might interfere with the absorption properties of the BRET-based assay (fluorescent, coloured compounds). To distinguish between false-positive hits or bona fide specific inhibitors, these compounds should be tested against a BRET signal

produced from an unrelated PPI. In case a hit molecule is identified, it should be confirmed by a new BRET measurement performed in triplicate and also tested on the control strain expressing only the energy donor, to confirm that it does not interfere with the luciferases or the luciferins. This homogeneous assay (no wash steps are required) can be easily adapted to perform HTS of large libraries of chemical compounds. With this protocol, up to 800 compounds can be screened manually per day.

2.2.5 DISCUSSION

In this study, we used Nutlin-3 and Nutlin-3a, known inhibitors of the p53-HDM2 interaction, to validate the yeast BRET-based assay as a robust method to identify P212s. Indeed, as proof of concept, the cell-based screening assay described here has permitted the discovery, among more than 5000 compounds tested, of first-in-class chemical structures that can inhibit the CDK5/p25 interaction involved in various human diseases and notably in Alzheimer's disease^{11,27}. Among these inhibitors, tamoxifen was discovered, and additional studies have demonstrated that treatment of neuronal cells with this compound affects Tau phosphorylation, a substrate of CDK5^{27,28}. Contrary to these previous research study, we comprehensively describe here all steps of the protocol, the statistical Z'-factor (adapted to BRET in yeast, the Z-yBRET factor), and finally the possibility of designing alternative versions of the screening assay by modifying the donors. In this study, we have improved this yeast BRET protocol by using the high-efficiency small donor luciferase NLuc rather than the RLuc used previously. This results in higher protein expression and signal intensity/stability and represents a significant improvement when dealing with poorly expressed heterologous proteins. New donor/acceptor couples are still being discovered and optimized and their use may further enhance the BRET signals produced in our yeast PPI assay. Important advances have been made with the Nano lanterns, which are direct donor-acceptor fusion proteins optimized for BRET-based high bioluminescence²⁹. New RLuc8 mutants fused to mutated acceptors such as mVenus, mTurquoise, and mKusabiraOrange2 lead to a BRET signal more than 8000 mBRET^{29,30}. The protocol described here in association with new advances in BRET couples should contribute to the discovery of new promising therapeutic candidates that inhibit a variety of PPIs.

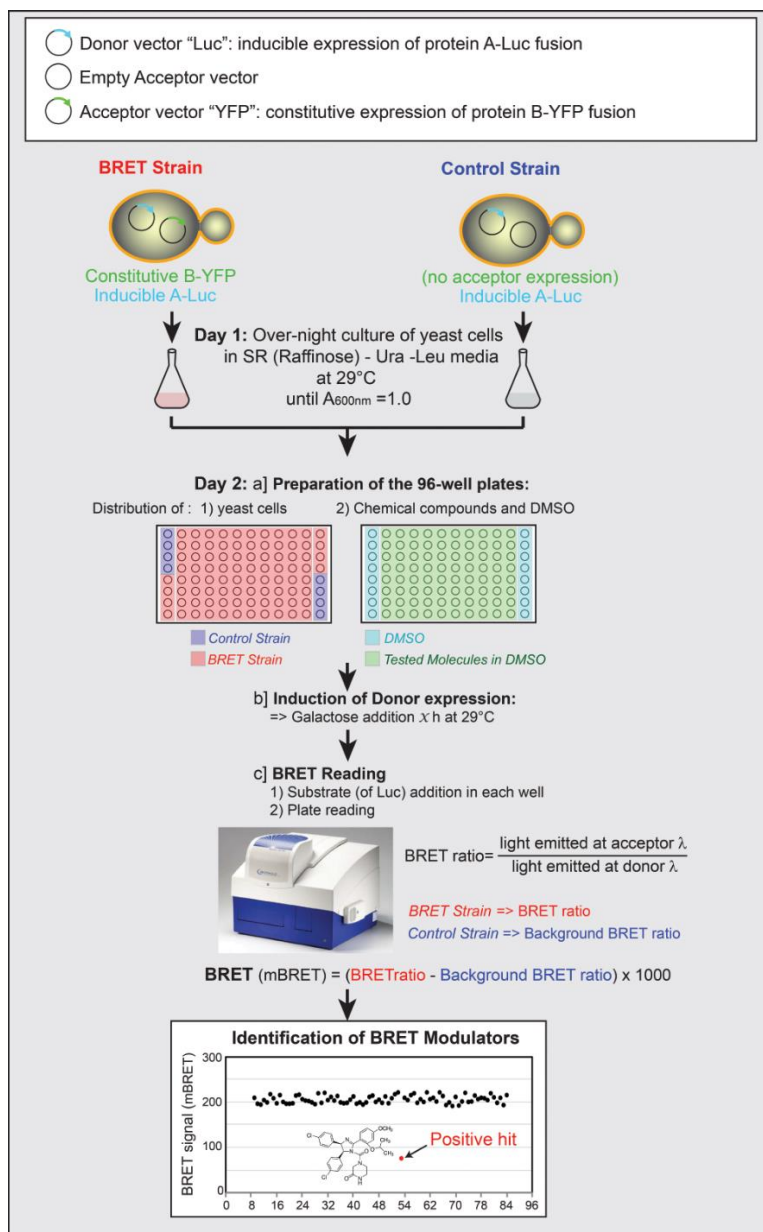


Figure 4. Workflow of the proposed Bioluminescence Resonance Energy Transfer (BRET)–based screening assay in yeast. In the first (A1 to H1) and in the 12th column (A12 to H12) of each 96-well plate, strains expressing the protein A-Luc donor fusion protein alone (control strain, A1:D1, and E12:H12) and both donor and acceptor fusion proteins (BRET strain, E1:H1, and A12:D12) are treated with DMSO as controls. The other 80 wells are dedicated to the screening of 80 compounds. Luc = RLuc or NLuc.

2.3 MATERIALS AND METHODS

Chemicals

D(+)-galactose and D(+)-raffinose were purchased from ACROS Organics (Geel, Belgium). Yeast nitrogen base without amino acids and Bacto peptone were purchased from BD Biosciences (Franklin lakes, NJ). D(+)-glucose, Bacto yeast extract, dimethylsulfoxide (vehicle control), 3,3',5'-triiodo-L-thyronine sodium salt (T3), Nutlin-3, Nutlin-3a, FK-506 monohydrate, and the different amino acids complements were purchased from Sigma (St. Louis, MO).

Reagents

Coelenterazine h was purchased from Interchim (Montluçon, France) and Nano-Glo Luciferase Assay Substrate from Promega (Madison, WI). *erg6* yeast mutant strain was obtained from Euroscarf No.Y00568 BY4741; MATa; his3Δ1; leu2Δ 0; met15Δ 0; ura3Δ 0; YML008c::kanMX4 (www.euroscarf.de). The antibodies used are anti-GFP (#ab290; Abcam, Cambridge, UK) and anti-RLuc (#MAB4400; Millipore, Billerica, MA).

Equipment

Mithras LB940 fluorometer/luminometer (Berthold Technologies, Bad Wildbad, Germany) microplate reader was used with the following emission filters: • RLuc/NLuc: counting time, 2.00 s; emission filter (No. 39450), 480 nm (±10 nm) • eYFP: counting time, 2.00 s; emission filter (No.39451), 530 nm (±12.5 nm) Measurement operation is performed by well, and each plate is read three times in a cycling manner.

BRET Calculation

The BRET ratio was calculated by dividing the signal measured at 530 nm by the signal measured at 480 nm. Then, the BRET signal was calculated as the BRET ratio subtracted by the BRET background ratio (obtained when the donor protein was expressed alone) and multiplied by 1000 to express results in millibRET (mBRET):

$$\text{BRET} = (\text{BRET ratio} - \text{Background BRET ratio}) \times 1000$$

detailed in reference⁶.

Statistical Analysis

Data were expressed as mean \pm SD or as percentage \pm %RSD (percentage relative standard deviation: SD x 100/mean). Statistical analyses were done by Student t test, and significance levels used are *p < 0.05, **p < 0.01, ***p < 0.001, and n.s. = not significant.

Vector Constructions

The centromeric vectors p415 (*LEU2*, *GAL1* inducible promoter) and p416 (*URA3*, *GPD* constitutive promoter) were used to express the chimeric proteins¹⁹. *TRP1* selectable marker gene cannot be employed with *erg6* mutant strain, because *trp1-erg6* double mutant is synthetic lethal. Donor (HDM2-RLuc or HDM2-NLuc) proteins were cloned into p415, and acceptor proteins (p53-YFP and p53m[F19A]-YFP) were cloned into p416. Both C- or N-terminal fusion vectors are available upon request.

Table I. List of the yeast plasmids used in this study.

Expressed Protein	Backbone	Marker	Origin	Promoter
HDM2-RLuc	p415GAL1	<i>LEU2</i>	CEN/ARS	<i>GAL1</i>
HDM2-NLuc	p415GAL1	<i>LEU2</i>	CEN/ARS	<i>GAL1</i>
p53-YFP	p416GPD	<i>URA3</i>	CEN/ARS	<i>GPD</i>
p53m-YFP	p416GPD	<i>URA3</i>	CEN/ARS	<i>GPD</i>

Table II. List of primers used in this study.

Primer name (restriction enzyme)	Sequence (5'-...-3')
oSB22 Fw (<i>Bam</i> HI/ <i>Nhe</i> I)	CTCTGGATCCGCTAGCATGTGCAATACCAACATGTCTG
oSB23 Re (<i>Age</i> I)	CTACCGGTCCGGGAAATAAGTTAGCAC
oSB34 Re (<i>Xho</i> I/ <i>Bsr</i> GI)	CGCCTCGAGTGACATTACTGCTCGTTCTTCAGCAC
NLuc Fw (<i>Cpo</i> I/ <i>Age</i> I)	CCCATCGGTCCGGGACCGGTAGCAACCATGGTCTTCACACTCGAAGATTT
NLuc Re (<i>Xho</i> I)	AATTATTTTACTCGAGTCACGCCAGAATGCGTTCGCA
HDM2 Fw (<i>Bam</i> HI/ <i>Cpo</i> I)	TAAATATAAAGGATCCGGTCCGATGTGCAATACCAACATGTCTG
HDM2 Re (<i>Age</i> I/ <i>Cpo</i> I)	GCTACCGGTCCCGGACCGATGGGGAAATAAGTTAGCACAAATCA
NheI-hCDK5_Sens (<i>Nhe</i> I)	ACCCAAGCTAGCATGCAGAAATACGAGAAAC
hCDK5-AgeI_AS (<i>Age</i> I)	GTGGCGACCGGTGGACAGAAGTCGGAGAAG
pcDNA3-HindIII_AS (<i>Hind</i> III)	ACCTCTACAAGCTTGGTATGGCTGATTATG
oSB28 Fw (<i>Bam</i> HI/ <i>Nhe</i> I)	CTCTGGATCCGCTAGCATGGAGGAGCCGCAGTCAGATCC
oSB29 Re (<i>Age</i> I)	CTACCGGTGGGTCTGAGTCAGGCCCTTCTG

ABBREVIATIONS

ATP Adenosine triphosphate

BRET Bioluminescence Resonance Energy Transfer

CDK Cyclin-Dependent Kinase

CML Chronic myelogenous leukemia

FKBP12 12 kDa FK-506 Binding Protein

FRET Förster Resonance Energy Transfer

HDM2 Human Double Minute 2

HTS High-Throughput Screening

mBRET milliBRET

NCoR Nuclear Receptor co-repressor

NLuc Nanoluc Luciferase

P212 Protein-protein interaction inhibitor

PBS Phosphate-Buffered Saline

PPI Protein-Protein Interaction

RLuc *Renilla* Luciferase

SD Synthetic Dextrose medium

SR Synthetic Raffinose medium

TGF β R Transforming Growth Factor β Receptor

TR T3 Thyroid hormone receptor

YFP Yellow Fluorescent Protein

REFERENCES

1. Santos F. P., Quintas-Cardama A. New Drugs for Chronic Myelogenous Leukemia. *Curr Hematol Malign Rep.* 2011;6:96–103.
2. Peng Z., Luo H. W., Yuan Y. et al. Growth of Chronic Myeloid Leukemia Cells Is Inhibited by Infection with Ad-SH2-HA Adenovirus That Disrupts Grb2-Bcr-Abl Complexes. *Oncol Rep.* 2011;25:1381–1388.
3. Colas P. High-Throughput Screening Assays to Discover Small-Molecule Inhibitors of Protein Interactions. *Curr Drug Disc Technol.* 2008;5:190–199.
4. Klein C., Vassilev LT. Targeting the p53-MDM2 Interaction to Treat Cancer. *Br J Cancer.* 2004;91:1415–1419.
5. Issad T., Jockers R. Bioluminescence Resonance Energy Transfer to Monitor Protein-Protein Interactions. *Methods Mol Biol.* 2006;332:195–209.
6. Bacart J, Corbel C, Jockers R, Bach S, Couturier C. The BRET technology and its application to screening assays. *Biotechnol J.* 2008;3(3):311-324.
7. Mager W. H., Winderickx J. Yeast as a model for medical and medicinal research. *Trends Pharmacol Sci.* 2005;26:265-273.
8. Goffeau A., Barrell B. G., Bussey H., Davis RW. Life with 6000 genes. *Science.* 1996;274(546):563-547.
9. Emter R., Heese-Peck A., Kralli A. ERG6 and PDR5 Regulate Small Lipophilic Drug Accumulation in Yeast Cells via Distinct Mechanisms. *FEBS Lett.* 2002;521:57–61.
10. Lee D. H., Goldberg AL. Selective inhibitors of the proteasome-dependent and vacuolar pathways of protein degradation in *Saccharomyces cerevisiae*. *J Biol Chem.* 1996;271:27280-2728.
11. Corbel C, Wang Q, Bousserouel H, et al. First BRET-based screening assay performed in budding yeast leads to the discovery of CDK5/p25 interaction inhibitors. *Biotechnol J.* 2011;6(7):860-870.
12. Zhao H. F., Kiyota T., Chowdhury S., Purisima E. et al. A mammalian genetic system to screen for small molecules capable of disrupting protein-protein interactions. *Anal Chem.* 2004;76:2922-2927.
13. Mazars A., Fahraeus R. Using BRET to Study Chemical Compound-Induced Disruptions of the p53-HDM2 Interactions in Live Cells. *Biotechnol J.* 2010;5:377–384.
14. Falcone C., Mazzoni C. External and internal triggers of cell death in yeast. *Cell Mol Life Sci.* 2016.
15. Hamdane M., Sambo A. V., Delobel P. et al. Mitotic-Like Tau Phosphorylation by p25-Cdk5 Kinase Complex. *J BiolChem.* 2003;278:34026–34034.

16. Zahiri J., Bozorgmehr J. H., Masoudi-Nejad A. Computational Prediction of Protein-Protein Interaction Networks: Algorithms and Resources. *Curr Genomics*. 2013;14:397-414.
17. Gonzalez M. W., Kann MG. Chapter 4: Protein interactions and disease. *PLoS Comput Biol*. 2012;8.
18. Couturier C., Jockers R. Activation of the leptin receptor by a ligand-induced conformational change of constitutive receptor dimers. *J Biol Chem*. 2003;278:26604-26611.
19. Mumberg D., Muller R., Funk M. Yeast vectors for the controlled expression of heterologous proteins in different genetic backgrounds. *Gene*. 1995;156:119-122.
20. England C. G., Ehlerding E. B., Cai W. NanoLuc: A Small Luciferase is Brightening up the Field of Bioluminescence. *Bioconjug Chem*. 2016.
21. Carry J. C., Garcia-Echeverria C. Inhibitors of the p53/HDM2 Protein-Protein Interaction-Path to the Clinic. *Bioorg MedChem Lett*. 2013;23:2480–2485.
22. Couturier C, Deprez B. Setting Up a Bioluminescence Resonance Energy Transfer High throughput Screening Assay to Search for Protein/Protein Interaction Inhibitors in Mammalian Cells. *Front Endocrinol (Lausanne)*. 2012;3:1-13.
23. Vassilev L. T., Vu B. T., Graves B. et al. In Vivo Activation of the p53 Pathway by Small-Molecule Antagonists of MDM2. *Science*. 303:844–848.
24. Chen Y. G., Liu F., Massague J. Mechanism of TGF beta receptor inhibition by FKBP 12. *EMBO J*. 1997;16:3866-3876.
25. Safer J. D., Cohen R. N., Hollenberg A. N., Wondisford FE. Defective release of corepressor by hinge mutants of the thyroid hormone receptor found in patients with resistance to thyroid hormone. *J Biol Chem*. 1998;273:30175-30182.
26. Zhang, J. H., Chung T. D., Oldenburg KR. A Simple Statistical Parameter for Use in Evaluation and Validation of High Throughput Screening Assays. *J Biomol Screen*. 1999;4:67–73.
27. Corbel C., Zhang B., Le Parc A. et al. Tamoxifen Inhibits CDK5 Kinase Activity by Interacting with p35/p25 and Modulates the Pattern of Tau Phosphorylation. *Chem Biol*. 2015;22:472–482.
28. Patrick G. N., Zukerberg L., Nikolic M., de la Monte S. et al. Conversion of p35 to p25 deregulates Cdk5 activity and promotes neurodegeneration. *Nature*. 1999;402:615-622.
29. Saito K., Chang Y. F., Horikawa K. et al. Luminescent Proteins for High-Speed Single-Cell and Whole-Body Imaging. *Nat Commun*. 2012;3:1262.
30. Takai A., Nakano M., Saito K., Haruno R. et al. Expanded palette of Nano-lanterns for real-time multicolor luminescence imaging. *Proc Natl Acad Sci U S A*. 2015;112:4352-4356.

Chapter 3

Identification of novel antibiotics targeting RNA polymerase

3.1 INTRODUCTION

Antibiotic resistance is an increasingly important global problem, with a high number of deaths every year (Fig.1). After a “Golden Era” (1940-1960), when all the principal antibiotics currently in use were discovered, there has been a significant decreasing in the number of new antibacterial compounds commercially available, as a consequence of the expansion of resistant strains and the failure in drug development by pharmaceutical industries. This “nightmare scenario” was due to several causes, the overuse and misuse of antibiotics, related to inappropriate prescriptions (choice of agent, duration of therapy, etc.) and the easy supply in many countries or online. Secondly, the widespread use in cattle and agriculture, mainly to promote growth and to prevent infections, has led to the release of antibiotics in the air and water, with the possible ingestion by humans of resistant bacteria, causing infectious diseases. Finally, this field was neglected by the pharmaceutical industry due to the low profits, associated with the high costs of clinical trials, the usually short treatment therapy, in addition to the unpredictable rate of resistance development^{1,2}.

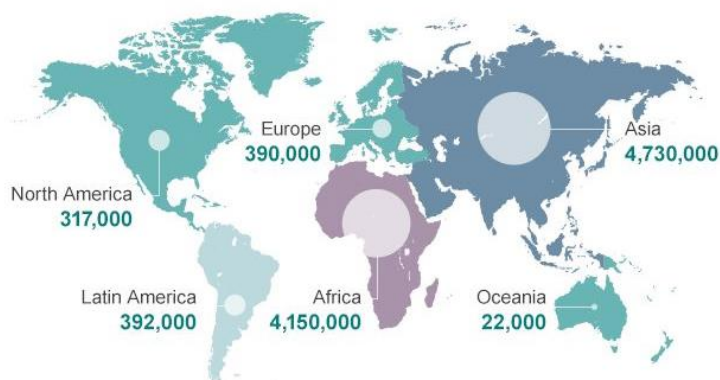


Figure 1. Global deaths attributable to antimicrobial resistance every year by 2050³.

The number of currently exploited bacterial targets is scant. The most successful antibiotics hit only three targets or pathways: the ribosome, cell wall synthesis and DNA gyrase or DNA topoisomerase⁴⁻⁷ (Table I).

Table I. Antibiotic targets and pathways.

Drug type	Drug	Derivation	Species range	Primary target	Pathways affected
Fluoroquinolones*					
DNA synthesis inhibitor	Nalidixic acid, ciprofloxacin, levofloxacin and gemifloxacin	Synthetic	Aerobic Gram-positive and Gram-negative species, some anaerobic Gram-negative species (<i>C. perfringens</i>) and <i>M. tuberculosis</i>	Topoisomerase II (DNA gyrase), topoisomerase IV	DNA replication, SOS response, cell division, ATP generation, TCA cycle, Fe-S cluster synthesis, ROS formation, and envelope and redox-responsive two-component systems
Trimethoprim-sulfamethoxazole					
DNA synthesis inhibitor	Co-trimoxazole (a combination of trimethoprim and sulfamethoxazole in a 1:5 ratio)	Synthetic	Aerobic Gram-positive and Gram-negative species	Tetrahydrofolic acid synthesis inhibitors	Nucleotide biosynthesis and DNA replication
Rifamycins					
RNA synthesis inhibitor	Rifamycins, rifampin and rifapentine	Natural and semi-synthetic forms of ansamycins (derived from <i>S. mediterranei</i>)	Gram-positive and Gram-negative species, and <i>M. tuberculosis</i>	DNA-dependent RNA polymerase	RNA transcription, DNA replication and SOS response
β-lactams*					
Cell wall synthesis inhibitors	Penicillins (penicillin, ampicillin, oxacillin), cephalosporins (cefazolin, cefoxitin, ceftriaxone, cefepime) and carbapenems (imipenem)	Natural and semi-synthetic forms of carbonyl lactam ring-containing azetidinone molecules (from <i>P. notatum</i> , <i>C. acremonium</i> and <i>S. cattleya</i>)	Aerobic and anaerobic Gram-positive and Gram-negative species	Penicillin-binding proteins	Cell wall synthesis, cell division, autolysin activity (regulated by LytSR-VncRS two-component system), SOS response, TCA cycle, Fe-S cluster synthesis, ROS formation, and envelope and redox-responsive two-component systems
Glycopeptides and glycolipopeptides					
Cell wall synthesis inhibitor	Vancomycin; teicoplanin	Natural and semi-synthetic forms of amino sugar-linked peptide chains (for glycopeptides) or of fatty acid-bearing, amino sugar-linked peptide chains (for glycolipopeptides) derived from actinobacteria	Gram-positive species	Peptidoglycan units (terminal D-Ala-D-Ala dipeptide)	Cell wall synthesis, transglycosylation, transpeptidation and autolysin activation (VncRS two-component system)
Lipopeptides					
Cell wall synthesis inhibitors	Daptomycin and polymyxin B	Natural and semi-synthetic forms of fatty acid-linked peptide chains (from <i>S. roseosporus</i> and <i>B. polymyxa</i>)	Gram-positive species (daptomycin), Gram-negative species (polymyxins)	Cell membrane	Cell wall synthesis and envelope two-component systems
Aminoglycosides					
Protein synthesis inhibitors	Gentamicin, tobramycin, streptomycin and kanamycin	Natural and semi-synthetic forms of amino sugars (-mycins from <i>Streptomyces</i> spp. and -micins from <i>Micromonospora</i> spp.)	Aerobic Gram-positive and Gram-negative species, and <i>M. tuberculosis</i>	30S ribosome	Protein translation (mistranslation by tRNA mismatching), ETC, SOS response, TCA cycle, Fe-S cluster synthesis, ROS formation, and envelope and redox-responsive two-component systems
Tetracyclines					
Protein synthesis inhibitors	Tetracycline and doxycycline	Natural and semi-synthetic forms of four-ringed polyketides (from <i>S. aureofaciens</i> and <i>S. rimosus</i>)	Aerobic Gram-positive and Gram-negative species	30S ribosome	Protein translation (through inhibition of aminoacyl tRNA binding to ribosome)
Macrolides					
Protein synthesis inhibitors	Erythromycin and azithromycin	Natural and semi-synthetic forms of 14- and 16-membered lactone rings (from <i>S. erythraea</i> and <i>S. ambofaciens</i>)	Aerobic and anaerobic Gram-positive and Gram-negative species	50S ribosome	Protein translation (through inhibition of elongation and translocation steps) and free tRNA depletion

Table I (cont). Antibiotic targets and pathways.

Streptogramins					
Protein synthesis inhibitors	Pristinamycin, dalbapristin and quinupristin	Natural and semi-synthetic forms of pristinamycin I (group B, macrolactone ringed-peptides) and pristinamycin II (group A, endolactone oxazole nucleus-bearing depsipeptides) (from <i>Streptomyces</i> spp.)	Aerobic and anaerobic Gram-positive and Gram-negative species [‡]	50S ribosome	Protein translation (through inhibition of initiation, elongation and translocation steps) and free tRNA depletion
Phenolics					
Protein synthesis inhibitor	Chloramphenicol	Natural and semi-synthetic forms of dichloroacetic acid with an aromatic nucleus and aminopropanediol chain (from <i>S. venezuelae</i>)	Some Gram-positive and Gram-negative species, including <i>B. fragilis</i> , <i>N. meningitidis</i> , <i>H. influenzae</i> and <i>S. pneumoniae</i>	50S ribosome	Protein translation (through inhibition of elongation step)

*Drug efficacy can vary across species range based on drug generation. ‡ When used as a combination of pristinamycin I and pristinamycin II. *B. fragilis*, *Bacillus fragilis*; *B. polymyxa*, *Bacillus polymyxa*; *C. acremonium*, *Cephalosporium acremonium*; ETC: electron transport chain; *H. influenzae*, *Haemophilus influenzae*; *M. tuberculosis*, *Mycobacterium tuberculosis*; *N. meningitidis*, *Neisseria meningitidis*; *P. notatum*, *Penicillium notatum*; ROS, reactive oxygen species; *S. ambofaciens*, *Streptomyces ambofaciens*; *S. aureofaciens*, *Streptomyces aureofaciens*; *S. cattleya*, *Streptomyces cattleya*; *S. erythraea*, *Saccharopolyspora erythraea*; *S. mediterranei*, *Streptomyces mediterranei*; *S. pneumoniae*, *Streptococcus pneumoniae*; *S. rimosus*, *Streptomyces rimosus*; *S. roseosporus*, *Streptomyces roseosporus*; *S. venezuelae*, *Streptomyces venezuelae*; TCA, tricarboxylic acid⁵.

Unlikely, bacteria have rapidly become expert in managing our weapons both via antibiotic resistance and via antibiotic tolerance, reducing the efficacy in the treatment of infectious diseases, correlated to high risk of clinical complication⁸. Bacteria have evolved different strategies to survive the action of antibiotics: i) alteration or destruction of the compounds: bacteria may be able to alter the antibiotic molecules, producing an enzyme that introduces chemical modifications (principally acetylation, phosphorylation and adenylation), or destroying the compound, for example, β -lactamases cleave the amide bond of β -lactam ring^{5,9}. ii) Alteration of permeability and/or efflux pump: since many antibiotic targets are cytoplasmic, bacteria may be capable to restrict the penetration of different toxic compounds, altering the expression levels, the type and the functions of porins. For example, vancomycin has no effect on Gram-negative bacteria because it fails in the outer membrane penetration. On the other hand, bacteria could increase the extrusion of drugs by efflux pumps, which may affect a wide range of compounds, such as fluoroquinolones and β -lactams^{5,9}; iii) Target modification: to decrease the affinity of antibiotics with their targets, bacteria could mutate a gene sequence, altering the target site, such as in the case of the resistance to rifampin, where a single point mutation in *rpoB* gene (encoding for the β subunit of the enzyme) blocks the inhibitory effect of the antibiotic on the DNA-dependent RNA polymerase (RNAP)¹⁰. The enzymatic alteration of the binding site is another common strategy: for example, the macrolide resistance is due to methylation

of the 50S ribosomal subunit¹¹; iv) the overproduction of the antibiotic target; v) the acquisition of foreign DNA from the environment through horizontal gene transfer^{5,9} (Fig.2).

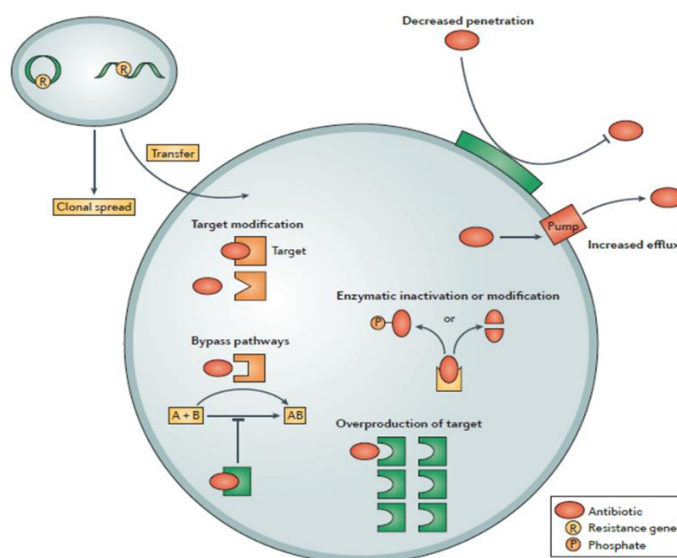


Figure 2. Main mechanisms of antibiotic resistance⁸.

Other mechanisms are also possible: bacteria may be able to survive a transient exposure to high antibiotic concentration: it refers to tolerance, a phenomenon principally due to slow-growth and growth-lag of bacteria¹². These are phenotypic “non-growing” variants of active dividing cells produced stochastically in the population, which tolerate the action of bactericidal compounds. In the model organism *Escherichia coli*, the toxin-antitoxin system has been characterized for its involvement in the production of tolerance phenotype^{8,12}.

Owing to the rise of antibiotic tolerance and resistance, in addition to the spread of multi-drug resistant “ESKAPE” pathogens (*Enterococcus faecium*, *Staphylococcus aureus*, *Klebsiella pneumoniae*, *Acinetobacterium baumannii*, *Pseudomonas aeruginosa* and *Enterobacter spp.*) there is an urgent need to develop new strategies in the identification of new compounds or novel druggable targets.

Transcription is a key biological process for life and represents an attractive drug target, rarely exploited in antibiotic research. Eukaryotes possess three different RNAPs associated with several regulators, while prokaryotes have only one enzyme able to convert all the genomic information in RNAs with different functions^{13–15}. The bacterial RNAP core enzyme has a molecular weight of

approximately 350 kDa and consists of five subunits: two α -subunits, each containing a N-terminal domain necessary for enzyme assembling and a C-terminal domain that interacts with regulatory elements; one β subunit and one β' subunit that form the enzyme active site, and an ω subunit involved in the RNAP assembling and in the interaction with different transcriptional modulators¹⁶ (Fig.3). The amino acids sequence, 3D structures and the functions of all these subunits are highly conserved among bacteria. Starting from 1995, several RNAP structures have been resolved, mainly from *E. coli*, *Thermus aquaticus/Thermus thermophiles* and *Bacillus subtilis/Bacillus stearothermophilus*¹⁷. The RNAP core enzyme has a “crab claw” structure that forms the primary channel accommodating the active site. Here, the β and β' subunits create one “pincer” of the claw, which interacts with DNA portions downstream the enzyme active site¹⁸. In addition, the enzyme presents a second channel, the nucleoside triphosphate (NTP) entry site, when DNA is bound¹⁹. Although catalytically active, the core enzyme alone is unable to start the transcription efficiently and specifically. To this end, the interaction with the initiation factor σ and the formation of the holoenzyme confers to the RNAP the ability to specifically recognize the promoter DNA sequences -10 and -35. Once the DNA has been melted, and the open complex shaped, the σ factor is released as part of the promoter clearance process^{16,20–26}. All bacteria present an essential σ factor, orthologous to *E. coli* σ^{70} , which is responsible of the ‘housekeeping’ genes transcription during the exponential growth. Most bacteria also have a complement of “alternative” σ factors (six in *E. coli*) that recognise promoters of genes involved in adaptive response to specific signal, such as stress and morphological development²⁷.

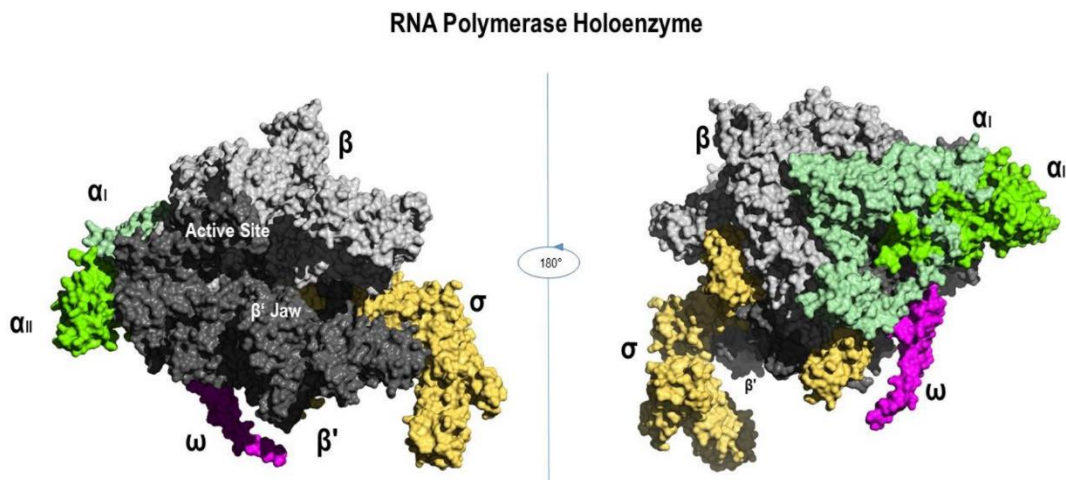


Figure 3. Bacterial RNAP holoenzyme is made up of a core enzyme (five subunits: β (grey), β' (dark grey), ω (magenta), α_I (pale green), α_{II} (green)) to which the σ factor (light orange) is associated (PDB 4YG2). This factor is responsible for the correct placement of the transcriptional machinery on DNA promoter and the acceleration of the open complex formation; it specifically promotes, in *E. coli*, the transcription initiation of housekeeping genes during the log growth phase.

Bacterial RNAP represents a suitable drug target for different reasons: i) as mentioned above, it is essential for the pathogen propagation; ii) its subunits and the associated transcription factors are highly conserved among bacteria, allowing to develop antibiotics of broad-range²⁸. iii) Bacterial RNAP is different to the corresponding eukaryotic enzyme, ensuring selectivity and reducing the possibility of cytotoxicity²⁹; iv) the availability of different high resolution structures that can be used for the rational design of new drugs³⁰.

To date, only two classes of antibacterial drugs targeting RNAP are used in clinical practice: i) the rifamycins (rifampin, rifapentine, rifabutin and rifamixin) bind within the cleft close to the active site of RNAP, sterically inhibiting the growth of RNA product³¹; ii) the lipiarmycins (fidaxomicin) bind to a region distant from the enzyme active site and allosterically inhibit the DNA binding to RNAP; fidaxomicin is principally used for the treatment of *Clostridium difficile* infections³². Recently, another class of antibacterial agents is under investigation: the myxopyronins bind to a site distant from active centre and lock the clamp in a partly closed conformation, preventing the loading of DNA^{33,34}. All these compounds have the inherent disadvantage of being subjected to resistance, due to mutations of the respective binding site on RNAP.

As an alternative to the use of the active site as an antibiotic target, the interaction between the RNAP core enzyme and the σ factor can be envisaged as a possible target for drug discovery to search for small molecules able to prevent the assembly of the transcription complex holoenzyme. Indeed, the specific factors σ is not conserved between bacterial and eukaryotic cells³⁵; moreover, the high resolution determination of three-dimensional structures of complex between RNAP core and the house-keeping initiation factor σ^{70} in Gram-negative bacteria and σ^A in Gram-positive bacteria, has allowed the identification of the main regions involved in the interaction: the coiled coil β' CH (Clamp Helix) region (β' 260-309 *E. coli* (*rpoC* gene)) and the 2.2 σ^{70} domain (σ^{70} 379-449 *E. coli*, (*rpoD* gene))³⁶ (Fig.4). Structural studies have revealed that the principal residues involved in the interaction form polar bonds between basic residues (R275, R278, R281) of the subunit β' and σ acid residues (D403, E407), in addition to hydrophobic interactions²⁰. Specific amino acids contained in the first α -helix of the σ 2.2 domain are also important for the interaction, as revealed by targeted mutagenesis in *B. subtilis* σ^A (amino acids E166, Q165, M169, D162 e M172)^{36,37}. Overall, these experiments demonstrate the existence of a clear hotspot between the two proteins, making this interaction an attractive target for the addressing of small molecules, that, intercalating between the σ^{70} acidic patch and the β' basic patch, can strongly obstruct the transcription initiation complex formation.

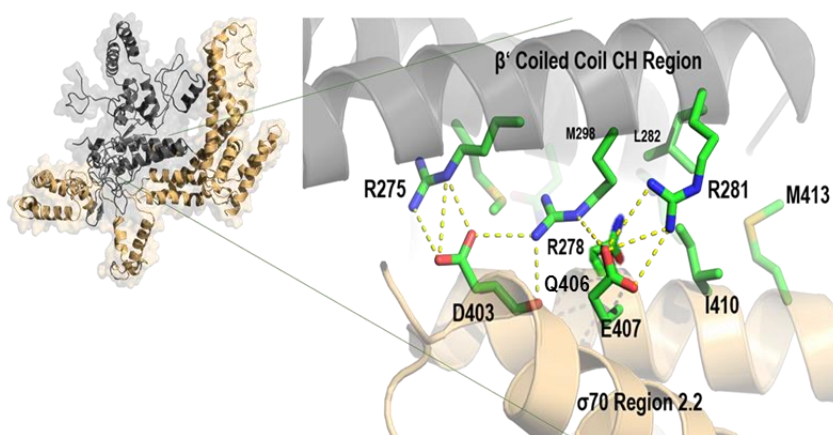


Figure 4. Interaction between β' subunit (grey) and σ^{70} factor (light orange) of *E. coli* (PDB 4YG2). The image shows key residues involved in the interaction. Salt bridges can be observed between R275 and D403; E407 and R281; other hydrophobic amino acids that have been proved to be important for the interaction (Table II) are shown.

Table II

2.2 σ^{70} domain			β' CH region		
<i>T. Thermophilus</i> (PDB 1IW7)	<i>E. Coli</i> (PDB 4YG2)	<i>B. Subtilis</i>	<i>T. Thermophilus</i> (PDB 1IW7)	<i>E. Coli</i> (PDB 4YG2)	<i>B. Subtilis</i>
E215	E407	E166	R553	R278	R267
Q214	Q406	Q165	R550	R275	R264
Q218	I410	M169	K556	R281	R270
D211	D403	D162	M573	M298	M287
I221	M413	M172	N569	N294	N283
			L557	L282	L271
			I566	I291	I280
			E570	E295	E284

These tables show the residues of two interacting subunit of RNAP colored and sorted by the importance in the interaction, as obtained by mutagenesis experiments. Highlighted in red are the key residues whose mutation results in considerable loss of affinity, while the less critical are in green. Residues are reported for bacteria species *T. thermophilus*, *E. coli* and *B. subtilis*.

To date, all the attempts to target the $\beta' - \sigma$ interaction were conducted using *in vitro* assays, that allowed to identify molecules with high potency *in vitro*, but demonstrated several problems, such as poor antibacterial activity, low specificity for RNAP, unfavourable physiochemical properties.

In the first work a small molecule library was screened using an ELISA assays to identify molecules able to disrupt the *E. coli* RNAP holoenzyme assembly. The SB-molecule series was able to inhibit the RNAP core - σ interaction with an IC_{50} ranging from 2 μ M to 15 μ M. The principal problem of the SB series was the lack of specific mode of action, targeting different bacteria components. The possible development of analogues was complicated by the absence of a structure activity relationship model³⁸. Subsequently, Glaser et al. performed a LRT-based High Throughput Screening (HTS) of commercial small molecule library from Chembridge Corp., identifying three compounds able to disrupt RNAP core - σ^{70} interaction in a dose-dependent manner, with an IC_{50} ranging from 3 μ M to 28 μ M. Their activity was also confirmed by *in vitro* transcription assay and growth inhibition of *E. coli*, but showed insolubility problems³⁹. Hüsecken et al. tried a peptide-based approach to generate a new class of inhibitors, starting from the rationale design of peptides able to target different regions of the RNAP core - σ^{70} interface, subsequently tested *in vitro* transcription assay and confirmed by ELISA assay and by molecular dynamic simulation. They found a peptide mimicking σ^{70} 2.2, able to inhibit the PPI and the holoenzyme assembling at low micromolar concentration, but the efficacy of this peptide was not tested on bacteria cells⁴⁰.

Other attempts with small molecules led to the identification of the GKL series, a class of indole-containing compounds capable of interfering with RNAP complex assembling, selected by a structure-based drug design³⁶. Starting from the key residues in the σ^A and the β' -CH region involved in the formation of intermolecular interaction, they constructed a pharmacophore model and used it to select potential inhibitors within an in-house compound library. This approach led to the identification of GKL001-003, being GKL003 the most active molecule, that was able to specifically bind to β' -CH region (revealed via isothermal titration calorimetry) with a high potency in *in vitro* transcription assay ($K_i \sim 6$ nM). Nevertheless it displayed low antimicrobial potency against both Gram-positive and Gram-negative bacteria (MIC >2 mM), probably due to the low solubility of the compound³⁶. Starting from these observations, the same authors synthesized a library of thirty bis-indoles compounds analogues to GKL001-003. Each compound was assayed both to determine its ability to inhibit the $\sigma^{2.2}/\beta'$ -CH interaction, by ELISA assay at 15 μ M, and its effectiveness in reducing cell growth of *B. subtilis* and *E. coli* at 200 μ M. Most of the molecules effectively inhibited the interaction *in vitro*, and showed moderate inhibition of *E. coli* growth, but did not show any antibacterial activity against *B. subtilis*. Cellular permeability can be influenced by molecular size and the chemical characteristics of the compound, thereby affecting the antibacterial activity. A possible solution was the identification and synthesis of smaller inhibitors, with lower molecular weight in order to overcome the solubility and permeability problems⁴¹. Using this strategy, the same research group analyzed 41 mono-indole or a mono-benzofuran compounds, characterized by a lower molecular weight, but these compounds showed a lower activity in comparison with the molecules of the previous work⁴². Nevertheless, unlike bis-indoles, which preferentially inhibited the growth of *E. coli*, many mono-indoles inhibit cell growth of *B. subtilis* and *E. coli*. This observation suggests that the mono-indole scaffold can potentially be developed for broad-spectrum antibacterial agents. The Structure Activity Relationship analysis (SAR) carried out on this library suggested that two important aspects should be taken into account for a rational design of antibacterial agents: the molecular size and the hydrophilicity-lipophilicity balance, in order to generate compounds capable of crossing the outer membrane of the Gram-negative and cell wall of Gram-positive bacteria, whilst retaining a high solubility⁴³. The same authors subsequently generated an improved pharmacophore model, used for the identification of a drug lead through *in silico* screening of the public mini-library Maybridge, in order to find molecules capable of inhibiting the holoenzyme formation targeting the interaction $\sigma^{70}/\sigma^A 2.2 - \beta'$ -CH. Twenty-seven molecules have been identified and tested by ELISA assay, and only one showed significant activity at low concentration.

Its activity was also demonstrated in an *in vitro* transcription assay, exhibiting an IC_{50} of about 0.05 μ M. When tested for its antimicrobial activity, the compound showed a greater inhibition against the Gram positive bacterium *B. subtilis*, with a value of MIC of 50 μ M. The low activity of the compound is thought to be due to its scarce permeability⁴⁴.

All these results confirm the RNAP - σ^{70} interaction as an appropriate target for novel antibiotic discovery, as well as the potential of indoles group to disrupt this PPI. To effectively screen for candidate compounds capable of interfering with the RNAP (β' subunit) - σ^{70} interaction, we set-up a high-throughput (HT) platform that combines sequential *in vivo* and *in vitro* assays as a novel antibiotic discovery pipeline with a screening throughput of up to 800 compounds/day. The proposed antibiotic discovery pipeline includes: i) a highly sensitive *in vivo* HT, yeast Bioluminescent Resonance Energy Transfer (yBRET) assay, which allows to reproduce the β' - σ^{70} interaction in yeast and to screen for interaction inhibiting compounds. This platform can be applied to the random screening of large pre-existing compound libraries, but it can also be focused on specific sets of compounds selected *in silico* based on the known three-dimensional structure of the RNAP - σ^{70} complex as well on available information on known inhibitors to be used as pharmacophore models; ii) different *in vitro* tools to validate and further characterize the inhibitory activity of hit compounds; iii) *in vivo* bacterial assays to evaluate the ability of selected compounds to inhibit bacterial growth. This strategy applied to small molecule libraries of different origin, proved to be an effective tool for the identification and characterization of novel antibiotics targeting β' - σ^{70} interaction.

3.2 RESULTS AND DISCUSSION

3.2.1 OPTIMIZATION AND VALIDATION OF THE β' - σ^{70} INTERACTION IN THE YEAST BRET PLATFORM

β' - σ^{70} INTERACTION MODEL CONSTRUCTION IN yBRET

The availability of 3D structures of RNAP holoenzyme complex and the awareness of residues involved in the interactions between β' and σ^{70} , guided the design of the constructs for BRET analysis^{18,20,36,44}. To reproduce the β' - σ^{70} interaction in yBRET, we initially cloned two different portions of *E. coli* β' -CH region (residues 1-334 and 220-334), and the full-length sequence of σ^{70} (*E. coli*), since no previous study has been reported using only the 2.2 domain. To identify the combinations with the highest BRET signals, the coding sequences of β' and σ^{70} have been cloned in-frame with both the donor and the acceptor, in either C-terminal or N-terminal orientation.

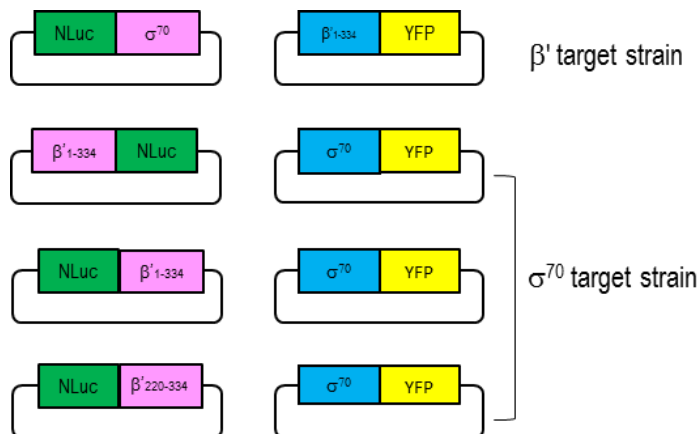
For screening purpose, we usually consider combinations with BRET signals higher than 100 mBRET. In addition, the acceptor-fusion protein (preferably the inhibitor target protein) is constitutively expressed, while the expression of the donor-fusion protein is induced, after the candidate compound addition, by supplementation of the inducer. This allows the binding of the small molecule inhibitors before complex formation⁴⁵. The signal deriving from the induced luciferase-fusion protein may also be informative about the toxicity of the molecule tested. Therefore, the donor-fusion proteins were expressed under the control of the galactose-inducible *GAL1* promoter (p415), while the acceptor-fusion protein under a constitutive promoter (p416, *GPD* promoter), in the hyper permeable $\Delta erg6$ yeast strain to maximize the uptake of luciferase substrate and small molecule compounds. To select the best combinations, we performed a preliminary test, where the donor fusion protein expression was induced for 2 h with 2% galactose (Table III).

Table III. yBRET β' - σ^{70} interaction combinations.

A		B	
Constructs		Constructs	
β' target strain		σ^{70} target strain	
σ^{70} -NLuc + β' (1-334)-YFP	68	β' (1-334)-NLuc + σ^{70} -YFP	216
σ^{70} -NLuc + YFP- β' (1-334)	39	β' (1-334)-NLuc + YFP- σ^{70}	6
NLuc- σ^{70} + β' (1-334)-YFP	151	NLuc- β' (1-334) + σ^{70} -YFP	278
NLuc- σ^{70} + YFP- β' (1-334)	41	NLuc- β' (1-334) + YFP- σ^{70}	11
σ^{70} -NLuc + β' (220-334)-YFP	28	β' (220-334)-NLuc + σ^{70} -YFP	58
σ^{70} -NLuc + YFP- β' (220-334)	11	β' (220-334)-NLuc + YFP- σ^{70}	2
NLuc- σ^{70} + β' (220-334)-YFP	18	NLuc- β' (220-334) + σ^{70} -YFP	279
NLuc- σ^{70} + YFP- β' (220-334)	6	NLuc- β' (220-334) + YFP- σ^{70}	16

BRET signals obtained with different combinations of constructs. The expression of donor fusion proteins was induced for 2 h with 2% galactose. The table A shows the combinations for the construction of the β' target strain (both 1-334 and 220-334 portions), while table B the combinations for σ^{70} target strain.

The YFP-X fusion proteins always gave weaker signals than the corresponding X-YFP fusions, regardless the combination considered, while the donor orientation less affected the signal strength. Four combinations gave a BRET signal higher than 100 mBRET and included both β' and σ^{70} target strains (Fig.5). These combinations were chosen for further analysis on signal sensitivity and specificity.

**Figure 5.** Schematic representation of selected combinations with highest BRET signal.

Increasing inducer (galactose) concentrations were tested to find the optimal expression levels of donor fusion protein, necessary to obtain a stable and reliable signal in addition to the sensitivity required for the trustworthy detection of inhibitory compounds to measure the modulation of BRET signal (Table IV).

Table IV. Inducer-dependent BRET signal modulation.

A			B		
NLuc- σ^{70} + β' (1-334)-YFP			β' (1-334)-NLuc + σ^{70} -YFP		
% of galactose	mBRET	NLuc	% of galactose	mBRET	NLuc
2	151	400491	2	216	488317
0,5	134	323013	0,5	216	322427
0,1	128	113072	0,1	214	289280
0,05	120	97414	0,05	213	216164
0,025	113	62823	0,025	185	51185
0,01	104	14052	0,01	177	22029
0,005	100	3350	0,005	161	6216

C			D		
NLuc- β' (1-334) + σ^{70} -YFP			NLuc- β' (220-334) + σ^{70} -YFP		
% of galactose	mBRET	NLuc	% of galactose	mBRET	NLuc
2	278	105513	2	287	47155
0,5	278	143054	0,5	268	70735
0,1	274	128140	0,1	265	67620
0,05	274	111805	0,05	269	60972
0,025	278	39900	0,025	280	22872
0,01	299	19587	0,01	279	11190
0,005	309	3442	0,005	269	1477

BRET and luciferase signals evaluated at different galactose concentrations. BRET signals deriving from NLuc values < 20000 units are considered not trustworthy for screening purposes.

Two σ^{70} -target strains (NLuc- β' (1-334) + σ^{70} -YFP and NLuc- β' (220-334) + σ^{70} -YFP) showed an absence of BRET signal modulation at any galactose concentration considered (Table IVC-D). In absence of modulation it is difficult to infer about the donor:acceptor ratio present in the cell. In the other two strains, the BRET signal increased with the inducer concentration until it reached a plateau. In these cases, at low galactose concentrations, the donor fusion protein is probably present in limiting molar concentration respect to the donor fusion protein. When the donor:acceptor ratio is close to 1:1 the BRET signal is at the highest sensitivity for the detection of a protein-protein interaction inhibitor.

We therefore selected these last interactions for the subsequent assays (Table IVA-B), and the highest galactose concentration rising the BRET signal before the plateau was chosen, which guaranteed for both strains a sensitive, high and stable BRET signal and a reliable luciferase value (higher than 20000 units). The inductor concentration was 0,5% and 0,025% for β' -target strain (NLuc- σ^{70} + β' (1-334)-YFP) and for σ^{70} -target strain (β' (1-334)-NLuc + σ^{70} -YFP), respectively.

EVALUATION OF β' - σ^{70} INTERACTION SIGNAL SPECIFICITY

The donor saturation assay allows to verify the specificity of the interaction in a BRET set-up. This assay is carried out to assess whether the BRET signal observed results from occasional collisions due to the cytosolic crowding or from a specific interaction bringing the energy donor and acceptor in proximity. The donor saturation assay consists on the inducible expression of the acceptor fusion protein at various concentrations of galactose for 20 h at 20 °C, whereas the donor expression is constitutive. The long time required for the induction is due to the maturation of the chromophore and 20 °C represents the ideal temperature for the expression of the YFP. The result obtained shows precisely the exponential increase of the BRET signal followed by a plateau phase that is expected for a specific interaction measured in BRET (Fig.6).

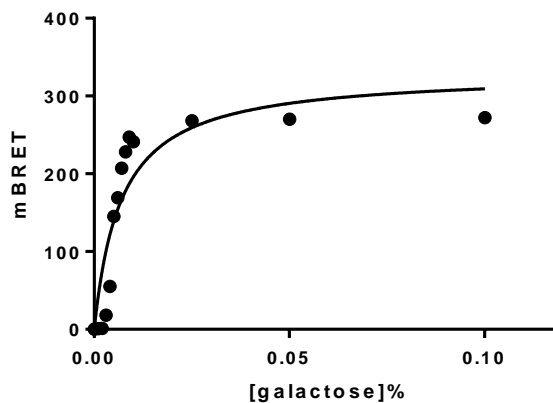


Figure 6. Donor saturation assay for β' - σ^{70} interaction in BRET. The expression of the acceptor fusion protein (β' (1-334)-YFP) was induced o/n at 20 °C at different galactose concentrations, while the expression of the donor fusion protein (NLuc- σ^{70}) was controlled by a constitutive promoter (p190 *TEF*).

Another way to test interaction specificity is to verify the influence of mutations in key residues on the BRET signal. We therefore created mutant versions of β' and σ^{70} by replacing two amino acids known to be critical for the interaction^{36,37}: R275 and R278 on β' were substituted with alanine residues, while Q406 and E407 on σ^{70} were substituted with a lysine and alanine residues, respectively. The BRET signals of two mutant versions, NLuc- σ^{70} + β' mut (1-334)-YFP and NLuc- σ^{70} mut + β' (1-334)-YFP, were compared to the wild-type signal: the results revealed an almost complete loss of the BRET signal with σ^{70} mutant, and a 40% reduction for β' mutant (Fig.7). These data indicated once again the specificity of the interaction reconstituted with the two fusion proteins inside yeast cells.

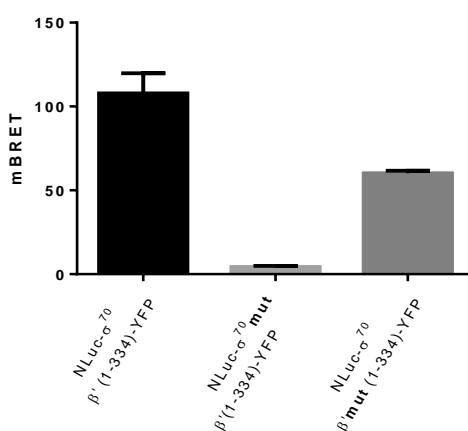


Figure 7. BRET signal comparison between wild-type and σ^{70} mut or β' mut combinations. The expression of the donor fusion proteins was induced for 2 h with 0.5% galactose (mean \pm SD; error bars represent SD, n=3)

VALIDATION OF SCREENING PLATFORM WITH INDOLE-CONTAINING MOLECULES

The efficacy of molecules containing indole groups as inhibitors of the interaction β' - σ^{70} , by targeting β' has been previously demonstrated^{36,44}.

To validate the yBRET assay, we therefore evaluated an in-house mini library of 27 indole derivatives, 10 mono-indoles and 17 bis-indoles, supplied by Prof. Gilberto Spadoni, Dipartimento di Scienze Biomolecolari, University of Urbino "Carlo Bo" (Supplementary Table 1). The molecules were assayed at a final concentration of 20 μ M on the β' -target strain (NLuc- σ^{70} + β' (1-334)-YFP), and seven molecules had an inhibitory activity devoid of significant toxicity. The two mono-indoles UCM 1315 and

UCM 1316 were not selected for further analysis due to their toxic effect on yeast cells, measured by a significant drop of luciferase signal (Fig.8). These results indicate that the β' -target strain is sensitive to the detection of potential β' - σ^{70} interaction inhibitors.

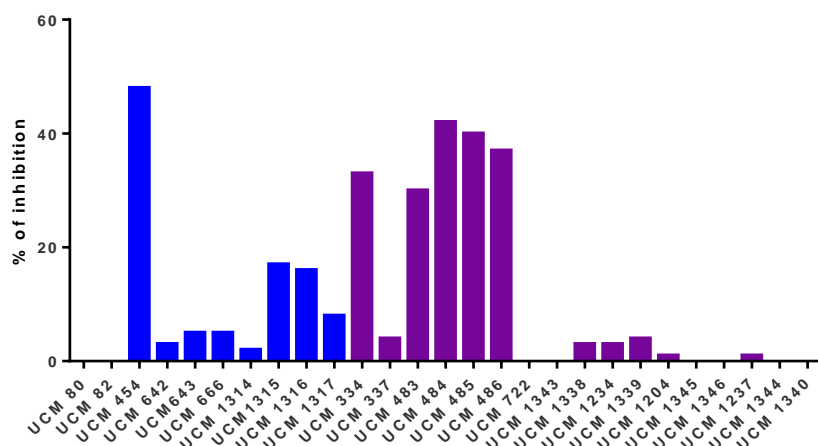


Figure 8. Screening of indoles and bis-indoles mini-library in yBRET assay. The histogram shows the percentage of inhibitions for each molecule tested at 20 μ M. The mono-indole compounds are coloured in blue and the bis-indoles in purple. The structures of these molecules are shown in Supplementary Tables 1.

3.2.2 VALIDATION OF yBRET RESULTS USING AN ELISA ASSAY

To confirm the yBRET results in an independent experimental set-up we reproduced the β' - σ^{70} interaction in an *in vitro* ELISA-based assay.

To this aim, we produced the two recombinant proteins in *E. coli*, fused to two different tags, Glutathione-S-Transferase (GST)- β' (1-334) and His-tag- σ^{70} . The GST-Thioredoxin (from *Pyrococcus furiosus*) protein was used as negative control of interaction. His-tag- σ^{70} was successfully expressed and purified, while GST- β' (1-334) purification failed during the elution with glutathione from the immobilized glutathione Sepharose column. So, the cell lysate of *E. coli* expressing GST- β' (1-334) at high level was used as a source of tagged β' during ELISA assays. The concentration of GST- β' (1-334) was determined by densitometric analysis of lysates subjected to PAGE analysis in the presence of standards at known concentration.

The β' - σ^{70} interaction was first reproduced in ELISA using σ^{70} at two molar concentrations (250 nM and 500 nM) and different concentrations of β' (2.5 μ M, 1.25 μ M, 750 nM and 250 nM), in a combinatorial way. All the combinations tested exhibited a stable signal, in comparison to the negative controls performed to monitor the non-specific signal: the interaction between σ^{70} and GST-Thioredoxin and the incubation of β' supernatant in absence of σ^{70} . Using σ^{70} at 250 nM, the same conditions were also assayed in the presence of a molecule known to interfere in the β' - σ^{70} interaction³⁸, and we chose to use both proteins at 250 nM concentration for the highest test sensitivity (Fig. 9).

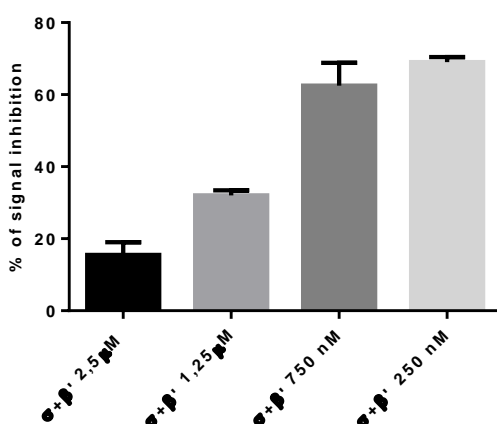


Figure 9. Sensitivity of ELISA assay in the presence of a β' - σ^{70} interaction inhibitor. Plates were coated with 100 μ l of His-tag- σ^{70} at 250 nM. GST- β' at different concentrations was incubated for 10' with SB2 500 μ M before the contact with His-tag- σ^{70} . The histogram shows the percentage of inhibition for each GST- β' concentration; the maximum signal inhibition was obtained with GST- β' at 250 nM. (mean \pm SD; error bars represent SD, n=2)

Using these optimized conditions, we tested the molecules that showed an inhibitory activity against the β' - σ^{70} interaction in yBRET, along with two inactive molecules of the same mini-library (the mono-indole UCM 80 and the bis-indole UCM 722) and four molecules known to be β' - σ^{70} interaction inhibitors^{36,38,39,44}. These molecules, tested at a final concentration of 500 μ M, confirmed their efficacy as potential antibiotics molecules, as well as the reliability of our new drug discovery platform (Fig.10).

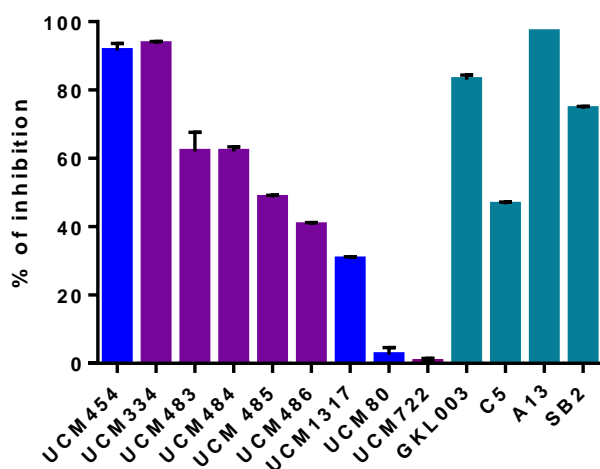


Figure 10. Activity of indoles mini-library molecules in ELISA assay. The ELISA assay was conducted both on molecules known to inhibit the interaction, used as positive controls, and on selected molecules from indoles mini-library. Mono-indole compounds are coloured in blue, the bis-indoles in purple and the positives controls in mid blue. (mean \pm SD; error bars represent SD, n=2)

To compare their potency, UCM 454, UCM 483, and the positive control GKL003 were assayed in a dose-response ELISA assay. UCM 334 was not selected for further analysis since it resulted insoluble in PBS.

Molecules from the indole mini-library appeared to be at least ten time less efficient than GKL003, with IC_{50} values ranging from 52.27 μ M to 93.25 μ M (Fig.11).

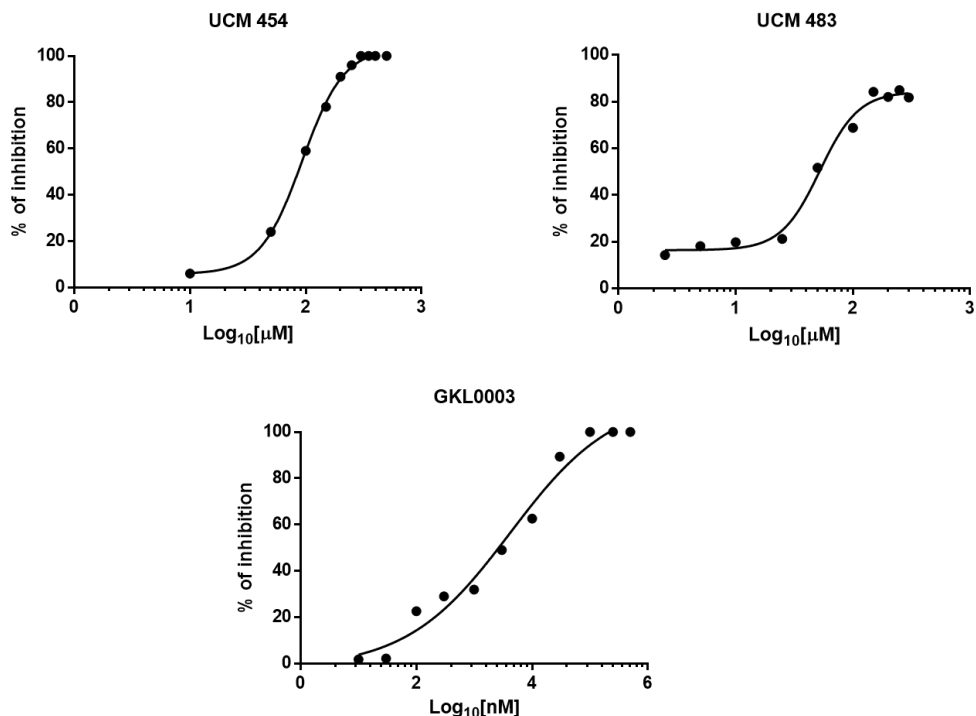


Figure 11. Inhibitory activity on β' - σ^{70} interaction of indole-containing molecules assayed at different concentrations in ELISA assay. The IC_{50} is calculated as a measure of molecule potency.
 UCM 454: $IC_{50}=93.25 \mu M$ $r^2=0.9988$
 UCM 483: $IC_{50}=52.27 \mu M$ $r^2=0.9901$
 GKL0003: $IC_{50}=4.1 \mu M$ $r^2=0.98$

3.2.3. *IN SILICO* SELECTION AND SCREENING OF SMALL-MOLECULE LIBRARIES

A burning point of target-based drug discovery, once a proper assay has been finely gauged, is the selection of the compounds to be screened. We have performed the yBRET platform on untargeted compounds libraries and on specific sets of compounds selected *in silico* based on the known three-dimensional structure of the RNAP- σ^{70} complex as well as on available information on known inhibitors.

Computational approaches were applied to the Compounds Australia Library (Griffith University) to identify a subset of 5.000 commercial small molecules belonging to ChemDiv (San Diego, CA USA) and Enamine Ltd companies, starting from 50.0000 compounds, to select molecules with the higher probability to be active inhibitors of the β' - σ^{70} interaction.

Firstly, the database was filtered by molecular weight (MW): only compounds with molecular weight greater than or equal to 250 were kept, since compounds with lower MW are less likely to inhibit PPIs. Then, starting from the crystallographic structure of *E. coli* RNAP (PDB: 4YG2), three models were built on the σ^{70} interaction surface, whose derived molecules will likely target the β' surface (Table V, Fig 12).

Table V. Pharmacophore elements identified on σ^{70} subunit for the three models.

Pharmacophore model A	Pharmacophore model B	Pharmacophore model C
Two hydrogen bond donor groups on two H atoms of Q406 ammine group	Two hydrogen bond donor groups on two H atoms of Q406 ammine group	Two hydrogen bond donor groups on two H atoms of Q406 ammine group
Two hydrophobic sites on Q406 and I410 side chains	One hydrogen bond acceptor group on the Q406 carbonyl oxygen	One hydrogen bond acceptor group on the Q406 carbonyl oxygen
One negatively charged site on the acidic group of E407	Two hydrophobic sites on side chains of Q406 and I410	Two hydrophobic sites on side chains of Q406 and L402
	One negatively charged site on the acidic group of E407	Two negatively charged sites on the acidic group of E407 and D403

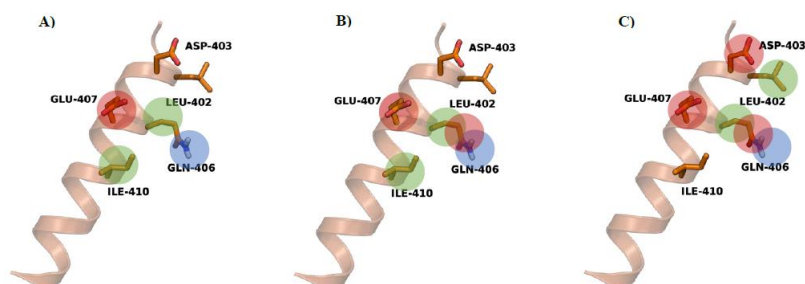
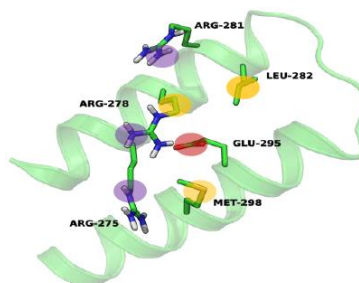


Figure 12. Pharmacophore model on σ^{70} . The three pharmacophore models, built on σ^{70} region 2.2, exploited for the compounds screening. Negatively charged sites are shown in red, hydrogen bond donor groups in blue, hydrophobic and aromatic groups in green.

One model was built on the β' interaction surface, rejecting positively charged molecules, being unable to cross the yeast and bacterial cell wall (Table VI, Fig 13).

Table VI. Pharmacophore elements identified on β' subunit for the model.

Pharmacophore model D
Three positively charged sites on guanidium groups (R275, R278 and R281)
Three hydrophobic sites on side chains of L282, R278 and M298
One negatively charged site on the acidic group of E295

**Figure 13.** Pharmacophore model on β' . Representation of pharmacophore model built on β' . Negatively charged site is shown in red, positively charged sites in purple and hydrophobic/aromatic groups in yellow.

Other criteria, based on the similarity with known β' - σ^{70} interaction inhibitors, were also used for compound selection: the top 250 compounds according to the shape similarity score for both reference inhibitors (C5 and GKL003) were chosen, along with all compounds containing an indole ring or a carboxylic acid.

Seven small-molecule libraries of different origin (see Materials and Methods) were also screened against β' - σ^{70} interaction, for a total of other 13.898 compounds of synthetic and natural origin.

Molecules were tested in yBRET at 20 μ M and added to exponentially growing yeast before donor protein induction. BRET signal was read after 2 h of incubation at 30 °C, and molecules reducing NLuc signal more than 50% were considered toxic to yeast cells.

The 5000-selected Australia Compound Library was assayed with both the β' -target and the σ^{70} -target strains. Considering the rate of success of these two strains in the identification of potential inhibitors in this library, the other libraries were screened with β' -target strain only. Molecules that significantly reduced BRET signal were re-assayed at the same concentration and at 10 μ M and subsequently the inhibitory activity of confirmed hits was verified with the *in vitro* ELISA assay.

Table VII

LIBRARY	TARGET STRAIN	N. COMPOUNDS	YBRET	ELISA	N. SCAFFOLD
AUSTRALIA COMPOUND LIBRARY	β'	5000	18	7	6
AUSTRALIA COMPOUND LIBRARY	σ^{70}	5000	6*	-	-
NCI	β'	1596	-	-	-
REC3	β'	1040	4	1	1
ICBMS	β'	4320	11	6	4
ICNS	β'	4640	9	2	1
ENZO	β'	502	5	-	-
PRESTWICK	β'	1200	4	-	-
MARC3	β'	600	-	-	-

This table summarizes the results obtained from the screening of the eight libraries: the yBRET column refers to the number of molecules identified *in vivo*; the ELISA column shows the number of compounds that were confirmed to disrupt the interaction *in vitro*, and the last column refers to the number of different scaffolds identified in selected hits compounds. * molecules with similar chemical structures to ELISA-confirmed compounds identified in Australia Compound Library using β' -target strain

The screening of Australia Compound Library performed on the β' -target strain led to the identification of seven molecules able to inhibit the interaction both *in vivo* and *in vitro*. Some of these molecules contain in their structure an indole group, confirming once again the potential of this chemical class. The seven hits were purchased from public vendors, along with structural analogues of the best two compounds, to extensively investigate the inhibitory activity of these chemical classes (Table VIII). The six molecules identified to targeted σ^{70} were not purchased since their principal chemical features were similar to those of molecules selected against β' -target strain.

The ReC3 library is a compound collection created in the KISSf of Roscoff, assembling molecules from different libraries. The unique hit discovered came from a compound collection of the *Institut de Chimie des Substances Naturelles* (ICNS), directed by Dr. Catherine Guillou (CNRS-ICNS, Gif-sur-Yvette, France), which kindly provided the hit molecule, along with three structural analogues (Table VIII). This molecule was not present in the ICNS library we screened.

The ICBMS library led to isolate six molecules inhibiting the interaction; thanks to a collaboration with Dr. Arnaud Comte (*Université Claude Bernard-Lyon 1*), it was possible to identify the chemical structure of hit compounds and to classify them in four major scaffolds. Dr. Comte kindly provided a tiny amount of three hits with 34 structural analogues, in order to investigate the class activity. The other hit compounds will be purchased in short-term.

In the case of ICNS, it was possible to identify two molecules able to inhibit the interaction and, in collaboration with Dr. Catherine Guillou (CNRS-ICNS, Gif-sur-Yvette, France), the chemical structure

of compounds was identified (Supplementary Table 5). These molecules belong to the same scaffold and they will be re-purchased shortly together with structural analogues.

Table VIII

Small-molecule library	HIT commercial ID	Vendor	n. structural analogues	Analogues commercial ID	Vendor
Australia Compound Library	L390-1378	Chemdiv	8	L390-2620 F812-0882 G210-0090 V013-2659 L036-0366 8019-9090	Chemdiv
				Z1191880202 Z1191882607	Enamine
	L557-0318	Chemdiv	13	L557-0168 L557-0360 L557-0164 L491-0070 L557-0300 L556-0122 L556-0204 L556-0024 L556-0100 L556-0114 L556-0137 L556-0264 L557-0204	Chemdiv
	M530-2099	Chemdiv	-	-	-
	Z1021075756	Enamine	-	-	-
	Z126203636	Enamine	-	-	-
	F538-0554	Chemdiv	-	-	-
ReC3	2009/0540	CNRS-ICSN	3	2009/0746 2009/0770 2009/0771	CNRS-ICSN
ICBMS	15-B02	ICMBS	13	08-G10-09 08-H07-09 08-H11-09 08-H09-09 12-E09-09 12-F02-09 12-G10-09 15-A06-09 14-G07 14-H10 15-H02 15-H09 17-A06	ICMBS
	17-H04	ICMBS	3	17-B08 17-B11 17-F11	ICMBS
	37-A03	ICMBS	18	U181-10-10-L-H03 U181-10-10-L-H08 U181-10-13-L-C04 U181-10-13-L-C06 U181-10-20-L-A02 U181-10-20-L-A11 U522-12-36-L-F11 U524-12-36-L-G05 U524-12-36-L-G06 U524-12-36-L-G08 U524-12-36-L-G09 U524-12-36-L-G11 U524-12-36-L-H05 U524-12-36-L-H06 U524-12-36-L-H07 U524-12-36-L-H11 U522-12-37-L-A02 U524-12-37-L-A05	ICMBS

The list of selected hits with structural analogues.

As expected from a screening campaign, hit compounds identified through yBRET assay belong to different chemical classes, differing in the nature of the cyclic scaffold and the nature and position of the substituents. However, it is possible to highlight some structural elements shared by many of the selected compounds. An indole ring is present in L557-0318, L390-1378, G581-0350 and L557-0335 (Supplementary Table 2) as well as in the most potent inhibitors of β' - σ^{70} interaction reported to date (i.e., GLK003 and its derivatives). An indole structure can be envisaged in the compound from the ReC3 library 2009/0540 as part of its tetracyclic ring (Supplementary Table 3) and potential indole bioisosteres can be seen in compounds Z1021075756, C448-0959, C448-1002 and G581-0350 (Supplementary Table 2), which have one or more additional nitrogen atoms in the six-membered ring of their indole-like structure. Although not an indole, a bicyclic nucleus is present in M530-2099 in which a benzofuran ring constitutes the central portion of the compound (Supplementary Table 2). All the compounds have side chains characterized by the presence of polar groups not ionizable at physiological pH, mostly amide (L390-1378, M530-2099, Z126203636, C208-0595, C448-0959, C448-1002, C654-0156, G581-0350) and urea (L557-0318, F538-0554, G418-0274, L557-0335) groups (Supplementary Table 2). Interestingly, GKL003, the best characterized σ^{70} -beta' inhibitor has a N,N'-diacylhydrazine group.

A total of 32 molecules (8 hits and 24 structural analogues) were primarily tested in yBRET at 10 μ M to re-confirm the inhibition of the hits compounds and to evaluate the activity of new molecules.

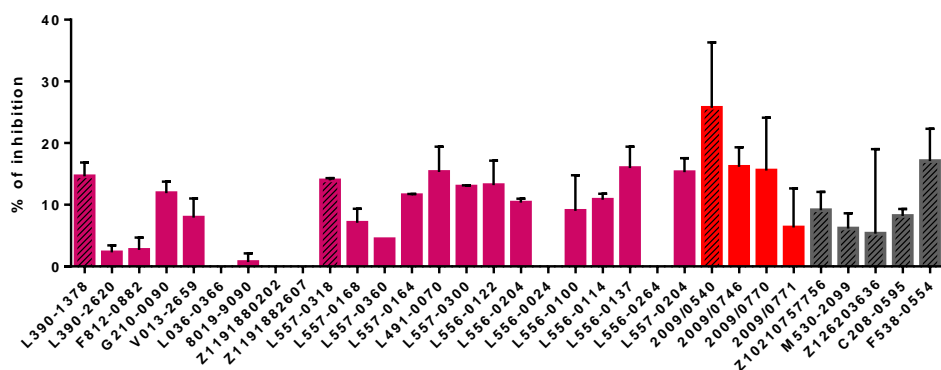


Figure 14. Results of yBRET assay of hits and structural analogues tested at 10 μ M; Hit molecules (striped bars) are followed by their structural analogous. Bars represent mean \pm SD; Indoles are in purple, indole-tetracyclic ring containing molecules in orange, the other hit molecules are in grey. The structures of these molecules are shown in Supplementary Tables 2 and 3.

Once re-purchased the seven hits from Australia Compound Library and the hit acquired from the ICNS institute (resulting from the ReC3 library) confirmed their efficacy; concerning the analogues, fifteen molecules showed significant inhibition: two compounds were analogues of the hit L390-1378, ten of L557-0318, and three of 2009/0540 (Fig. 14). We subsequently evaluated the inhibitory capacity of all molecules in ELISA assay, to validate the results obtained in yBRET.

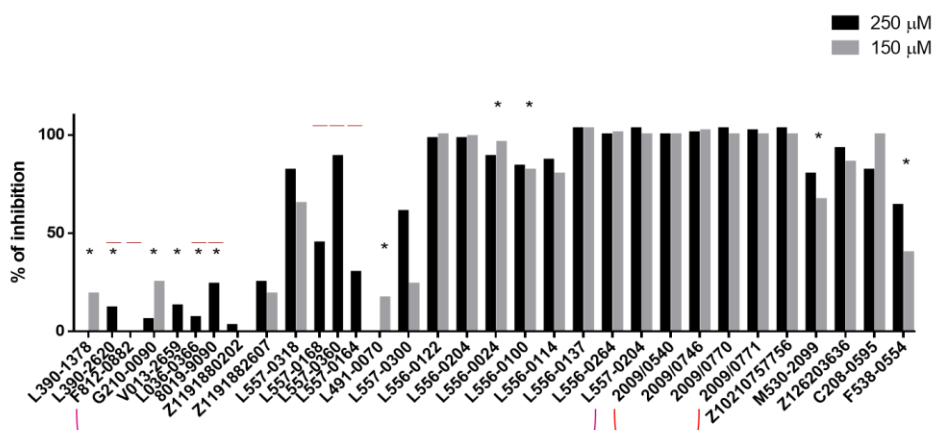


Figure 15. Results of ELISA assay of hits and structural analogues tested at 250 μM (black bars) and 150 μM (grey bars); * indicate insoluble molecules in PBS; - indicate data not available at 150 μM . The molecules in the order as in Figure 14. Indoles are grouped with purple bracket, indole-tetracyclic ring containing molecules with orange bracket. The structures of these molecules are shown in Supplementary Tables 2 and 3.

Molecules were tested at 250 μM . Seven of the eight hits compounds exhibit their efficacy as potential antibiotics molecules, while the hit L390-1378, once re-purchased, resulted insoluble in PBS, as well as all the structural analogues correlated to this molecule (Fig. 15). Lowering the concentration to 150 μM allowed to assay these molecules as soluble, but at this concentration they have lost their activity. Decreasing the concentration of the compounds the turbidity disappeared, nevertheless the molecules were no more active; the same consideration was applied also to the compounds L491-0070, L556-0024, L556-0100 (analogues of L557-0318), M530-2099 and F538-0554. All the other molecules confirmed their inhibitory activity (Fig. 15). To verify whether this group of molecules targeted β' , we performed an ELISA assay incubating four of the most active compounds at two different concentrations with His-tag- σ^{70} instead GST- β' , prior His-tag- σ^{70} - GST- β' complex formation. Results showed a significant decrease in the percentage of inhibition in comparison to the data obtained with β' , suggesting that they likely bind β' (Fig. 16).

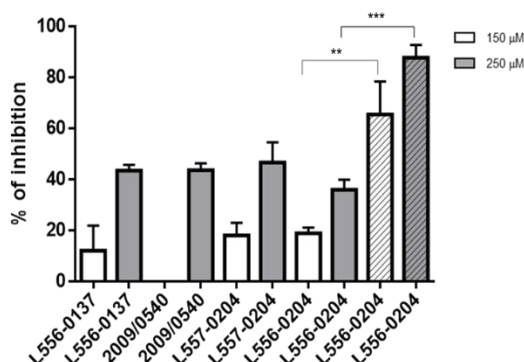


Figure 16. Results of ELISA assay where molecules were first incubated at 150 μ M and 250 μ M for 10' minutes with His-tag- σ^{70} before GST- β' addition. Striped bars with streaks refers to molecule incubated with GST- β . ** t-test p-value < 0.001; *** t-test p-value < 0.0001.

We selected the most active compounds among indole- and indole-tetracyclic ring containing molecules to assess their inhibitory capacity in a dose-response ELISA assay. The percentage of inhibition was tested at eight different concentrations ranging from 10 μ M to 250 μ M (Fig.17). The curves of C208-0595 and L556-0264 are not shown, since they rapidly lost effect at concentrations lower than 120 μ M and 80 μ M, respectively.

IC₅₀ were calculated as a measure of molecule potency and ranged between 37 µM and 52 µM for the molecules derived from Australia Compound Library, whereas for the molecules associated to ReC3 library the IC₅₀ was 65 µM and 83 µM. The results were compared to the reference compound GKL003, which exhibit an IC₅₀ at least 10 times lower respect to newly identified molecules.

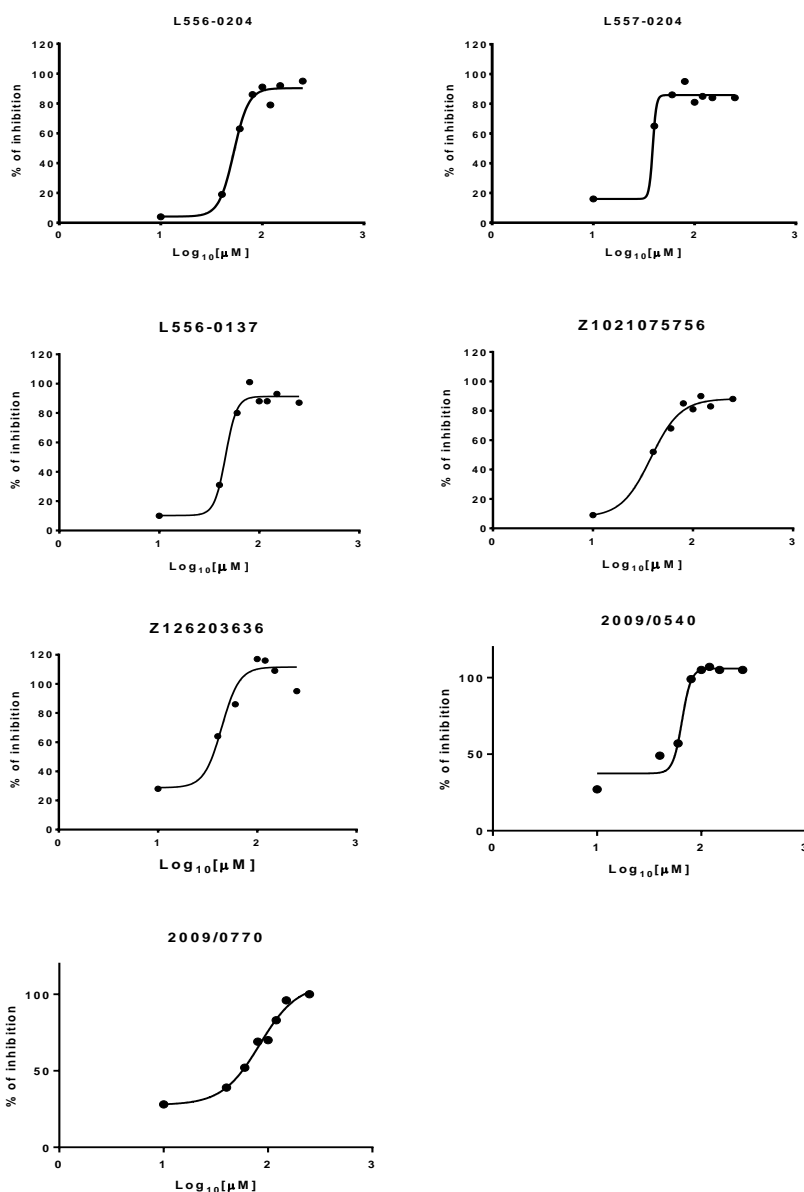


Figure 17. Inhibitory activity on β' - σ^{70} interaction of molecules assayed at different concentrations in ELISA assay. The IC₅₀ is calculated as a measure of molecule potency.

L556-0204: IC₅₀=52.36 μ M r²=0.9828

L557-0204: IC₅₀=38.63 μ M r²=0.9739

L556-0137: IC₅₀=46 μ M r²=0.9786

Z1021075756: IC₅₀=37.84 μ M r²=0.9849

Z126203636: IC₅₀=43.85 μ M r²=0.9020

2009/0540: IC₅₀=65.31 μ M r²=0.9673

2009/0770: IC₅₀=83.36 μ M r²=0.9848

Concerning the molecules from ICBMS library, for three hits (15-B02 and 17-H04 belonging to the same scaffold, plus 37-A03) it was possible to retrieve the molecules and structural analogues. In this case, we decided to perform only the ELISA assay at 100 μM given the limited availability of compounds. Two hit molecules, 15-B02 and 37-A03, confirmed their activity on the interaction, while for 17-H04, originally validated at 150 μM , it was not possible to monitor any effect at this concentration. Ten structural analogues exhibited significant inhibition and will be re-purchased at high quantity to performed subsequent analyses (Fig.18).

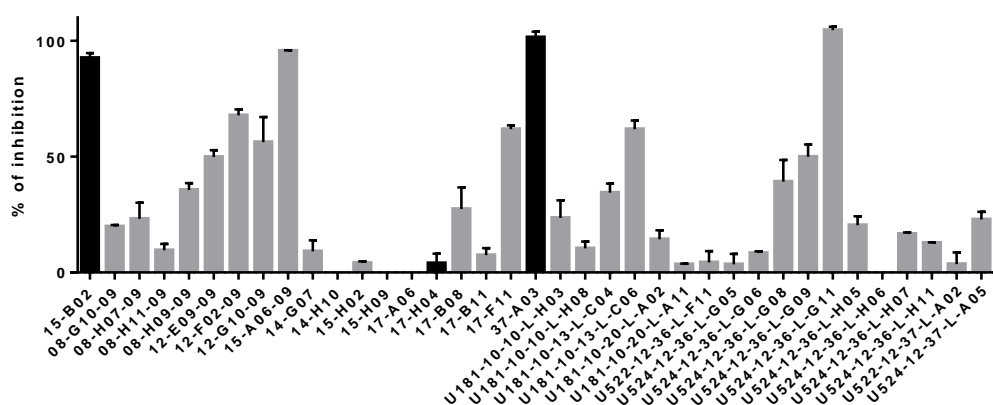


Figure 18 Results of ELISA assay of hits and structural analogues from ICBMS library, tested at 100 μM . Each hit molecule, coloured in black, is followed by its structural analogues, coloured in grey. The structures of these molecules are shown in Supplementary Tables 4.

3.2.4 RNAP-INHIBITORY AND ANTIBACTERIAL ACTIVITY OF MOLECULES IDENTIFIED IN γ BRET SCREENING AND VALIDATED IN ELISA

An *in vitro* transcription assay was performed to verify whether these molecules, able to inhibit β' - σ^{70} interaction, were also able to interfere with the RNA polymerase holoenzyme assembly. We selected six most potent molecules for each scaffold: a mono-indole (UCM 454) and a bis-indole (UCM 483) from the in house-mini library of indole derivatives; L556-0204, L556-0137, and L557-0204, the best three structural analogues derived from a hit of Australia Compound Library, and 2009/0540 from the ReC3 library.

Firstly, we assessed the activity of molecules at two fixed concentrations of 25 μM and 50 μM , in a non-competitive inhibition assay, prior to RNAP core - σ^{70} interaction. The results were compared with

those of the best characterized inhibitor of β' - σ^{70} interaction, GKL003, and of the RNAP enzyme activity inhibitor Rifampicin. Molecules were initially incubated with 87.5 nM RNAP core enzyme, followed by the addition of 875 nM recombinant His-tag- σ^{70} . The DNA template was added and the mixture was incubated at 37 °C for 15 minutes. The reaction started with the addition of a mix of radiolabelled and unlabelled NTPs and allowed to continue for 10 minutes.

Table IX

Compounds	25 μ M	50 μ M
UCM 454	0	83
UCM 483	8	32
L556-0204	0	100
L556-0137	12	100
L557-0204	0	100
2009/0540	41	77
GKL003	90	100
Rifampicin	97	100

Results of molecules activity in *in vitro* transcription inhibition assay. The percentage of transcription inhibition is reported at 25 μ M and 50 μ M.

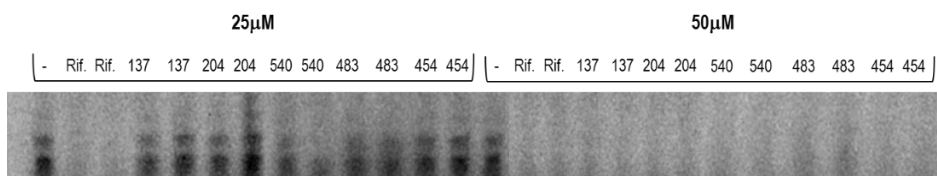


Figure 19. Determination of hit compounds activity using *in vitro* transcription assay. Molecules were tested at 25 μ M and 50 μ M. The band shown in the autoradiograph corresponds to the 175 nt transcription product. -: DMSO, vehicle control; Rif: Rifampicin; 137: L556-0137; 204: L556-0204; 540: 2009/0540; 483: UCM 483; 454: UCM 454.

All molecules, except UCM 483, caused an almost complete loss of transcript at 50 μ M; at lower concentration, only 2009/0540 exhibited a significant reduction of RNAP activity (Table IX, Fig.19).

A dose-response assay was performed on the L556 series, along with the positive control GKL003. These molecules were tested at ten different concentrations ranging from 5 μ M to 400 μ M.

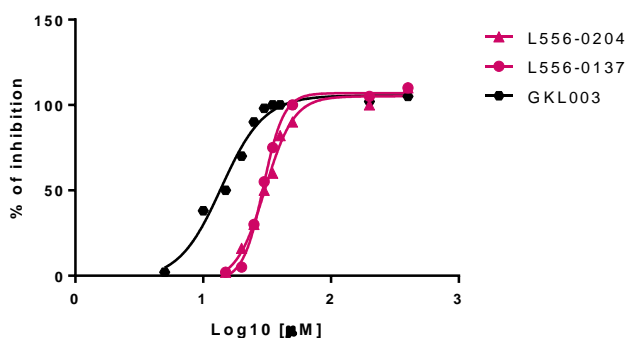


Figure 20. Inhibitory activity on RNA holoenzyme complex assembly in *in vitro* transcription inhibition assay. Molecules were tested at 10 different concentrations. The IC_{50} is calculated as a measure of molecule potency.

L556-0204: $IC_{50}=31.12\ \mu M$ $r^2=0.9942$

L556-0137: $IC_{50}=29.78\ \mu M$ $r^2=0.9979$

GKL003: $IC_{50}=13.49\ \mu M$ $r^2=0.9804$

Molecules of the L556 series brought to a coherent sigmoid curve, with an IC_{50} close to $30\ \mu M$ for both compounds, approximately double that of the control molecule (Fig.20).

Having established the ability of molecules to inhibit *in vitro* transcription, we evaluated their efficacy directly on bacteria. The assay was conducted in a 96-well plate by monitoring the cells growth in the presence of molecules dissolved in DMSO, or of an equivalent quantity of DMSO as negative control. Antimicrobial activity of hit compounds was determined monitoring growth inhibition of non-pathogen bacteria, the Gram-positive *B. subtilis* and the Gram-negative *E. coli*, in presence of molecules. Preliminary tests on *E. coli* showed that the activity of the compounds was enhanced by the addition of Polymixin B (PMBN), suggesting limited cross of bacterial outer membrane. To increase outer membrane permeability, *E. coli* was treated with $1\ \mu g/ml$ PMBN in combination with the hit molecules. Similarly, we analyzed the growth of wild type W303 yeast strain in the presence of hits molecules, to verify their toxicity for eukaryotic cells.

Based on results obtained in different *in vitro* assays, we decided to carried out growth inhibition test on eight molecules: UCM 454, L556-0204, L556-0137, L557-0204 and 2009/0540, which showed the best activity in all test performed, plus other three compounds with IC_{50} in the range of $37-83\ \mu M$ in ELISA assay: Z1021075756, Z126203636 and 2009/0770. Bacterial growth was monitored for 6 h, in the presence of fixed concentration of molecules ($200\ \mu M$).

Table X

Compound	DH10	DH10+ PMBN	<i>B. subtilis</i>	<i>S. cerevisiae</i>
UCM 454	2	30	0	-
L556-0204	30	100	88	0
L556-0137	28	61	99	5
L557-0204	36	97	59	0
2009/0540	19	91	16	2
Z1021075756	0	40	22	-
Z126203636	14	46	3	-
2009/0770	14	55	0	-

Percentage of bacterial growth inhibition activity at 6 h for molecules tested at 200 μ M, on Gram-negative *E. coli* DH10 in presence or in absence of Polymyxin (PMBN) and on Gram-positive *B. subtilis* (WB800N). Best hits of *in vitro* transcription were also tested on the eukaryotic cells of yeast *S. cerevisiae*.

The inhibitory activity for all molecule assayed on *E. coli* increased considerably in the presence of PMBN, since all tested compounds exhibited a greater inhibition when this compound was present. Molecules L556-0204, L556-0137, L557-0204 and 2009/0540 were confirmed as most active compounds: L556-0204 was able to inhibit growth of both bacterial strains, L556-0137 displayed superior inhibitory activity against Gram-positive *B. subtilis* over Gram-negative *E. coli*, while L557-0204 and 2009/0540 were more active against *E. coli*. These molecules did not show any inhibitory activity against *S. cerevisiae*. The other four compounds, UCM 454, Z1021075756, Z126203636 and 2009/0770, revealed a mild inhibition only on *E. coli* (Table X).

The antibacterial activity of the most active molecules was monitored at different concentrations for 7.5 h, on both bacterial strains.

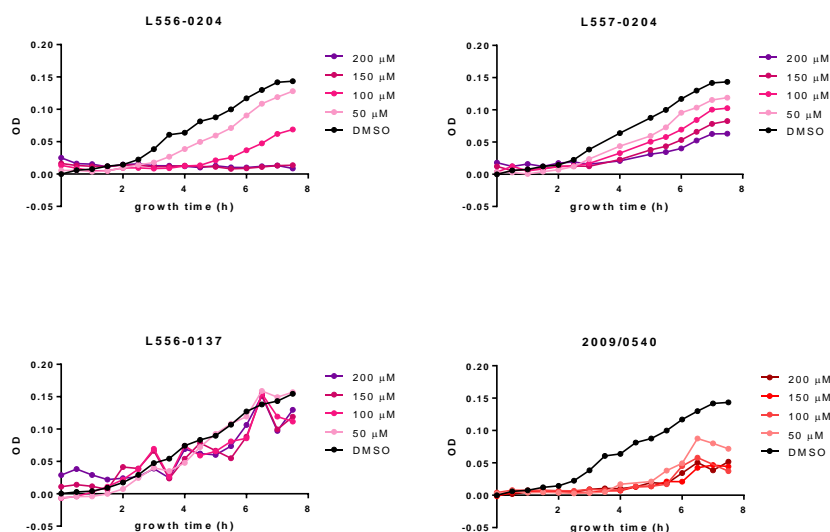


Figure 21. *E. coli* growth inhibition in the presence of hit molecules and 1 µg/ml Polymyxin B.

The most active compound against *E. coli* was L556-0204, which completely inhibited growth over the eight hours assayed at 200 µM and 150 µM, and still retaining high inhibitory activity at 100 µM. 2009/0540 exhibited a high inhibition activity down to 50 µM during the first six hours, and L557-0204 inhibition activity followed a dose-dependent behaviour. L556-0137 did not show a significant inhibitory activity (Fig.21).

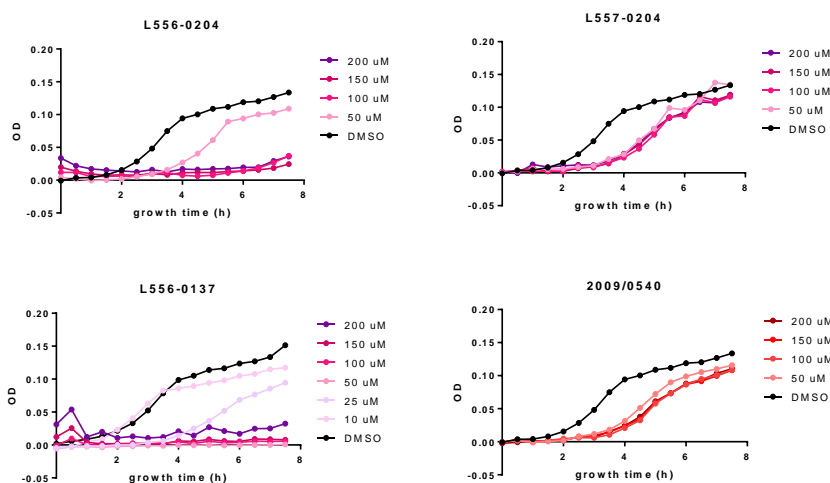


Figure 22. *B. subtilis* growth inhibition in the presence of hit molecules.

The most active compound against *B. subtilis* was L556-0137, which completely inhibited growth at all concentrations tested; L556-0204 displayed a similar trend, decreasing its efficacy at 50 μM . L557-0204 and 2009/0540 did not show a significant inhibitory activity after 6 h (Fig. 22).

To compare the antimicrobial activity of hit molecules with the reference compounds GKL003 and Rifampicin, we measured the bacterial growth for 7.5 h in the presence of compounds at 100 μM . In accordance with literature data, Rifampicin completely blocks bacterial growth at this concentration, while GKL003 had no inhibitory activity, both on *B. subtilis* and *E. coli* (Fig.23), confirming the best potency of the newly identified molecules on bacterial growth.

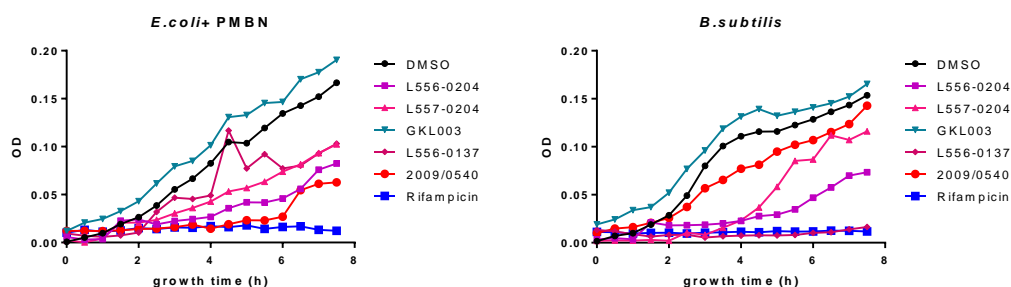


Figure 23. *E. coli* and *B. subtilis* growth inhibition in the presence of hit molecules and reference compound GKL003 and Rifampicin, at 100 μM .

3.2.5 MOLECULAR MODELLING

The pharmacophore ligand-based model was built based on indole-containing compounds with inhibitory activity detected in ELISA assay and belonging to different scaffolds. In particular, compounds from four different scaffolds of the Australia Compound Library (L556-0122, Z1021075756, M530-2099 and C208-0595), from the indole mini-library (UCM 454 and UCM 483), and GKL003 were chosen for this purpose. For each compound the conformation allowing the spatial superposition of the same chemical features (e.g., hydrogen bond donors, hydrogen bond acceptors, positively charged groups, negatively charged groups, hydrophobic regions) was selected. This provided a three-dimensional picture of the nature and relative arrangement of the chemical features relevant for the interaction with the target protein. It was possible to hypothesize a pharmacophore ligand-based model on the target β' for the chemical class of indoles. The identification of four principal

regions (hydrophobic, hydrogen bond acceptors, hydrogen bond donors and rings) have allowed a representation of possible ligand-target association (Fig.24).

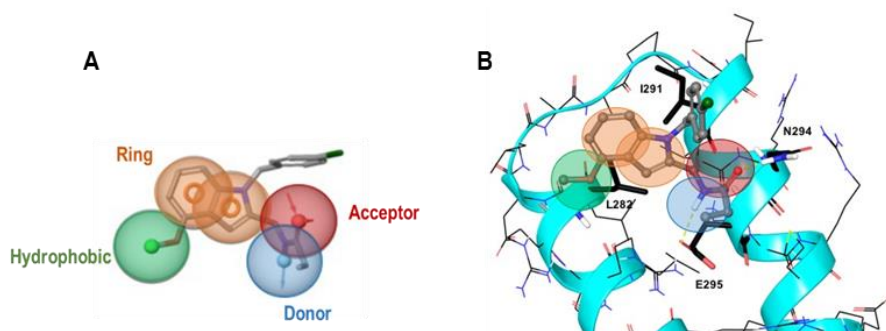


Figure 24. A) Four chemical features of hit compounds are highlighted with different colours, graphed on UCM 454 molecule; B) Representative UCM 454 compound fitted to the pharmacophore model, focusing on residues involved in the interaction with principal chemical features of molecule.

3.2.6 DISCUSSION

In this study, we describe the setting-up of a high-throughput platform that combines sequential *in vivo* and *in vitro* assays as a novel antibiotic discovery pipeline, applied to the search of small molecules able to prevent the assembly of the transcription complex holoenzyme, by targeting *E. coli* β' - σ^{70} interaction.

We successfully reproduced the interaction in an *in vivo* yBRET assay and in an *in vitro* ELISA assay, validating this pipeline with the screening of an in-house mini library of indole derivates, since the efficacy of molecules containing indole groups as inhibitors of β' - σ^{70} interaction has been previously demonstrated^{36,44}. Moreover, two different yBRET strains were optimized, for the identification of molecules preferentially targeting σ^{70} (σ^{70} -target strain) or β' (β' -target strain). The screening of specific sets of *in silico* selected compounds was conducted on both strains, while only β' -target strain was used to screen other small-molecule libraries of different origins. The yBRET-ELISA pipeline led to the identification of sixteen compounds able to inhibit the interaction both *in vivo* and *in vitro*. Among these, it was possible to identify different chemical classes that shared structural elements with known inhibitors, while others were completely new. Some molecules, e.g. L557-0318 and L557-0335, share the same scaffold structure, despite being identified in two different screenings in which β' and σ^{70} , respectively, were constitutively expressed. This poses the question as to whether they bind different

proteins or not. This result highlights the issue of the relationship between the constitutive expression of one protein and the preferential binding of test compounds to this protein instead of the inducible one. Even though ELISA assays suggest that L557-0318 and other indole-containing molecules preferentially target β' , further tests are needed to clarify the binding partner of these compounds (e.g., Surface Plasmon Resonance).

Most of the chemical classes were further validated by testing structural analogues for their ability to disrupt $\beta' - \sigma^{70}$ interaction, and some of these molecules proved to be able to interfere with the RNA polymerase holoenzyme assembly, with potency comparable to the most characterized $\beta' - \sigma^{70}$ interaction inhibitor GKL003. The IC_{50} of L556 series was approximately double that of the GKL003 (13.49 μ M), which showed a higher value in comparison with literature data ($K_i \sim 6$ nM)³⁶. This was probably due to a different RNAP core enzyme: σ^{70} ratio in our assay (1:10) respect to the one used by Ma et al. (1:0.5)³⁶. When tested on bacteria our newly identified molecules performed much better than GKL003 that has been reported to lose efficacy below 2 mM. Most of our newly identified molecules displayed growth inhibition at 200 μ M, with some still retaining activity at 50 μ M, concentration which corresponds to about 30-40 μ g/mL for these molecules.

We suggest that the use of an *in vivo* system from the beginning of the screening procedure may have led to the identification of molecules characterized by a more powerful antimicrobial activity, respect to the use of solely *in vitro* assays. Indeed, hits are characterized by the lack of acid or basic groups, significantly ionized at physiological pH, and this might be related to the peculiar characteristic of the yBRET assay. In fact the two interacting proteins β' and σ^{70} are expressed inside the yeast cell and highly ionized compounds might be penalized for their limited ability to cross yeast cellular wall and membrane.

In the close future, these new antimicrobics will be tested on different bacterial strains, including the “ESKAPE” bacterial pathogens (*Enterococcus faecium*, *Staphylococcus aureus*, *Klebsiella pneumoniae*, *Acinetobacter baumannii*, *Pseudomonas aeruginosa*, and *Enterobacter species*) and other bacteria that are resistant to presently available antibiotics.

Finally, exploiting the pharmacophore-ligand based model based on hit compounds, new potential inhibitors will be selected or synthesized, expanding the number of compounds to screen on this interaction.

3.3 MATERIALS AND METHODS

Strains and vectors

Strains

E. coli DH10B™ T1R strain (F- mcrA Δ(mrr-hsdRMS-mcrBC) φ80lacZΔM15 ΔlacX74 recA1 endA1 araD139 Δ(ara,leu)7697 galU galK - rpsL nupG tonA) (Invitrogen); exploited for vector construction and bacterial growth inhibition assay.

E. coli BL21+(DE3)™ strain (F-, ompT, hsdSB (rB-, mB-), dcm, gal, λ(DE3), pLysS, Cmr); exploited for protein overexpression (Agilent Technologies).

B. subtilis WB800N strain (nprE aprE epr bpr mpr::ble nprB::bsr Δvpr wprA::hyg cm::neo; NeoR); exploited for bacterial growth inhibition assay.

S. cerevisiae erg6 yeast strain (BY4742 background: MATa; his3Δ1; leu2Δ 0; met15Δ 0; ura3Δ 0; YML008c::kanMX4) was obtained from Open Biosystems (Huntsville, AL, USA) and employed in the yBRET system.

S. cerevisiae W303-1A strain (leu2-3,112 trp1-1 can1-100 ura3-1 ade2-1 his3-11, 15) was used for growth inhibition assay.

Vectors

All sequences used in this study were amplified with PCR and inserted in frame with the donor or the acceptor using *CpoI* restriction enzyme digestion and DNA ligation, using vectors shown in chapter 2 (paragraph 2.2.1). The centromeric vectors p415 (*LEU2*, *GAL1* inducible promoter) and p416 (*URA3*, *GPD* constitutive promoter) were used to express the chimeric proteins⁴⁶. *TRP1* selectable marker gene cannot be employed with *erg6* mutant strain, because *trp1-erg6* double mutant is synthetic lethal. Donor proteins were cloned into p415, and acceptor proteins were cloned into p416. Both C- or N-terminal fusion vectors are available upon request. Vector p190 (*LEU2*, *TEF* constitutive promoter) and p215 (*URA*, *GAL1*) were used to express chimeric proteins in the donor saturation assay.

pGEX and pET 28b (+) were used for the expression of gene in *E. coli* as fusion with *Schistosoma japonicum* GST at the carboxyl terminus and N-terminal His Tag®/thrombin/T7•Tag® configuration plus an optional C-terminal His Tag sequence, respectively.

BRET calculation and screening analysis protocol

The BRET ratio was calculated by dividing the signal measured at 530 nm by the signal measured at 480 nm. Then, the BRET signal was calculated as the BRET ratio subtracted by the BRET background ratio (obtained when the donor protein was expressed alone) and multiplied by 1000 to express results in milliBRET (mBRET): $\text{BRET} = (\text{BRET ratio} - \text{Background BRET ratio}) \times 1000^{45}$.

The rationale of the assortment takes into account three factors: (i) an interaction inhibition of at least 15% on average, compared to the non-treated plate specific controls; (ii) a percentage of mBRET median lower than 85% compared to the median calculated on the non-treated plate specific controls; (iii) an SSMD statistics considered at least as “weak inhibition” (SSMD represent the ratio of mean to the standard deviation of difference between a test compound and a negative reference group with no specific inhibition/activation effects).

Small molecule libraries

GKL003 was purchased from Glxxx Laboratories (Southborough, MA (USA)), C5 from Maybridge Chemical Co. Ltd (Altrincham, United Kingdom), while A13 and SB2 were purchased from Interchim (Montluçon, France). Mini-library of indole derivates was supplied within a collaboration with University of Urbino "Carlo Bo", Prof. Gilberto Spadoni, Dipartimento di Scienze Biomolecolari. Four libraries are available in our laboratory: Australia Compound Library, *Institut de Chimie des Substances Naturelles* (ICSN), *Institut de Chimie et Biochimie Moléculaire et Supramoléculaire* (ICBMS) and National Cancer Institute (NCI), which contained compounds of synthetic and natural origin. We screened the other four libraries at the Kinase Inhibitor Specialized Screening facility (KISSf, Station Biologique de Roscoff, France) of Stéphane Bach. Enzo chemical collection is characterized by extracts from terrestrial plants, Prestwick chemical collection by FDA approved compounds, essential chemical compound of Roscoff (ReC3 library) and Marine chemical compound collection (MarC3) include bioinspired molecules from marine organisms.

Expression and purification of His-tag- σ^{70} and GST- β'

The full length of σ^{70} was cloned in pET 28b vector that joins the N-terminal extremity of the protein to a 6xHistidines TAG, and expressed in BL21 codon plus *E. coli* strain. The best expression condition, in which the protein was most expressed and mainly soluble has been evaluated as the 3 h induction at 30 °C in LB medium, adding 1mM isopropyl- β -D-thiogalactopyranoside (IPTG). The protein was

then extracted from cells and purified through His-Tag selective, Cobalt resin, low-pressure affinity chromatography. The combined eluted fractions were stored in 50 mM NaH₂PO₄, 150 mM NaCl and glycerol 20%, pH 8 at 680 ng/μL.

The β' 1-334 aa sequence was cloned in a pGEX vector that joins the N-terminal extremity of the protein to the GST protein, and expressed in BL21 codon plus *E. coli* strain. The best expression condition, in which the protein was most expressed and mainly soluble, has been evaluated as the 24 h induction at 20 °C in Auto Induction Medium. The protein was then extracted from cells via sonication but no one of the assayed purification methods worked, since the protein binds the Glutathione resin so tightly that each tested condition for the elution was unable to detach the protein. Therefore, β' lysis supernatant was used for the subsequent experiments.

ELISA assay

His-tag- σ⁷⁰ and GST- β' proteins were recombinantly expressed in BL21 codon plus *E. coli* strain. σ⁷⁰ was diluted to 250 nM in phosphate buffered saline (PBS), and 100 μl of the solution were added into NUNC Maxisorp microtiter plate wells. Following o/n incubation at 4 °C wells were washed three times with 300 μl of PBS and blocked with 400 μl of 1% (w/v) BSA in PBS at RT for 2 h. Plates were then washed three times with wash buffer (PBS, 0.05% (v/v) Tween-20). 100 μl of 250 nM GST- β' diluted in PBS was incubated with 2.5 μl of the compounds at different concentrations (or DMSO as control) for 10 minutes at 37 °C, and added to the wells followed by incubation at RT for 1 h. Wells were washed three times with 300 μl of wash buffer, 100 μL of rabbit anti-GST primary antibody (1:2000 in PBS) were added, and the plate was incubated at RT for 1 h. After washing, HRP-conjugated goat anti-rabbit secondary antibody (1:20000 in PBS) was added to each well and incubated at RT for 1 h. Interactions were detected by the addition of 100 μl of ABTS substrate to each well. The signal was measured, after 30 minutes of incubation at 30°C, reading absorbance at 415 nm using a microplate reader (TriStar² LB 942, Berthold Technologies). The inhibitory activity of each compound was then calculated as IC₅₀ value.

In vitro transcription assay

The ability of compounds to impair the RNA polymerase activity was verified in an *in vitro* transcription assay, using the RNAP core enzyme (New England BioLabs, cat. M0550S) and recombinant σ⁷⁰ of *E.*

coli. Molecules were analysed at 25 μ M and 50 μ M in a non-competitive inhibition assay, prior to RNAP core - σ^{70} interaction. Molecules were first incubated with 87.5 nM RNAP core at RT for 10 minutes, followed by the addition of 875 nM σ^{70} . The mixture was incubated at RT for 10 minutes. The template DNA (pDSP circular DNA⁴⁷) was added and the mixture is incubated at 37 °C for 15 minutes. The reaction starts with the addition of a mix of radiolabelled and unlabelled NTPs. The results were analysed on denaturing polyacrylamide gel (6 % polyacrylamide, 7 M urea), and images were captured using a phosphor-imaging system (Packard Cyclone Storage Phosphor Screen).

Antimicrobial activity

Antimicrobial activity of hit compounds was evaluated monitoring bacterial growth in the presence of different molecule concentrations. Bacteria were grown at exponential phase prior to growth inhibition test and then diluted to $OD_{600\text{ nm}} = 0.006$. W303-1A yeast strain was grown in YPD (Yeast peptone Dextrose) at 30 °C until $OD_{600\text{ nm}} = 0.5$ before growth inhibition assay. Bacterial (or yeast) growth was monitored for 7,5 h in the presence of molecules dissolved in DMSO, or of an equivalent quantity of DMSO as negative control (5% DMSO final concentration). The assay was conducted in triplicate in a 96-well plate by monitoring the cells growth every 30 minutes, reading the absorbance with a microplate reader (TriStar² LB 942, Berthold Technologies). Polymyxin B Nonapeptide used on Gram-negative bacteria was purchased from Sigma-Aldrich (Saint Louis, USA).

Statistical analysis

To calculate IC_{50} for inhibitory activity in ELISA and in *in vitro* transcription, experiments were conducted in triplicate, using at least ten different compound concentrations. Data were analysed in Prism (GraphPad Software Inc.) using nonlinear regression curve fitting.

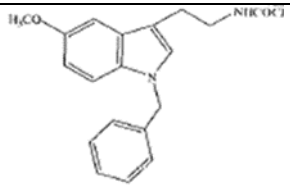
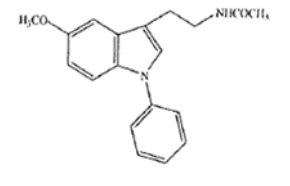
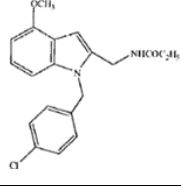
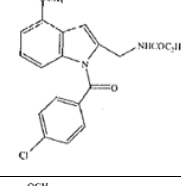
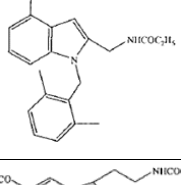
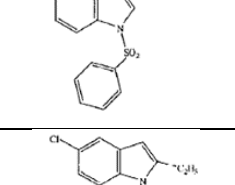
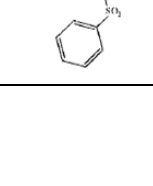
Student t test was used to find significant differences when comparing compound inhibitory activities.

Table XI. List of primers used in this study.

Primer name (restriction enzyme)	Sequence (5'....3')
σ^{70} Fw (<i>Cpol</i>)	TAAATATAAAT <u>CGGTCCG</u> ATGGAGCAAACCCGCAGTC
σ^{70} Re (stop codon) (<i>Cpol</i>)	AATTATTTTACGGACCGTTAATCGTCCAGGAAGCTACGC
σ^{70} Re (<i>Cpol</i>)	AATTATTTTACGGACCGATATCGTCCAGGAAGCTACGC
σ^{70} Q406K-E407A Fw	TGACCTGATTAAAGCTGGCAACATCGGTCTGATG
σ^{70} Q406K-E407A Re	CATCAGACCGATGTTGCCAGCTTTAATCAGGTCA
β' (1-334)Fw (<i>Cpol</i>)	TAAATATAAAT <u>CGGTCCG</u> ATGAAAGATTATTAAAGTTTCTGAAAGCG
β' (1-334)Re (<i>Cpol</i>)	AATTATTTTACGGACCGATTTTACCTTTGATCATGTCGGCC
β' (1-334)Re (stop codon) (<i>Cpol</i>)	AATTATTTTACGGACCGTCATTTACCTTTGATCATGTCGGCC
β' (220-334) Fw (<i>Cpol</i>)	TAAATATAAAT <u>CGGTCCG</u> ATGCGTATCAAACCTGCTGGAAGCG
β' R275A-R278A (220-334) Fw	AACGCTCTGAAACGTCTGCTGGATC
β' R275A-R278A (220-334) Re	GTTAGCGTTAATGACGCGACGATAC

3.4 SUPPLEMENTARY

Table 1. Structures of in-house mini library of 27 indole derivatives (collaboration with University of Urbino "Carlo Bo").

ID compound	Structure	Vendors
UCM 80		Mini-library Urbino
UCM 82		Mini-library Urbino
UCM 454		Mini-library Urbino
UCM 642		Mini-library Urbino
UCM 643		Mini-library Urbino
UCM 666		Mini-library Urbino
UCM 1314		Mini-library Urbino

UCM 1315		Mini-library Urbino
UCM 1316		Mini-library Urbino
UCM 1317		Mini-library Urbino
UCM 334		Mini-library Urbino
UCM 337		Mini-library Urbino
UCM 483		Mini-library Urbino
UCM 484		Mini-library Urbino
UCM 485		Mini-library Urbino
UCM 486		Mini-library Urbino
UCM 722		Mini-library Urbino
UCM 1343		Mini-library Urbino

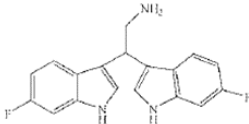
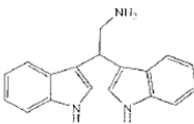
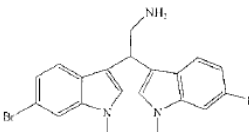
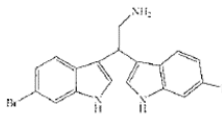
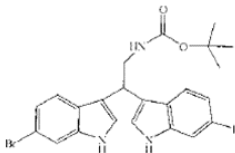
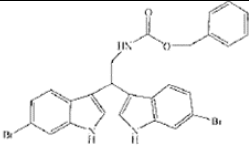
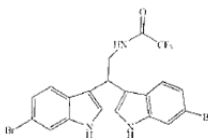
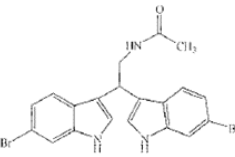
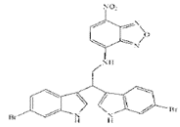
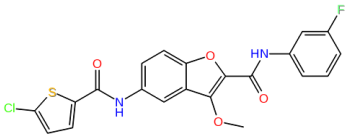
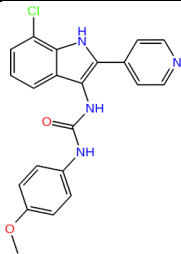
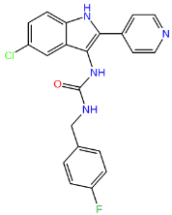
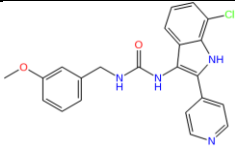
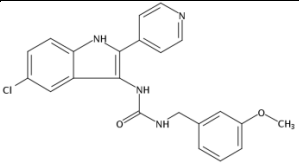
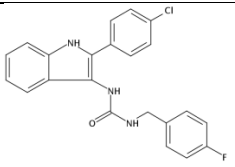
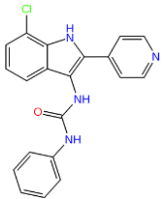
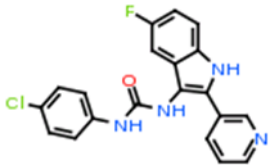
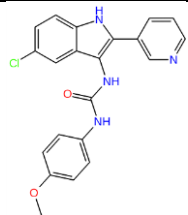
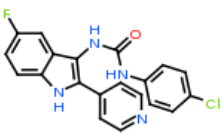
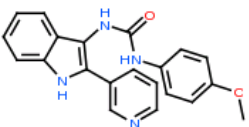
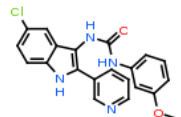
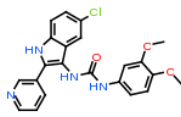
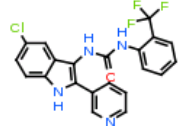
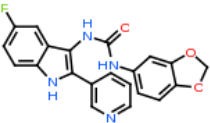
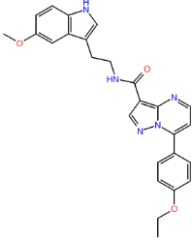
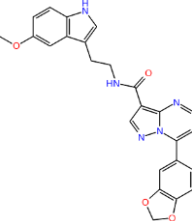
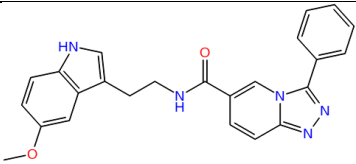
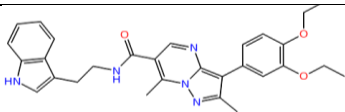
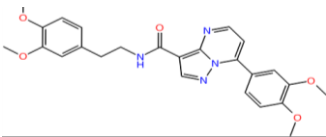
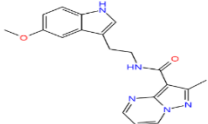
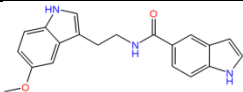
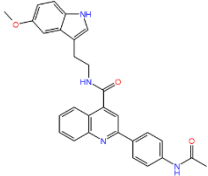
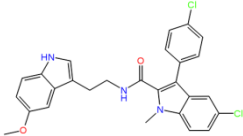
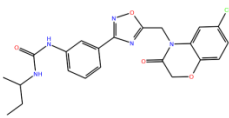
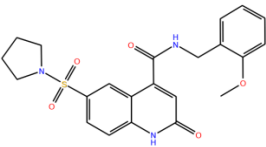
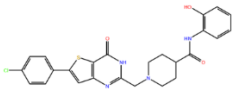
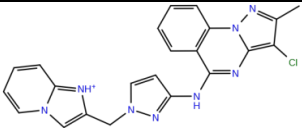
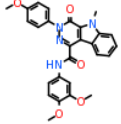
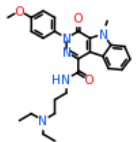
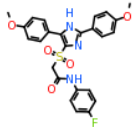
UCM 1338		Mini-library Urbino
UCM 1234		Mini-library Urbino
UCM 1339		Mini-library Urbino
UCM 1204		Mini-library Urbino
UCM 1345		Mini-library Urbino
UCM 1343		Mini-library Urbino
UCM 1273		Mini-library Urbino
UCM 1344		Mini-library Urbino
UCM 1340		Mini-library Urbino

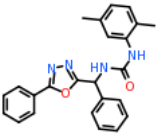
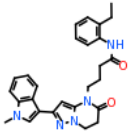
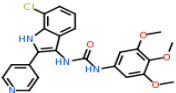
Table 2. Structure of hit compounds from Australia Compound Library and structural analogues.

ID compound	Structure	Vendors
M530-2099		ChemDiv
L557-0318		ChemDiv
L557-0168		ChemDiv
L557-0360		ChemDiv
L557-0164		ChemDiv
L491-0070		ChemDiv

L557-0300		ChemDiv
L556-0204		ChemDiv
L556-0122		ChemDiv
L557-0204		ChemDiv
L556-0024		ChemDiv
L556-0100		ChemDiv
L556-0114		ChemDiv
L556-0137		ChemDiv

L556-0264		ChemDiv
L390-1378		ChemDiv
L390-2620		ChemDiv
F812-0882		ChemDiv
G210-0090		ChemDiv
V013-2659		ChemDiv
Z1191880202		Enamine
Z1191882607		Enamine

L036-0366		ChemDiv
8019-9090		ChemDiv
F538-0554		ChemDiv
C208-0595		ChemDiv
Z126203636		Enamine
Z1021075756		Enamine
C448-0959		ChemDiv
C448-1002		ChemDiv
C654-0156		ChemDiv

G418-0274		ChemDiv
G581-0350		ChemDiv
557-0335		ChemDiv

Hit molecules against β' -target strain (highlighted in bold) are followed by their structural analogues; the six molecules identified to targeted σ^{70} are in grey.

Table 3. Structure of the hit compound from ReC3 library (highlighted in bold) and structural analogues.

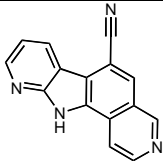
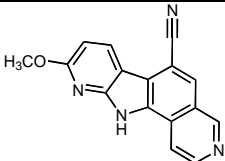
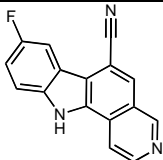
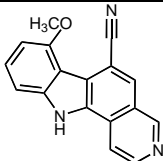
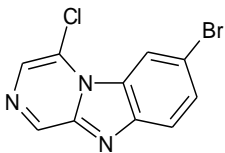
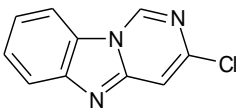
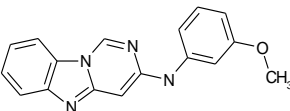
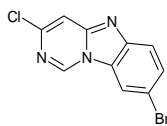
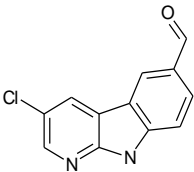
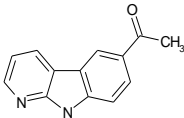
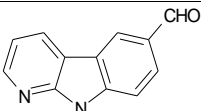
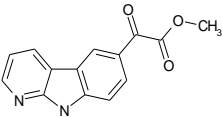
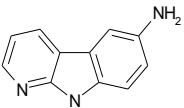
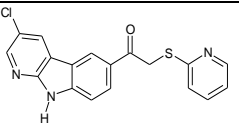
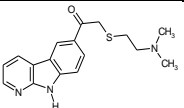
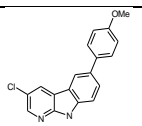
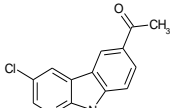
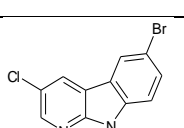
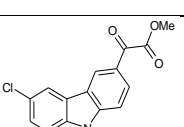
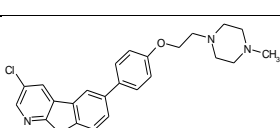
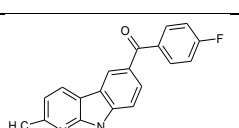
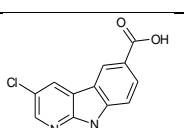
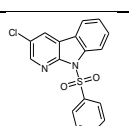
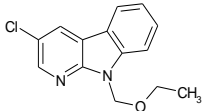
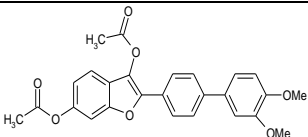
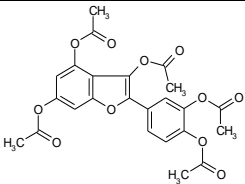
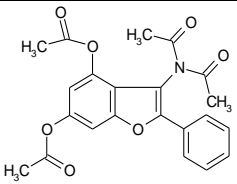
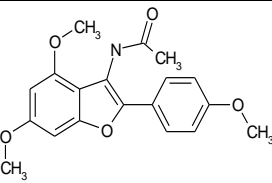
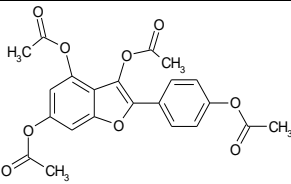
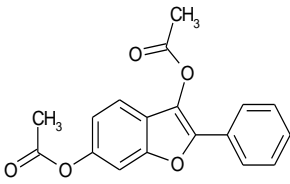
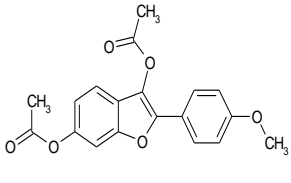
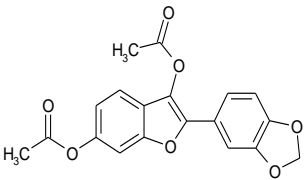
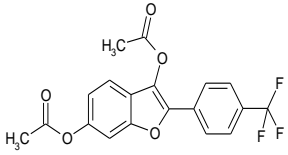
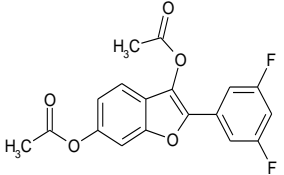
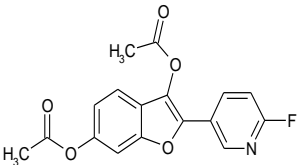
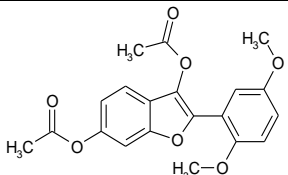
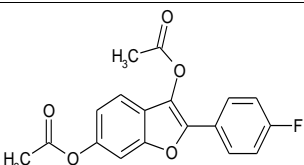
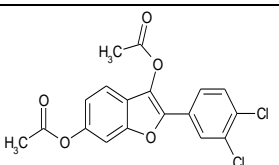
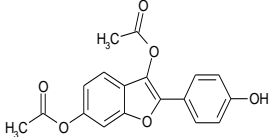
ID compound	Structure	Vendors
2009/0540		CNRS-ICNS
2009/0746		CNRS-ICNS
2009/0770		CNRS-ICNS
2009/0771		CNRS-ICNS

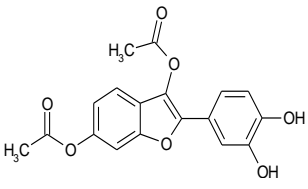
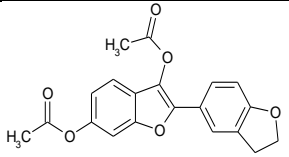
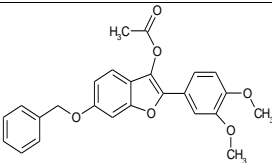
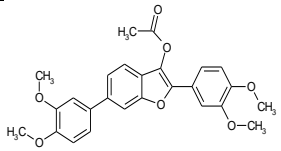
Table 4. Structure of hit compounds from ICBMS library and structural analogues.

ID compound	Structure	Vendors
ICMBS-PKRC 17-H04		ICBMS
ICMBS-PKRC- 17-B08		ICBMS
ICMBS-PKRC- 17-B11		ICBMS
ICMBS-PKRC- 17-F11		ICBMS
ICMBS-PKRC 15-B02		ICBMS
ICMBS-PKRC- 08-G10-09		ICBMS
ICMBS-PKRC- 08-H07-09		ICBMS
ICMBS-PKRC- 08-H11-09		ICBMS

ICMBS-PKRC-08-H09-09		ICBMS
ICMBS-PKRC-12-E09-09		ICBMS
ICMBS-PKRC-12-F02-09		ICBMS
ICMBS-PKRC-12-G10-09		ICBMS
ICMBS-PKRC-15-A02-09		ICBMS
ICMBS-PKRC-15-A03-09		ICBMS
ICMBS-PKRC-15-A06-09		ICBMS
ICMBS-PKRC-14-G07		ICBMS
ICMBS-PKRC-14-H10		ICBMS
ICMBS-PKRC-15-H02		ICBMS
ICMBS-PKRC-15-H09		ICBMS

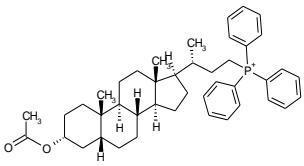
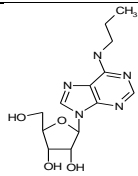
ICMBS-PKRC-17-A06		ICBMS
37-A03		ICBMS
U181-10-10-L-H03		ICBMS
U181-10-10-L-H08		ICBMS
U181-10-13-L-C04		ICBMS
U181-10-13-L-C06		ICBMS
U181-10-20-L-A02		ICBMS
U181-10-20-L-A11		ICBMS

U522-12-36-L-F11		ICBMS
U524-12-36-L-G05		ICBMS
U524-12-36-L-G06		ICBMS
U524-12-36-L-G08		ICBMS
U524-12-36-L-G09		ICBMS
U524-12-36-L-G11		ICBMS
U524-12-36-L-H05		ICBMS
U524-12-36-L-H06		ICBMS

U524-12-36-L-H07		ICBMS
U524-12-36-L-H11		ICBMS
U522-12-37-L-A02		ICBMS
U524-12-37-L-A05		ICBMS

Hit molecules (highlighted in bold) are followed by their structural analogous

Table 5. Structure of hit compounds from ICNS library.

ID compound	Structure	Vendors
ICSN22-24-L-A11		CNRS-ICNS
ICSN63-27-L-D03		CNRS-ICNS

ABBREVIATIONS

BRET Bioluminescence Resonance Energy Transfer

CH region coiled-coil region

DMSO Dimethyl sulfoxide

ELISA Enzyme-linked immunosorbent assay

GST Glutathione-S-Transferase

HT High Throughput

HTS High Throughput Screening

IPTG isopropyl- β -D-thiogalactopyranoside

mBRET milliBRET

MIC Minimal Inhibitory Concentration

MW Molecular Weigh

NLuc Nanoluc Luciferase

NTP Nulceoside Triphosphate

PBS Phosphate-buffered saline

PMBN Polymyxin B Nonapeptide

PPI Protein-Protein Interaction

RNAP RNA polymerase

SAR Structural Activity Relationship

yBRET yeast BRET

YFP Yellow Fluorescent Protein

REFERENCES

1. Ventola CL. The antibiotic resistance crisis: part 1: causes and threats. *PT*. 2015;40(4):277-283.
2. Allen HK, Donato J, Wang HH, Cloud-Hansen KA, Davies J, Handelsman J. Call of the wild: antibiotic resistance genes in natural environments. *Nat Rev Microbiol*. 2010;8(4):251-259.
3. O'Neill J. The Review on Antimicrobial Resistance. 2014.
4. Aminov R. History of antimicrobial drug discovery: Major classes and health impact. *Biochem Pharmacol*. 2017;133:4-19.
5. Kohanski MA, Dwyer DJ, Collins JJ. How antibiotics kill bacteria: from targets to networks. *Nat Rev Microbiol*. 2010;8(6):423-435.
6. Orhan DD, Özçelik B, Özgen S, Ergun F. Antibacterial, antifungal, and antiviral activities of some flavonoids. *Microbiol Res*. 2010;165(6):496-504.
7. Cushnie TP, Lamb AJ. Antimicrobial activity of flavonoids. *Int J Antimicrob Agents*. 2005;26(5):343-356.
8. Lewis K. Platforms for antibiotic discovery. *Nat Rev Drug Discov*. 2013;12(5):371-387.
9. Munita JM, Arias CA. Mechanisms of Antibiotic Resistance. *Mech Antibiot Resist*. 2016;4(2):1-37.
10. Floss HG, Yu TW. Rifamycin - Mode of action, resistance, and biosynthesis. *Chem Rev*. 2005;105(2):621-632.
11. Poehlsgaard J, Douthwaite S. Macrolide antibiotic interaction and resistance on the bacterial ribosome. *Curr Opin Investig Drugs*. 2003;4:140-148.
12. Brauner A, Fridman O, Gefen O, Balaban NQ. Distinguishing between resistance, tolerance and persistence to antibiotic treatment. *Nat Rev Microbiol*. 2016;14(5):320-330.
13. Lane WJ, Darst SA. Molecular Evolution of Multisubunit RNA Polymerases: Sequence Analysis. *J Mol Biol*. 2010;395(4):671-685.
14. Werner F, Grohmann D. Evolution of multisubunit RNA polymerases in the three domains of life. *Nat Rev Microbiol*. 2011;9(2):85-98.
15. Nudler E. RNA Polymerase Active Center: The Molecular Engine of Transcription. *Annu Rev Biochem*. 2009;78(1):335-361.
16. Vassylyev DG, Sekine S, Laptenko O, et al. Crystal structure of a bacterial RNA polymerase holoenzyme at 2.6 Å resolution. *Nature*. 2002;417(6890):712-719.
17. Murakami KS. Structural biology of bacterial RNA polymerase. *Biomolecules*. 2015;5(2):848-864.

18. Zhang G, Campbell EA, Minakhin L, Richter C, Severinov K, Darst SA. Crystal Structure of *Thermus aquaticus* Core RNA Polymerase at 3.3 Å Resolution. *Cell*. 1999;98:811-824.
19. Landick R. NTP-entry routes in multi-subunit RNA polymerases. *Trends Biochem Sci*. 2005;30:651-654.
20. Murakami KS. X-ray crystal structure of *Escherichia coli* RNA polymerase sigma70 holoenzyme. *J Biol Chem*. 2013;288(13):9126-9134.
21. Rhodius VA, Busby SJ. Interactions between activating region 3 of the *Escherichia coli* cyclic AMP receptor protein and region 4 of the RNA polymerase sigma(70) subunit: application of suppression genetics. *J Mol Biol*. 2000;299(2):311-324.
22. Blanco AG, Canals A, Bernués J, Solà M, Coll M. The structure of a transcription activation subcomplex reveals how σ 70 is recruited to PhoB promoters. *EMBO J*. 2011;30(18):3776-3785.
23. Bae B, Feklistov A, Lass-Napiorkowska A, Landick R, Darst SA. Structure of a bacterial RNA polymerase holoenzyme open promoter complex. *Elife*. 2015;4(September 2015):1-23.
24. Feng Y, Zhang Y, Ebright RH. Structural basis of transcription activation. *Science (80-)*. 2016;352(6291):1330-1333.
25. Vvedenskaya IO, Vahedian-Movahed H, Zhang Y, Taylor DM, Ebright RH, Nickels BE. Interactions between RNA polymerase and the core recognition element are a determinant of transcription start site selection. *Proc Natl Acad Sci*. 2016;113(21):2899-2905.
26. Finn RD, Orlova E V, Gowen B, Buck M, van Heel M. *Escherichia coli* RNA polymerase core and holoenzyme structures. *Embo J*. 2000;19(24):6833-6844.
27. Ruth MS, Record Jr. MT, DeHaseth PL. Mechanism of Bacterial Transcription Initiation: RNA Polymerase - Promoter Binding, Isomerization to Initiation-Competent Open Complexes, and Initiation of RNA Synthesis. *J Mol Biol*. 2011;412(5):754-771.
28. Perez JC, Groisman EA. Review Evolution of Transcriptional Regulatory Circuits in Bacteria. 2009;138(2):233-244.
29. Chopra I. Bacterial RNA polymerase: a promising target for the discovery of new antimicrobial agents. *Curr Opin Investig Drugs*. 2007;8:600-607.
30. Murakami KS, Darst SA. Bacterial RNA polymerases: The whole story. *Curr Opin Struct Biol*. 2003;13(1):31-39.
31. Campbell E, Korzheva N, Mustaev A, et al. Structural mechanism for rifampicin inhibition of bacterial rna polymerase. *Cell*. 2001;104:901-912.
32. Scott LJ. Fidaxomicin: A review of its use in patients with *Clostridium difficile* infection. *Drugs*. 2013;73(15):1733-1747.

33. Mukhopadhyay J, Das K, Ismail S, et al. The RNA Polymerase "Switch Region" Is a Target for Inhibitors. *Cell*. 2008;135(2):295-307.
34. Belogurov GA, Vassilyeva MN, Sevostyanova A, et al. Transcription inactivation through local refolding of the RNA polymerase structure. *Nature*. 2009;457(3):332-335.
35. Seshasayee AS, Sivaraman K LN. An overview of prokaryotic transcription factors : a summary of function and occurrence in bacterial genomes. *Subcell Biochem*. 4515;52:7-23.
36. Ma C, Yang X, Kandemir H, et al. Inhibitors of bacterial transcription initiation complex formation. *ACS Chem Biol*. 2013;8(9):1972-1980.
37. Johnston EB, Lewis PJ, Griffith R. The interaction of *Bacillus subtilis* sigmaA with RNA polymerase. *Protein Sci*. 2009;18(11):2287-2297.
38. André E, Bastide L, Michaux-Charachon S, et al. Novel synthetic molecules targeting the bacterial RNA polymerase assembly. *J Antimicrob Chemother*. 2006;57(2):245-251.
39. Glaser BT, Bergendahl V, Thompson NE, Olson B, Burgess RR. LRET-based HTS of a small-compound library for inhibitors of bacterial RNA polymerase. *Assay Drug Dev Technol*. 2007;5(6):759-768.
40. Hüsecken K, Negri M, Fruth M, Boettcher S, Hartmann RW, Hauptenthal J. Peptide-Based Investigation of the *Escherichia coli* RNA Polymerase σ 70 :Core Interface As Target Site. *ACS Chem Biol*. 2013;8(4):758-766.
41. Mielczarek M, Devakaram R V, Ma C, et al. Synthesis and biological activity of novel bis-indole inhibitors of bacterial transcription initiation complex formation. *Org Biomol Chem*. 2014;12(18):2882-2894.
42. Thach O, Mielczarek M, Ma C, et al. From indole to pyrrole, furan, thiophene and pyridine: Search for novel small molecule inhibitors of bacterial transcription initiation complex formation. *Bioorg Med Chem*. 2016;24(6):1171-1182.
43. Mielczarek M, Thomas R V., Ma C, et al. Synthesis and biological activity of novel mono-indole and mono-benzofuran inhibitors of bacterial transcription initiation complex formation. *Bioorganic Med Chem*. 2015;23:1763-1775.
44. Ma C, Yang X, Lewis PJ. Bacterial Transcription Inhibitor of RNA Polymerase Holoenzyme Formation by Structure-Based Drug Design: From in Silico Screening to Validation. *ACS Infect Dis*. 2015;2(1):39-46.
45. Corbel C, Sartini S, Levati E, et al. Screening for Protein-Protein Interaction Inhibitors Using a Bioluminescence Resonance Energy Transfer (BRET)–Based Assay in Yeast. *SLAS Discov*. 2017;22(6).
46. Mumberg D, Muller R, Funk M. Yeast vectors for the controlled expression of heterologous proteins in different genetic backgrounds. *Gene*. 1995;156:119-122.

47. Rivetti C, Guthold M, Bustamante C. Wrapping of DNA around the E . coli RNA polymerase open promoter complex. *EMBO J.* 1999;18(16):4464-4475.

Chapter 4

Screening of inhibitors targeting human immuno-modulatory interactions

4.1 INTRODUCTION

The immune system is one of the most complex networks of human body, designed to protect the organism from disease-causing factors. Its principal task is to distinguish “self” from “non-self”: this implies to recognise infectious organisms, harmful substances and its own changed cells, for example in neoplastic or autoimmune diseases. The human immune responses against any “non self” could be of two types: innate or adaptive. The innate response provides immediate defence through physical, chemical and microbiological fence, and through recruitment of different cell types, such as neutrophils, monocytes, macrophages, natural killer cells, etc. The adaptive immunity works with an antigen-specific reaction, using T and B lymphocytes, spending long time to develop. This kind of response also relies on immunological memory to ensure a more rapid reaction if the pathogen exposure recurs. The antigen recognition relies on transmembrane glycoproteins on T cell surfaces, known as co-receptors: CD4 recognises antigens presented by Major Histocompatibility Complex (MHC) class II, while CD8 those presented by MHC class I. Crosslinking of T cell receptor (TCR) causes aggregation with the CD3 complex, leading to phosphorylation of tyrosine on cytoplasmic tail and transduction of signals to nucleus, where the genes for T cell proliferation are activated (Fig.1). On T cell surface there are also co-signalling molecules that are not involved in the antigen recognition, but contribute to the signal transduction: co-stimulatory receptors deliver positive signal for the activation of naïve T cells, while co-inhibitory receptors decrease the signalling of T cells (also known as immune checkpoints)¹.

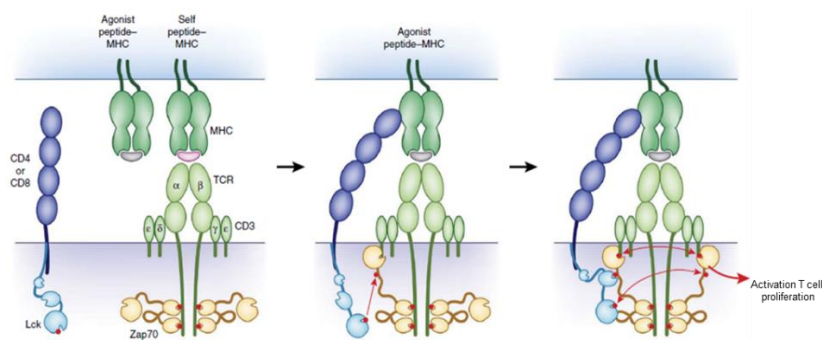


Figure 1. TCR receptor activation through the interaction with CD4 or CD8 co-receptors. In the basal state cytosolic tails are phosphorylated (red dots) and bound to auto-inhibited Zap70. Lck initiates activation by phosphorylating Zap70 and creating a binding site for Lck SH2 domain. Lck promotes further local phosphorylation events. Zap70 trans-autophosphorylation of its activation loop results in its catalytic activation, leading to signalling cascade for T cell proliferation (modified by ²).

Over the past decade, immunotherapy developed as an approach to assist a compromised immune system, resolving different disorders with the use of monoclonal antibody (mAb) and recombinant fusion proteins (RFP) to target cell surface receptors/ligands expressed on immune system cells. These immunomodulatory biologics could modulate TCR and B cell receptors (BCR) to control lymphocyte response. They can be antagonist or agonist, according to the blockage of ligand-receptor interaction or the mimic of ligand³. The first immunomodulatory protein drug (therapeutic protein) on market was the mAb muromonab (Orthoclone OKT3), directed against CD3 complex, approved by FDA in 1986 for the prevention of transplanted rejection^{4,5}.

There are two principal families of co-signalling molecules for the therapeutic intervention: the immunoglobulin (Ig) superfamily and the tumour necrosis factor (TNF) / tumour necrosis factor receptor (TNFR) superfamily.

Ig superfamily molecules

The best characterized families of this group are CD28 and CD2/SLAM. The co-signalling CD28 receptor family contains different members such as CD28, CTLA-4, ICOS, BTLA and PD-1, expressed on T cell surface, that are characterized by a single Ig variable region-like (IgV) motif in the extracellular domain (Fig.2). CD28 and CTLA-4 interact either with B7-1/CD80 or with B7-2/CD86 ligands, which are expressed on antigen presenting cells (APC), through a MYPPPY motif: CD28 is a co-stimulatory molecule that promotes T cell activation, while CTLA-4 is a co-inhibitory receptor that inhibits signal

transduction. Different therapeutic proteins target these receptors to modulate T cell response: for example, in 2011 the FDA approved Ipilimumab, a mAb anti-CTLA-4, used for the treatment of metastatic melanoma⁶⁻⁸. The co-inhibitory receptor PD-1 has been widely investigated as well, together with its ligands B7H1/PD-L1 and B7DC/PD-L2. The cytoplasmic tail of PD-1 contains an immunoreceptor tyrosine-based inhibition motif (ITIM) and an immunoreceptor tyrosine-based switch motif (ITSM), that mediate the phosphorylation events^{9,10}. PD-1 controls the T cell activation and expansion of self-reactive T cells⁶. Different tumour cells highly express PD-1 on their surface, making themselves invisible to immune system; PD-1 is also overexpressed on virus specific CD8+ cells during chronic viral infection, conducting to T cell exhaustion¹¹. Antibodies against PD-1/PD-L1 interaction are promising therapies to reactivate T cell function against cancer, giving encouraging results in clinical trials: Pembrolizumab¹² and Nivolumab¹³ are anti-PD-1 already used in clinical practice, while Atezolizumab¹⁴, Avelumab¹⁵ and Durvalumab¹⁶ are anti-PD-L1 in clinical trials.

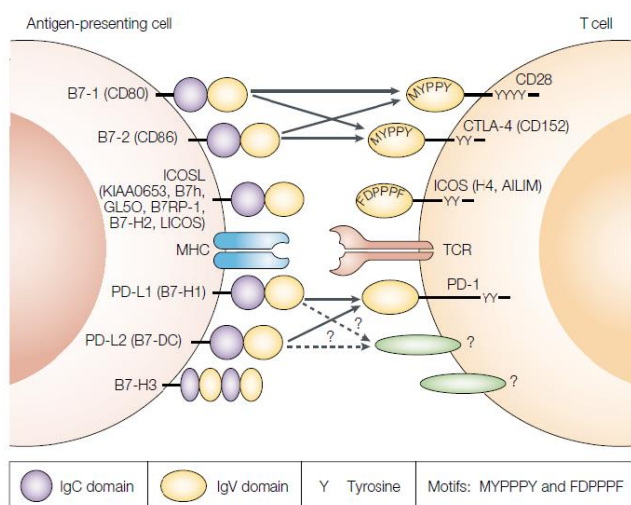


Figure 2. Structures of CD28 superfamily CD28 and CTLA-4 contain a MYPPPY motif essential for B7-1 and B7-2 binding, whereas ICOS has a FDPPPF motif and binds ICOSL. PD-1 is a receptor for both PD-L1 and PD-L2 ligands, which might also bind to other unidentified, receptors on T cells⁶.

The other best characterized Ig superfamily, the CD2 family, includes among its members CD2, CD48, CD58, signalling lymphocytic activation molecule (SLAM), CD244 (2B4) and CD229 (Ly-9) (Fig.3). These receptors are characterized by an IgV and an IgC motif in the extracellular domain, a transmembrane region and a cytoplasmic tail that varies among the CD2 members: in 2B4, SLAM and CD229 it contains tyrosine-rich motifs, in CD2 the tail is rich in proline and basic residues, while CD48

and CD58 have a very short cytoplasmic domain¹⁷. The majority of SLAM proteins and CD229 are self-ligand, whereas CD2 interacts principally with CD58, and 2B4 with CD48¹⁸. CD2-CD58 is a co-stimulatory interaction, promoting lymphocyte activation by enhancing adhesion between T cells and APC cells. The inhibition of this interaction leads to immunosuppression: Alefact is a recombinant human CD58-Ig fusion protein that targets CD2 inhibiting the interaction with its ligand and was used to treat psoriatic arthritis¹⁹. In last years, several peptides were also designed for the treatment of autoimmune disease, such as rheumatoid arthritis²⁰.

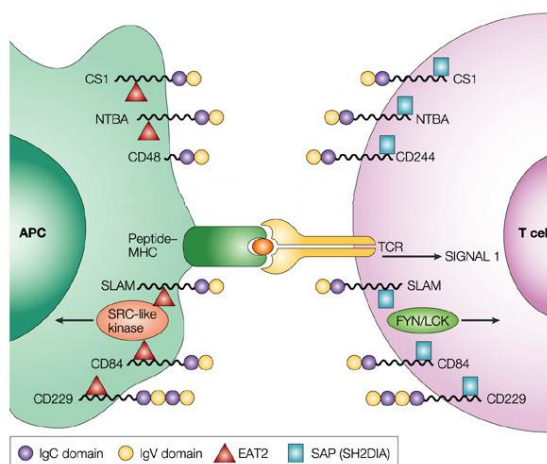


Figure 3. Structures of CD2/SLAM superfamily: receptors are characterized by an IgV and an IgC motif in the extracellular domain; the binding of the SLAM-family immunoglobulin-like receptors to their ligands induces the phosphorylation of their cytoplasmic tails, allowing the subsequent binding of SLAM-associated protein (SAP) and EAT2 through a tyrosine-containing motif located in their cytoplasmic regions. These two molecules can recruit and activate several SRC kinases, including FYN, that will modulate cell activation mediated by signals generated through the T-cell receptor (TCR) (modified by ²¹).

The TNF and TNFR superfamily

Members of this superfamily are essential for homeostasis and regulation of the immune system. TNF ligands count about nineteen members of which the best characterized are BAFF, 4-1BBL, CD30L, CD40L, CD70, CD95L, OX40L, LT α , LT β , RANKL, NGF, TNF α and TRAIL²² (Fig.4). These proteins are expressed on activated macrophages, monocytes, B and T lymphocyte and dendritic cells, and are characterized by an extracellular TNF homology domain (THD) that forms non-covalent homotrimers and by a type II transmembrane domain; alternatively, the extracellular domain of most of these ligands can be proteolytically cleaved by proteases (e.g. ADAM-17), into a soluble form²³. TNF mediate

interactions with thirty receptors of TNFR superfamily, characterized by cysteine-rich extracellular domains, and classified in three groups according to their cytoplasmic domain. The first group includes death domain receptors, such as CD95, TNFR1, DR3 (also called TRAILR1), DR4 (also called TRAILR2), DR5 and DR6, which following their activation recruit intracellular adaptors, such as FAS-associated death domain (FADD) and TNFR-associated death domain (TRADD), inducing cellular apoptosis. The second group is composed by decoy TNFR with DCR1, DCR2, DCR3 and OPG, characterized by the absence of intracellular signalling domains; they compete with other two groups of receptors for their corresponding ligands. The third group contains receptors with TNF receptor associated factors (TRAF) interacting motifs, which triggers recruitments of TRAF proteins to activate different signalling pathways involving NF- κ B, JNK, MAPK and p38 MAPK; this last group includes the majority of TNFR, of which BAFFR, 4-1BB, CD30, CD40, CD27, CD95, OX40 and NFGR are few examples^{3,24,25}. These proteins regulate haematopoiesis, innate immunity, immune surveillance, tumour regression and protection from bacterial and viral infections²⁶. A dysregulation of TNF/TNFR interaction leads to different diseases such as chronic heart failure²⁷, asthma²⁸, septic shock²⁹, Alzheimer's disease³⁰, tumorigenesis³¹, systemic lupus erythematosus³² and many others.

TNF/TNFR signalling pathway can be modulated by blocking the receptor-ligand interaction to reduce the pathogenic immune responses. Several therapeutic biologics has been approved for solid tumour treatment. Many others are currently in clinical trials, as Dacetuzumab a mAb that targets CD40 treating solid tumours or B-cell non-Hodking's lymphoma³³.

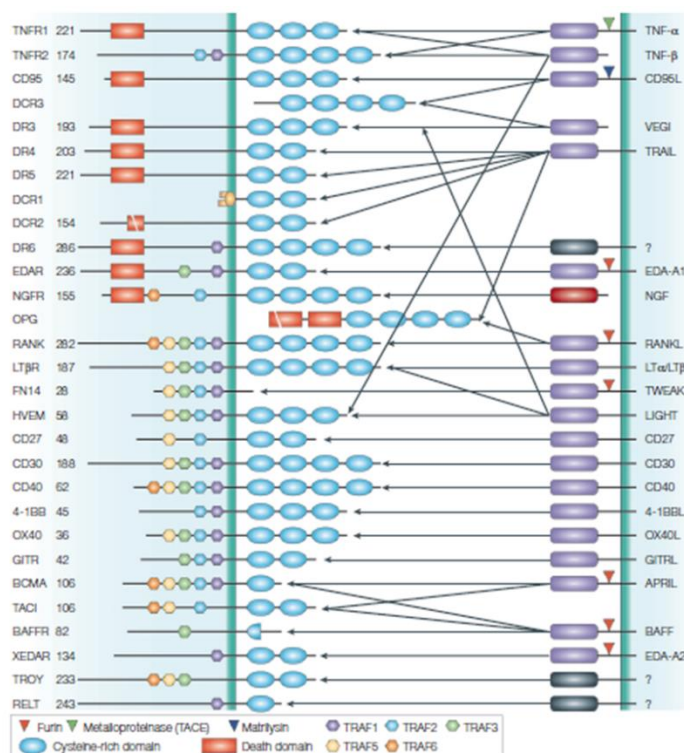


Figure 4. A diagrammatic representation of the ligands of the TNF superfamily and their receptors. All ligands are type II transmembrane proteins with a carboxy-terminal extracellular domain, an amino-terminal intracellular domain and a single transmembrane domain. Most members of the TNF superfamily are released from the cell surface by proteolysis through distinct proteases; the number on the left represent the number of amino acids in the cytoplasmic domain of the receptor.²².

4.2 EXHAUSTION

The phenomenon known as "exhaustion" is characterized by a progressive functional impairment, where CD8⁺ T cells become hyporesponsive to antigen stimulation, as during chronic viral infections (HBV, HCV, HIV, CMV) and tumour growth. This dysfunctional state is promoted by prolonged and high expression of inhibitory receptors on CD8⁺ T cell surface, persistent antigen exposure, CD4⁺ helper T cells availability and the stimulatory cytokines levels³⁴. Initial T-cell responses are elicited, but a spectrum of phenotypic and functional defects arises as the responding cells lose their functional capabilities in a progressive and stepwise manner. Interleukin-2 (IL-2) production is one of the first effector activities to be extinguished, followed by tumour necrosis factor-α (TNFα) production, whereas the ability to produce interferon-γ (IFN-γ) is more resistant to inactivation³⁵ (Fig.5). Infections elicit multi-epitope-specific T-cell responses, but not all specificities are equally prone to exhaustion; this

Figure 5. Hierarchical stages of T cell exhaustion. At the beginning of infection, naïve T cells are primed to differentiate into effector T cells. Clearance of infection and antigen allows a subset of these functional effector T cells to further differentiate into memory T cells capable of producing cytokines. During chronic infection, antigen load increases and T cells lose their functional capabilities in a progressive and stepwise manner. Furthermore, T cell exhaustion is also accompanied by a progressive increase in the amount and diversity of inhibitory receptors expressed.

The activity of each property is presented on a scale from high (+++) to low (—); 'CTL' indicates cytotoxic potential³⁷.

The activity of each property is presented on a potential³⁷.



4.3 2B4-CD48 INTERACTION

2B4 receptor belongs to CD2 superfamily, is expressed in NK cells, in a subset of memory-phenotype CD8+ $\alpha\beta$ T cells, $\gamma\delta$ T cells, in basophils and monocytes. It possess an IgV and two IgC motifs in the extracellular domain, a transmembrane hydrophobic region and a long cytoplasmic tail with four tyrosine-based switch motifs (ITSMs, TxYxxV/I). This receptor recognizes CD48, a GPI-anchored molecule expressed in lymphoid and myeloid cells⁴³.

The impact of the interaction between 2B4 and CD48 was widely studied in NK cells, demonstrating an activation role, both in mice and human ⁴⁴. More recently, studies conducted in 2B4-deficient mice revealed an inhibitory role of 2B4 in murine NK cells, where the absence of 2B4 displayed an increase of IFN- γ production and an enhanced cytotoxicity against CD48 expressing cells *in vitro* ^{45,46}; in human, 2B4 accomplishes its inhibitory role also in the early stages of NK cells differentiation ⁴⁷.

The immune modulation of 2B4 is principally dependent on two cytoplasmic mediators: the signalling lymphocyte activation molecule associated protein (SAP) and the EAT-2 family. SAP is recruited by phosphorylated ITSMs after 2B4-CD48 interaction and may carry out two different effects: first, it can block recruitment of the protein tyrosine phosphates SHP-2, the principal cytosolic mediator of inhibition; second it can recruit and activate the Scr family kinase Fyn via unusual SH2domain-SH3domain interaction ⁴⁸. A dysfunction or lack of SAP is the molecular cause of a congenital disease, the X-linked lymphoproliferative disease 1 (XLP1), where 2B4 only delivers inhibitory signals⁴⁹⁻⁵¹. EAT-2, instead, is negative regulator that acts during the NK cells recognition of viruses and tumours; this protein presents three potential mechanisms of action: i) the recruitment of protein tyrosine phosphatase SHP-1 or SHP-2, which block the signalling cascade for NK cell activation; ii) the recruitment of Scr kinase, which phosphorylate receptors with ITSMs leading to the activation of SHP-1 or SHP-2; iii) the recruitment of Scr kinase Csk which negatively regulates the function of other Scr kinases, such as Fyn.

Besides its role in NK cells, 2B4 was also recently characterized for its involvement in CD8 T-cell exhaustion, where the expression levels of 2B4 and CD48 define the signalling function. Low levels of 2B4 on lymphocytes cell surface trigger stimulatory effect determining an increase of IL-2 secretion; by contrast, high density of receptor causes an inhibitory effect, thereby decreasing IL-2 secretion, as

it occurs during the phenomenon of exhaustion. Indeed, excessive EAT-2 signalling may contribute to poor control of viral infections, leading to CD8 T-cell exhaustion⁵². In case of intermediate levels of 2B4, the concentration of CD48 ligand becomes crucial: low expression levels leads to stimulatory effect, while it turns into inhibition when highly expressed⁵³. More importantly, disruption 2B4-CD48 interaction with monoclonal antibodies, proved to be effective in reversing T cell functional deficiency in a variety of chronic diseases, including HBV, HCV, CML and HIV infections³⁹.

The 2B4 (also known as CD244) and CD48 complex structure has been determinate in mouse to a resolution of 1.6 Å. The N-terminal domains of these proteins are characterized by two antiparallel β sheets of strands designated AGFCC'C'' and DEB. Unlike other IgV domains, the 2B4 and CD48 ligand-binding domains lack the canonical disulphide bond between B and F strands. 2B4 β sheet AGFCC'C'' interacts with the corresponding β sheet of CD48, and the interaction is restricted to C and C' sheets. The 2B4-CD48 interaction is stabilized by hydrogen bonds, salt bridges, electrostatic and polar interactions between loop residues. The protein interface is more symmetrical in comparison with other interfaces of this family (e.g. CD2-CD58) and is predominantly hydrophilic, with 32 bound water molecules, of which 28 create hydrogen bonds between the two proteins. In general, 18 residues of 2B4 interact with 14 residues of CD48 through 18 direct hydrogen bonds and six salt bridges. Critical interaction residues were found with mutational analysis, among these Lys68 of 2B4 is responsible of two hydrogen bonds with Glu93 of CD48 and the Glu70 of 2B4, involved in a salt bridge with Arg87 of CD48^{54,55} (Fig.6). Initially all predicted N-linked glycosylation sites were thought to be non-essential for 2B4-CD48 interaction. Some years later, the N-glycosylation of 2B4 was demonstrated to be essential for the interaction, because the lack of these sugars prevents the binding with CD48, while sialic acids seem to negatively affect the interaction, since the removal of this posttranslational modification leads to an increase of interaction between the two proteins⁵⁶.

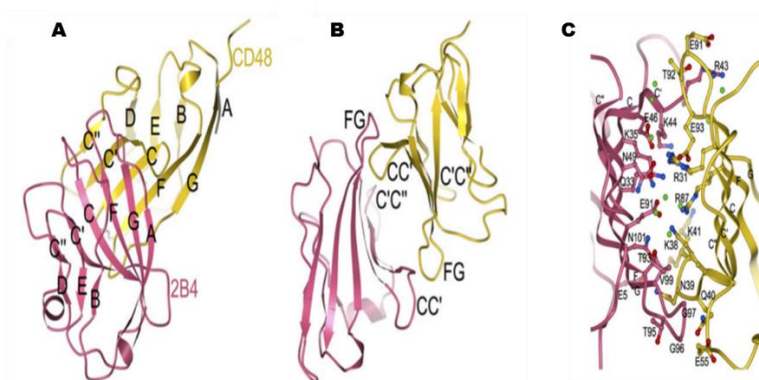


Figure 6. Structure of 2B4-CD48 complex. **A)** Face-to-face interaction between AGFCC'C'' β sheets of the two IgV domains. 2B4 is represented in pink and CD48 in yellow. **B)** Rotation of the complex of 90° around the vertical axis to visualize the proteins interface. **C)** View of residues involved in hydrogen bond or salt bridge interactions at 2B4-CD48 interface⁵⁴.

2B4-CD48 is an attractive drug target, since disruption of this interaction can reverse the dysfunctional state of CD8⁺ T cells observed in various chronic diseases. No active small molecule has been reported so far that could overcome the drawbacks associated with immunotherapy. Compounds able to disrupt this PPI could thus represent a therapeutic alternative for the treatment of refractory viral infections. The aim of this project is to discover small molecule inhibitors of 2B4-CD48 interaction that will provide a set of novel compounds amenable to further development and use as selective inhibitors of PPI involved in CD8⁺ T cell exhaustion associated to chronic infection.

4.4 RESULTS

4.4.1 CHIMERIC PROTEIN CONSTRUCTION FOR BRET ANALYSIS AND VALIDATION OF SIGNAL SPECIFICITY

Available 3D structure of the 2B4-CD48 complex guided the design of fusion proteins for BRET analysis⁵⁴. To reproduce 2B4-CD48 interaction in BRET, the ectodomain of the 2B4 receptor (aa 22-222) and its CD48 ligand (aa 29-134) were cloned in-frame with both the donor and the acceptor, in either C-terminal or N-terminal orientation. Since this interaction was the first examined in our yBRET platform, we performed a comparison between two different luciferases: the *Renilla* luciferase RLuc and the *Oplophorus gracilirostris* luciferase NLuc (NanoLuc, Promega), in order to confirm and extend the results obtained with p53-HDM2 (see chapter 2).

Table I. yBRET 2B4-CD48 interaction combinations.

Construct	mBRET	Substrate
2B4-RLuc + CD48-YFP	110	Coe
2B4-RLuc + YFP-CD48	40	Coe
RLuc-2B4 + CD48-YFP	260	Coe
RLuc-2B4 + YFP-CD48	2	Coe
CD48-RLuc + 2B4-YFP	77	Coe
CD48-RLuc + YFP-2B4	66	Coe
RLuc-CD48 + 2B4-YFP	4	Coe
RLuc-CD48 + YFP-2B4	7	Coe
2B4-NLuc + CD48-YFP	130	Coe
NLuc-2B4 + CD48-YFP	278	Coe
NLuc-2B4 + CD48YFP	370	Nglo

BRET signal obtained with different combinations of constructs. The expression of donor fusion proteins was induced for 2 h with 2% galactose; the orientations with the higher BRET signal are highlighted in bold. Coe: coelenterazine h, Nglo: Nanoglo® substrate.

Using RLuc luciferase, the highest BRET signal was obtained with the acceptor protein fused to the C-terminus of CD48, and 2B4 in the donor fusion protein in either orientation. For this reason, the NLuc luciferase was tested only fused to 2B4, in association with CD48 fused at C-terminal to YFP (Table I). Concerning the comparison between RLuc and NLuc, the BRET signals were very similar when the substrate coelenterazine h (optimal for *Renilla* luciferase) was used, whereas increased considerably when the substrate optimized for the NLuc (Nanoglo®) was used. NLuc-2B4 + CD48-YFP combinations revealed the highest BRET signals regardless the luciferase type.

We subsequently evaluated BRET signal as a function of time and inducer concentration, and the induction conditions were set at 2% galactose for 2 h. The expression of both fusion proteins was then evaluated under these conditions by Western blotting and their interaction by co-immunoprecipitation (Fig.7). The lack of the availability of a reliable anti-NLuc antibody, prevented the use of NLuc fusion protein at this stage, therefore the experiments were conducted using the RLuc-2B4 + CD48-YFP strain. Both fusion proteins were highly expressed and clearly interact as revealed by the co-immunoprecipitation experiment.

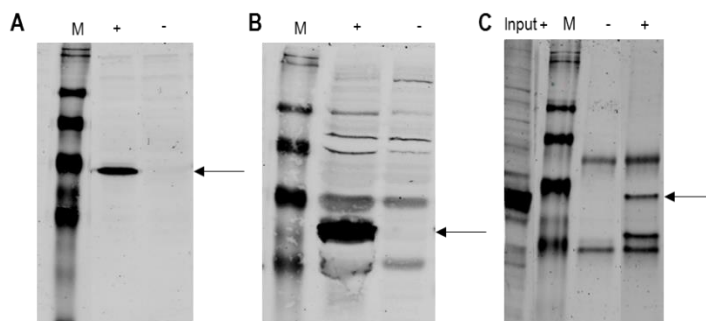


Figure 7. Protein expression evaluated by Western blotting analysis using 25 μ g of crude extract produced from the yBRET strain expressing RLuc-2B4 (A) and CD48-YFP (B), using a monoclonal anti-RLuc (antibody #MAB4400, Millipore) and a polyclonal anti-GFP (antibody #ab290, Abcam), respectively; (C) Co-immunoprecipitation from 2 mg of total extract of yBRET strain co-expressing RLuc-2B4 and CD48-YFP. Proteins were first immunoprecipitated using anti-RLuc antibody, and then revealed in WB using anti-GFP antibody. M: marker; +: yeast expressing RLuc-2B4 and CD48-YFP; -: yeast transformed with empty vectors; input +: 25 μ g of total extract. The arrow points to the detected protein.

The specificity of BRET signal was verified through a BRET donor saturation assay. For this purpose, the donor fusion protein (NLuc-2B4) was constitutively co-expressed with increasing levels of acceptor fusion protein (CD48-YFP). A non-specific BRET signal increases linearly whereas a specific BRET signal increases in a hyperbolic manner until it reaches a plateau. The curve obtained for this interaction shows the typical rise of BRET signal for specific interaction (Fig.8).

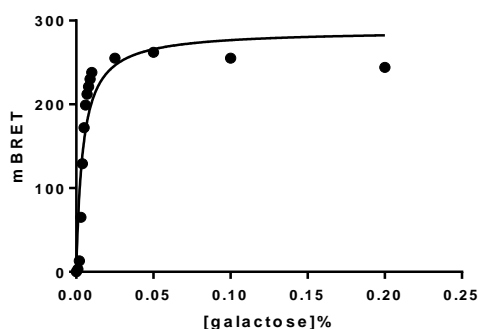


Figure 8. Donor saturation assay for 2B4-CD48 interaction in BRET. The expression of the acceptor fusion protein (CD48-YFP) was induced o/n at 20 °C at different galactose concentrations, while the expression of the donor fusion protein (NLuc- 2B4) was controlled by a constitutive promoter (*TEF* promoter).

To further verify the specificity of 2B4-CD48 interaction, we created a mutant version of 2B4 by replacing two amino acids assumed to be critical for the interaction (K68 and E70, KE) with alanine residues⁵⁵. BRET analysis were performed also on a triple mutant (K54A, H65A and T110A, KHT) kindly provided by Carsten Watzl (IfADo, Department of Immunology, Dortmund, Germany), able to completely disrupt the interaction in mammal cells assays⁵⁷. The results obtained from mutants' comparison in yBRET revealed a significant reduction of the BRET signal with KE mutant and almost complete loss of signal with KHT mutant, thus indicating once again the specificity of the 2B4-CD48 interaction reconstituted with the two fusion proteins inside the yeast cell. Finally, to analyse the contribution of non-specific BRET value due to stochastic interaction between the donor and acceptor inside the yeast cells, we have verified that the co-expression of the luciferase fusion protein (NLuc-2B4) and YFP only (i.e., YFP without CD48) did not produce any detectable BRET signal (Fig.9).

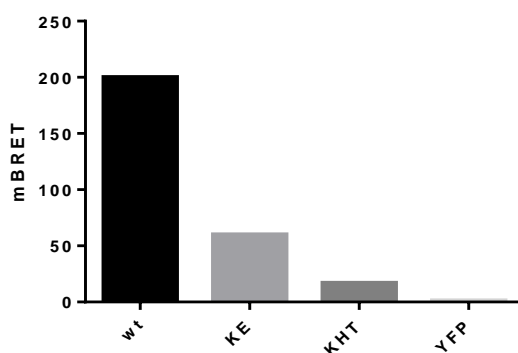


Figure 9. BRET signal derived from the co-expression of CD48-YFP with NLuc-wild-type 2B4 (wt), NLuc-2B4 K68A-E70A mutant (KE) and NLuc-2B4 K54A-H65A-T110A mutant (KHT), and of NLuc-2B4 with YFP (YFP). The expression of the donor fusion protein was induced for 2 h with 2% galactose.

4.4.2 SCREENING

Since no small molecules capable of selectively disrupting this interaction have been reported, we performed a screening on untargeted as well PPI inhibitors-enriched compound libraries (assembled considering the physicochemical and pharmacological profiles of PPI inhibitors)⁵⁸, for a total of over 14.000 compounds of synthetic and natural origin. To this purpose NLuc-2B4 was expressed under the control of the galactose-inducible *GAL4* promoter (p413 vector), and CD48-YFP in a constitutive manner (p190 vector, *TEF* promoter), in the hyper permeable $\Delta erg6$ yeast strain to maximize the

uptake of substrate and small molecule compounds. Molecules were tested in yBRET at 20 μ M and added to exponentially growing yeast before donor protein induction. NLuc-2B4 expression was induced by adding 2% galactose followed by incubation 2 h at 30 °C. Positive hits (i.e., compounds reducing the BRET signal by at least 15% without any sign of generalized cellular toxicity) were first confirmed in the same experimental set up.

Table II

Library	n. compounds	yBRET	n.scaffold
PPI-Australia Compound Library	5000	34	2
NCI	1596	-	-
ICNS	4640	-	-
Enzo	502	-	-
Prestwick	1200	-	-
Marc3	600	-	-
ReC3	1040	-	-

This table summarizes the results obtained from the screening of the seven libraries of different origin: the 'yBRET' column refers to the number of molecules identified *in vivo* and the 'number of scaffold' column refers to the different chemical structures identified in selected hit compounds.

The screening allowed the identification of 34 hits, all deriving from the PPI-enriched Australia Compound Library that could be classified into two chemical scaffolds: one molecule, the P300-1755, was the only representative of one scaffold, while the other 33 belonged to the second scaffold (Table II).

The P300-1755 hit contains a tricyclic ring system similar to known inhibitors of the CD28-CD80 interaction, which belong to the same Ig super family, increasing the interest for this compound⁵⁹⁻⁶¹. The hit molecule, P300-1755, was therefore purchased from the public vendor ChemDiv (San Diego, CA, USA), along with thirteen structural analogues to investigate the inhibitory activity of this chemical class.

The other 33 molecules, with lower inhibitory activity, are characterized by a strongly electrophilic methoxy-acrylester group and all belonged to CSIRO Institute (Clayton, Australia). 2B4 Cys106 residue is located in the interaction interface, immediately adjacent to an acid residue (E108) and a basic one (K155). It is possible to hypothesize that these three amino acids could create a triad, able to deprotonate cysteine, make Cys106 more reactive and prone to covalently bind electrophilic groups, explaining the activity of these molecules. The CSIRO Institute kindly provided the best seven

molecules of this class identified in the library. Other 25 structural analogues were also purchased or obtained within a collaboration with Dr. Silvia Rivara (Food and Drug Department, University of Parma), in order to assess the potential reactivity on cysteine.

4.4.3 CYSTEINE-REACTIVE MOLECULES

The seven hit compounds and the 25 structural analogues were tested at 50 μ M and 20 μ M in yBRET; the seven hits confirmed their activity, even if at higher concentration proved to be toxic for the yeast cells. Among the analogues, only two compounds were able to inhibit the interaction between 2B4-CD48, but showed high toxicity at 50 μ M; therefore, we performed an assay to test the active compounds at 5 μ M and 10 μ M, in order to monitor their efficacy in nontoxic conditions (Fig.10). The nine molecules retained the percentage of inhibition showed in previous assay and only the analogue #13 shown a toxic effect also at 10 μ M.

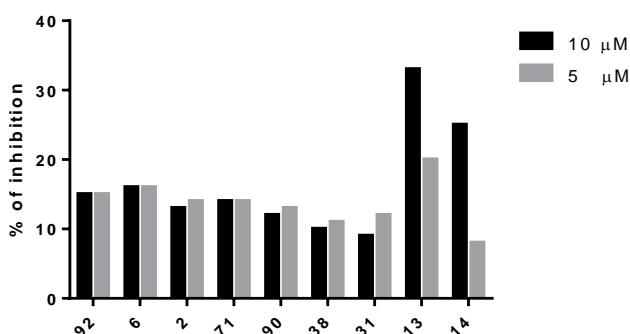


Figure10. Results of yBRET signal inhibition obtained with hits and the best structural analogues at 10 μ M and 5 μ M; all molecules showed inhibition without exhibit toxic effect, with the exception of analogue 13 at 10 μ M.

To verify the hypothesis that these molecules can inhibit 2B4-CD48 interaction by covalent binding to 2B4 Cys106, we have created a C106A mutant. In addition, to exclude the involvement of another cysteine present in the ectodomain, but located outside the proteins interface, Cys22 was replaced with alanine; finally, a double mutant (C22A, C106A) was also generated. Initially, we verified the BRET signal of three mutant versions, to ensure that the mutations did not influence the interaction strength. The mBRET signals were comparable in all cases, with a slight decrease when cysteine 106 was mutated (Fig.11).

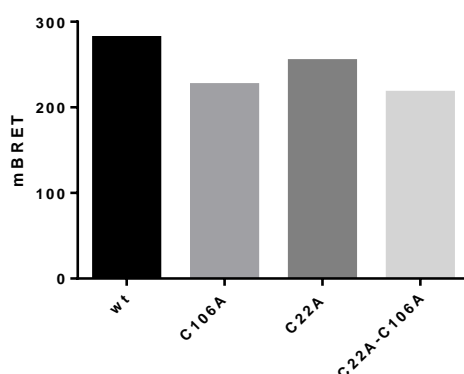


Figure 11. BRET signals derived from the co-expression of CD48-YFP with NLuc-wild-type 2B4 (wt), NLuc-2B4 C106A mutant (C106A), NLuc-2B4 C22A mutant (C22A), and NLuc-2B4 C22A-C106A mutant (C22A-C106A). The expression of the donor fusion protein was induced for 2 h with 2% galactose.

The activity of the nine methoxy-acrylester molecules was tested on three mutant strains and the wt at 10 μ M.

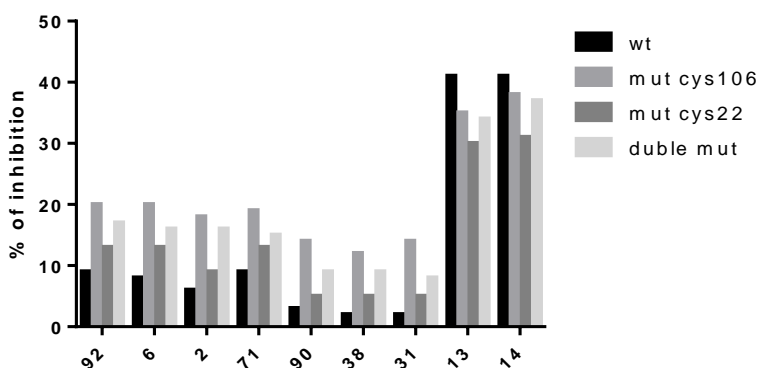


Figure 12. Results of the activity of methoxy-acrylester molecules on 2B4 cysteines, expressed as percentage on BRET signal decrease. The histogram show the percentage of inhibition for each molecule tested at 10 μ M on wild-type and three versions of mutants.

All molecules shown increased activity on mutants -especially mutants bearing the C106A mutation- in comparison to wild-type and this suggested that none of them was specifically targeting the Cys106. This is possibly due to a loosen interaction between 2B4 and CD48 in the mutant versions, so

molecules retained their activity. Since these compounds did not give any promising results, we decided to not pursue with the research of potential inhibitors within this chemical class.

4.4.4 P300-1755 AND STRUCTURAL ANALOGUE MOLECULES

P300-1755 together with thirteen structural analogues (Supplementary Table 1), were tested in yBRET at two different concentrations to re-confirm the inhibition of the hit compound and to evaluate the activity of new molecules.

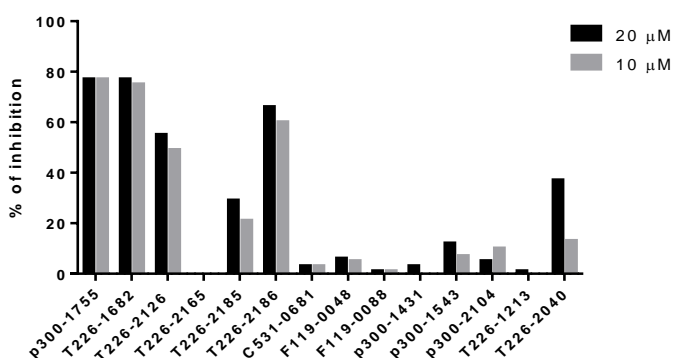


Figure 13. Results of yBRET assay of P300-1755 hit and its structural analogues at 20 μ M and 10 μ M; the percentage on BRET signal decrease is shown. The structures of these molecules are shown in Supplementary Tables 1.

P300-1755 confirmed its activity, retaining high inhibition also at 10 μ M; among structural analogues, T223-1682 showed a behaviour very similar to the hit compound, T226-2126 and T226-2186 exhibited a 50% of inhibition at both concentrations, while T226-2185 and T226-2040 displayed inhibitory activity under 50% at both conditions (Fig.13). These six molecules, plus one inactive compound of the same series (T226-2165) were subsequently tested to assess their ability to disrupt a preformed 2B4-CD48 complex, by the addition of compounds after one hour of yeast induction.

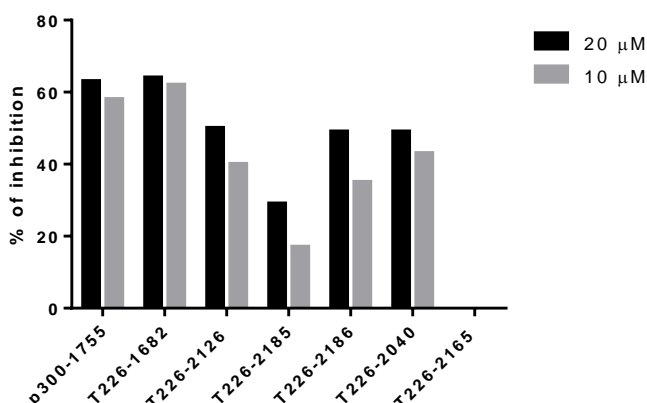


Figure 14. Results of yBRET assay carried out on induced yeast, in order to test the ability of the molecule to disrupt preformed protein complex at 20 μ M and 10 μ M.

Likewise, on induced yeasts with the protein complex already formed, the six compounds exhibit almost the same percentage of inhibition displayed by previous assay, validating their potential function as inhibitors; p300-1755 and T266-1682 were confirmed as the best molecules tested (Fig.14).

To monitor the ability of the molecules to interfere with the 2B4-CD48 interaction at sub-micromolar concentrations and in a dose-dependent manner, we performed a dose-response analyses, monitoring BRET signal decrease as a function of compound concentration (ranging from 0.25 μ M to 50 μ M).

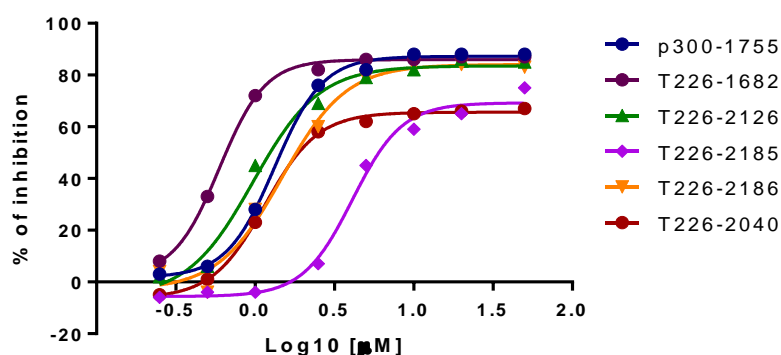


Figure 15. Inhibitory activity on 2B4-CD48 assayed of molecules at different concentrations in yBRET. The IC₅₀ is calculated as a measure of molecule potency.

P300-1755: IC₅₀=1.33 μM r²=0.9985

T226-1682: IC₅₀=0.60 μM r²=0.9983

T226-2126: IC₅₀=0.97 μM r²=0.9892

T226-2185: IC₅₀=4.10 μM r²=0.9902

T226-2186: IC₅₀=1.48 μM r²=0.9861

T226-2040: IC₅₀=1.50 μM r²=0.9989

All molecules showed dose-dependent trends, monitoring inhibitory activity also at lower concentrations. The IC₅₀ ranged between 0.6 μM and 4 μM, and T226-1682 has proven to be the best inhibitory compound on 2B4-CD48 interaction (Fig.15).

In all the assays performed, we have noticed that p300-1755 and T226-1682 compounds were prone to increase the NLuc signal, therefore to determine if there was a specific effect on this luciferase, we performed a dose-response curve also using the luciferase RLuc.

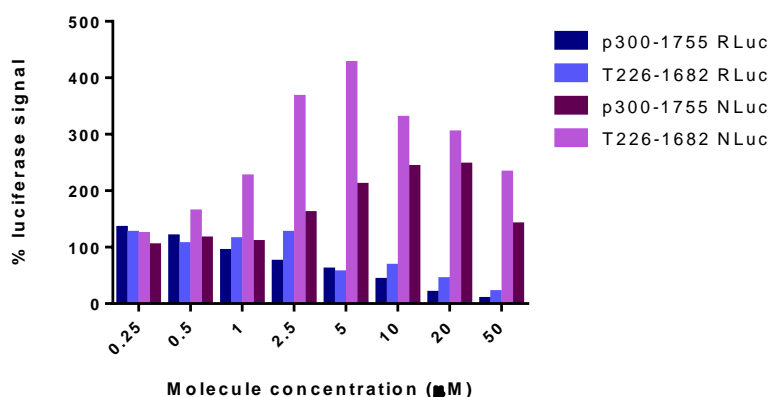


Figure 16. Results of yBRET assay performed on RLuc and NLuc in order to assess the effect of molecules on the luciferases; compounds are tested at different concentrations, ranging from 0.25 μM to 50 μM.

At all concentrations tested, both hit molecules raised the NLuc value in comparison with the DMSO-vehicle control (considered 100% of luciferase signal), instead the RLuc signal decreased with increasing molecule concentration. Despite these differences in luciferase signal, the molecules still retained inhibitory activity on BRET signal, even though the percentage of inhibition with RLuc strain was about half compared to results obtained with NLuc (Fig.16).

To understand the real inhibitory potential of p300-1755 and T226-1682 on this interaction, it was necessary to perform an independent experiment, reproducing 2B4-CD48 in an *in vitro* ELISA-based assay. Since the production of 2B4 is particularly hard in bacteria⁵⁴, because of post-translational modifications, we decided to purchase both recombinant human proteins expressed in mammalian cell lines. 2B4 was fused with a hIgG1-Fc tag, while CD48 had a His Tag (ThermoFisher, cat n°10042H02H25 and 10797H08H25). With this combination of proteins, it was possible to assemble only one orientation in ELISA assay, anchoring CD48 to the well and detecting 2B4 through anti-human IgG1-Fc secondary antibody (anti His-tag monoclonal antibody display a very low signal in ELISA). To overcome this limitation, we produced CD48 recombinant protein in *E. coli*, fused to Glutathione-S-Transferase (GST-CD48), in order to detect its signal with an anti-GST antibody.

The interaction was reproduced using different molar concentrations of proteins in a combinatorial way, summarized in the Table III.

Table III. Different combinations of 2B4-CD48 ELISA assay.

A		B	
anchored		anchored	
2B4- hlgG1-Fc 500ng	GST-CD48 800ng	CD48-His 1 μ g	2B4- hlgG1-Fc 400ng
	GST-CD48 200ng		2B4- hlgG1-Fc 100ng
2B4- hlgG1-Fc 250ng	GST-CD48 100ng	CD48-His 500ng	2B4- hlgG1-Fc 400ng
	GST-CD48 25ng		2B4- hlgG1-Fc 100ng
	GST-CD48 10ng	B	
anchored		anchored	
2B4- hlgG1-Fc 100ng	GST-CD48 40ng	GST-CD48 1 μ g	2B4- hlgG1-Fc 400ng
	GST-CD48 10ng		2B4- hlgG1-Fc 100ng

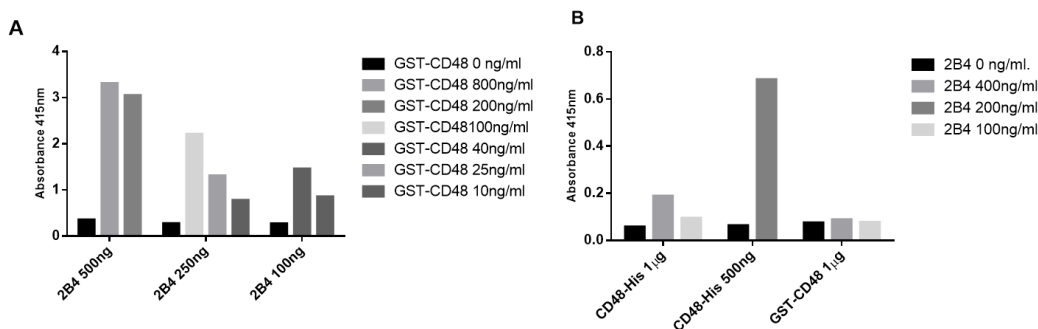


Figure 17. Detection of 2B4-CD48 interaction in ELISA assay. **A)** Plates were coated with 2B4-hlgG1-Fc (500 ng, 250 ng or 100 ng). 100 μ l of GST-CD48 at different concentrations was added to reproduce the interaction (see methods). **B)** Plates were coated with CD48-His-tag (1 μ g or 500 ng) or with CD48-GST (1 μ g). 100 μ l of 2B4-hlgG1-Fc was added at different concentrations to reproduce the interaction (see methods).

In comparison with the negative control (incubation of protein attached without the partner), 2B4-hlgG1-Fc anchored at 500 ng and 250 ng showed a saturation of the signal, which prevents monitoring differences in presence of potential inhibitors, while at 100 ng with 20 ng/mL of CD48 exhibited a stable and reliable signal. Regarding the results obtained with anchored CD48, we observed a signal with only one condition: His-tag CD48- at 500 ng with 200 ng/ml of 2B4 (Fig.17). These conditions were assayed in the presence of 200 μ M concentration of p300-1755 and T226-1682, to confirm their inhibitory activity against 2B4-CD48 interaction.

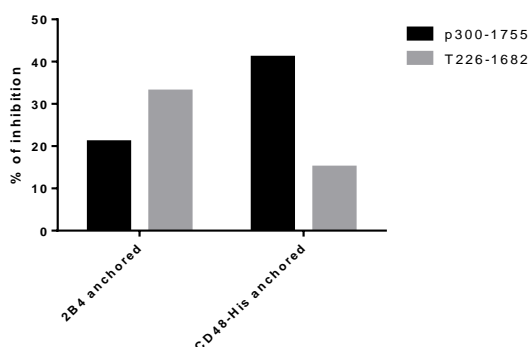


Figure 18. Activity of hit molecules in ELISA assay at 200 μ M.

Results obtained with 2B4-anchored showed an inhibitory activity for both molecules, with a higher percentage of inhibition for T226-1682; on CD48-anchored combination, instead, T226-1682 exhibited very low inhibitory activity in contrast to the high inhibition of p300-1755 (Fig.18). To measure their potency, we performed a dose-response ELISA-assay, monitoring their percentage of inhibition at seven different concentrations ranging from 50 μ M to 400 μ M. p300-1755 was tested on both protein orientations, while T226-1682 was tested only with CD48-anchored + 2B4, since its percentage of inhibition with the other condition was too low.

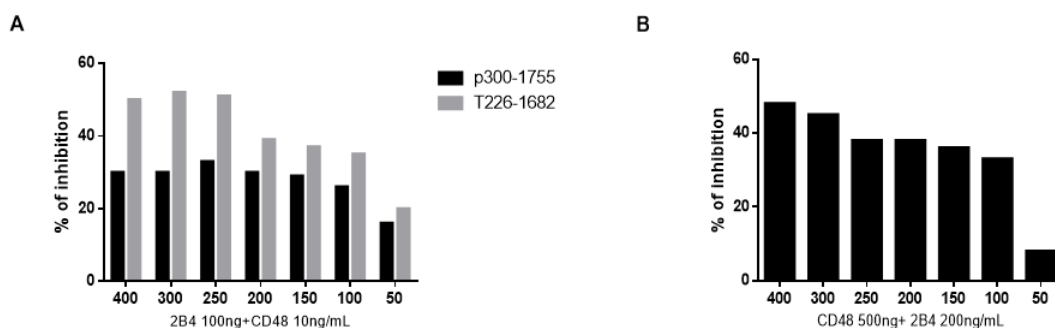


Figure 19. Inhibitory activity on 2B4-CD48 interaction of molecules assayed at different concentrations in ELISA assay. **A)** Activity of p300-1755 and T226-1682 on 2B4-hlgG1-Fc anchored combination; **B)** Activity p300-1755 on his-tag-CD48 anchored combination.

On 2B4-anchored combination, molecules appeared to be active at all concentrations tested, but none showed a dose-dependent trend; T226-1682 was confirmed more active than p300-1755 (Fig.19). On CD48-anchored p300-1755 exhibited inhibition until 50 μ M, once again there was not any evident dose-dependent behaviour. This assay has allowed us to validate the efficacy of p300-1755 and T226-1682 on the interaction between 2B4 and CD48 monitored in yBRET.

4.5 CD40-CD40L INTERACTION

The receptor-ligand complex formed by CD40 and CD40L, members of the TNFR and TNF superfamily, is an important co-stimulatory interaction for T and B cells activation. CD40 is a 48 kDa type I transmembrane receptor, expressed on the surfaces of B cells, monocytes, macrophages, platelets, follicular dendritic cells, eosinophils and activated CD8+ T cells⁶². Besides the hematopoietic tissue, it is also present in thymus, myofibroblasts, fibroblasts, epithelial, and endothelial cells⁶³. CD40L (also known as CD154) is a type II transmembrane protein, with a variable molecular weight of ~30 kDa, depending on post-translational modifications. It also exists as a soluble form with similar activity to the anchored protein. This ligand is transiently expressed as homo-trimeric protein on activated CD4+ T cells, CD8+ and $\gamma\delta$ T cells, but also on monocytes, activated B cells, vascular or epithelial endothelial cells⁶⁴. The function of CD40L in some of these cellular types is not well known, instead it participates in thrombotic disease when expressed on platelets⁶⁵. The best characterized function of CD40-CD40L complex is the adhesion and consequent signalling between APC and T cells⁶⁶. In the resting state of B cells, the interaction between CD40 and CD40L promotes survival, cells activation and differentiation of plasma cells and memory B cells⁶⁴.

During the interaction between receptor and ligand, CD40 recruits the cytoplasmic adapter protein TRAF to its cytoplasmic domains, activating signalling cascade that modulates transcriptional activity of survival and cellular growth genes²². Like other proteins of the TNF family, CD40L, also exists *in vivo* as a stable soluble trimer; in either form, its binding to CD40 is supposed to promote CD40 oligomerization with the consequent formation of TRAF binding site⁶⁴. TRAF family is composed by six components (TRAF1-6), able to activate different signalling pathways, including NF- κ B, MAPPK, PI3K and PLC γ . Some pathways are TRAF-independent, such as Janus family 3 (JAK3), which binds directly CD40 activating STAT5 phosphorylation⁶⁴. The CD40 signalling is necessary to different processes, among which the formation of germinal centre, the somatic hyper-maturation of immunoglobulins genes and the isotopic switching from IgM to IgG. The implications of this last process are dramatic in patients affected with X-linked hyper-IgM syndrome (XHIGM), where the mutations at the locus of CD40L prevent functional interaction with the receptor⁶⁷. CD40 and CD40L are also famous for their implication in pathologic autoimmune conditions or linked with phlogosis. In fact, in patients with systemic lupus erythematosus⁶⁸, Sjogren's syndrome⁶⁹, inflammatory chronic intestinal disease⁷⁰ and cardiovascular disease⁷¹, high levels of aberrant soluble isoforms of CD40L (sCD40L) were found. Besides being a biomarker, sCD40L probably actively promotes pathologic

progression. In other pathologic conditions (e.g. rheumatoid arthritis) CD40L is expressed at high levels in T cells⁷². In patients affected with Crohn's disease, the intestinal lesions are caused by accumulation of B cells expressing CD40 and of T cells that express CD40L⁷³. In the case of lupus, the *ex vivo* production of pathogenic autoantibodies by patient's lymphocytes could be blocked effectively with the administration of anti-CD40L antibodies⁷⁴. Likewise, the same antibodies reduce the production of interleukins and TNF- α by synovial cells explanted from patients with rheumatoid arthritis⁷⁵. CD40 signalling, as other members of TNFR superfamily, is highly pleiotropic. For example, in murine B lymphomas cell lines, the mAb anti-CD40 administration induces the arrest of growth and the same inhibitory effects on cellular proliferation is observed on cellular lines from patients affected by aggressive lymphomas of B cells⁷⁶. All these observations identify this interaction as potential therapeutic target.

The crystal structure of human extracellular domains of CD40-CD40L complex has been determined to a resolution of 3,5 Å. The extracellular portion of CD40L is a homotrimer, organized in a sandwich of two antiparallel β sheets with a α -helix, where the hydrophobic residues predominantly characterize the subunits interfaces. The more important structural arrangements take place in the flexible loop region and are not directly related to CD40 binding. The extracellular domain of CD40 possess three CRDs, each containing 2-3 parallel disulfide bridges, forming a ladder-like elongated structure that have a critical role in the stabilisation of the CD40 structure. This receptor binds to a groove between pairs of CD40L, interacting with both of them; so one CD40 trimer interacts with only two CD40, and one of the three potential CD40 interaction sites in the CD40L trimer remains empty⁷⁷ (Fig.20). This 2:3 molar ratio is unusual for the TNF/TNFR family, where all the structures are characterized by a 3:3 ratio. A possible explanation is the repulsion of charges in the determination of the molar ratio, since the complex is stabilized by hydrophilic and charged interactions, and only one-third of the interface have scattered non-polar residues. The proteins interface shows a charge complementarity, with a positive face on CD40L and a negative face on CD40. Critical interaction residues were found with mutational analysis, among these Glu74, Asp84 and Glu117 on CD40 and Lys143, His249, Arg203 and Arg207 on CD40L are responsible of the binding⁷⁷.

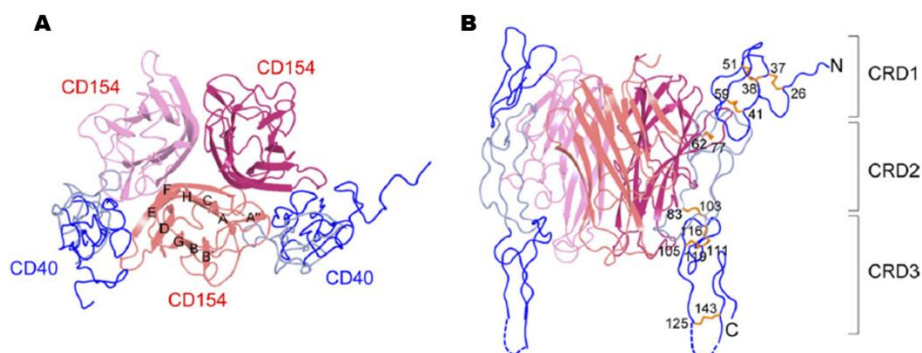


Figure 20. Structure of CD40-CD40L complex: (A) top view and (B) side view. The strands of CD154 are labeled. CRD1 and CRD3 of CD40 are coloured dark blue, and CRD2 is coloured light blue⁷⁷.

CD40 and CD40L are involved in many diseases such as lymphomas and autoimmune inflammation in the central nervous system. A number of antibodies that block this interaction have reached clinical trials against autoimmune diseases: antibody binds at a site that overlaps the expected CD40 binding site at each of the three-subunit interfaces of CD40L, but gives rise to thromboembolic complications. The aim of this project is to discover candidate small molecule inhibitors of CD40-CD40L interaction, developing also a surface BRET-based technology, which represents a new tool for the study of this protein interaction in conditions more similar to physiological ones. The technology can be extremely useful for the study of protein-protein complexes whose interaction, for different reasons (e.g. necessary formation of disulphide bridges, mass glycosylation), cannot be reproduced inside the cells.

4.6 RESULTS

4.6.1 STRUCTURAL ANALYSIS AND MODEL CONSTRUCTION IN YBRET

The first obstacle in the study of CD40-CD40L interaction is the pentameric nature of this protein complex that has generated several difficulties in the development of an effective BRET system, which is usually performed between two protein partners. To reproduce this interaction in yBRET, we initially analysed the crystal structure of protein complex. The extracellular domain of CD40L (aa 78-911) is a homotrimer that presents both N-terminal and C-terminal in the "upper" side of the complex (Fig.21). We decided to clone both the donor and the acceptor at the N-terminal of the ligand, since these residues are more exposed and less hidden in the grooves between monomers, while C-terminal sequences are directly involved in the interactions responsible for trimer formation, and any C-terminal fusions could cause excessively distorting monomers interface. The extracellular domain of CD40 (aa 77-858), instead, is characterized by a sort of "ladder-likier" elongated structure formed by eight

disulfide bridges, where the N-terminal and C-terminal are on the opposite site of protein complex; also in this case, we opted for a fusion at the N-terminal, since the useful distance in BRET between acceptor and donor is less than 10 nm, and a fusion at the C-terminal would bring luciferase too far from the YFP for energy transfer purpose. Furthermore, we also created these fusion proteins using a 10 amino acids poly-Gly-Ser linker to ensure dipole-dipole coupling between NLuc and YFP in CD40, and to reduce steric interference that could prevent CD40L complex formation.

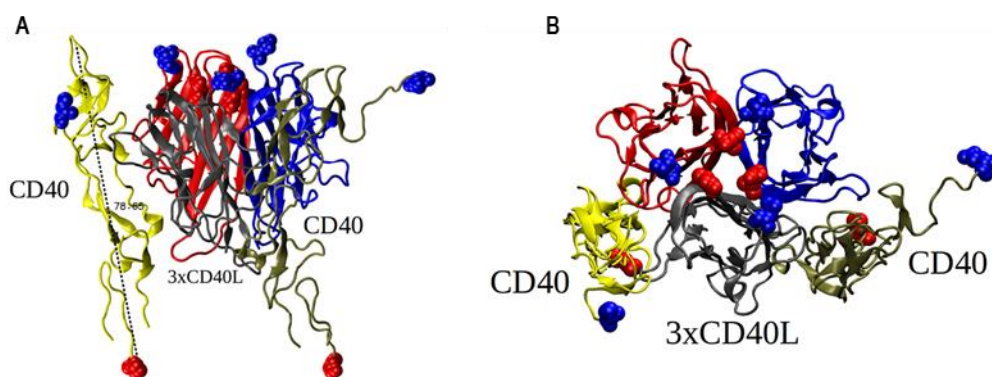


Figure 21. Pentamer structure visualized from (A) the top and (B) the bottom side of the complex formed by the ectodomains of CD40 and CD40L. The trimeric form of CD40L is contacted by two receptor units at trimeric grooves level. CD40 monomers are shown in yellow and dark green, CD40L monomers are in red, blue, and grey. The N-terminal are highlighted with blue spacefill, while C-terminal are red. The length of a CD40 monomer is also shown.

4.6.2 OPTIMIZATION OF CLASSICAL-CYTOSOLIC YBRET

Initially, we evaluated the efficiency of NLuc-CD40 and NLuc-CD40L fusion proteins expression in yeast by measuring NLuc emission signal. The NLuc-CD40L construct was highly expressed in both linker and no-linker versions, while we could not detect any NLuc-CD40 signal: as described above, the folding of this protein requires the formation of eight specific disulphide bridges, and it is presumable that in a relatively reducing environment like cytoplasm, this does not occur. Therefore, we started with the study of the trimer interaction by expression of CD40L fused with both NLuc and YFP, since any molecule capable of causing the dissociation of the three CD40L subunits probably could also prevent the pentameric complex assembling. Then, we evaluated the BRET signal in yeast expressing YFP-CD40L under the control of a constitutive promoter (*GDP* promoter), while the expression of NLuc-CD40L was induced with 2% galactose (*GAL1* promoter). The signal was

monitored in dependence of temperature and induction time. Heterotrimers formed by NLuc-CD40L and YFP-CD40L generated a reliable BRET signal, which was higher in the presence of poly-Gly-Ser-linker, thus confirming the usefulness in the orientation of BRET partner (Table IV).

Table IV

T°	20°				30°			
Induction Time	2h		4h		2h		4h	
	Linker	No linker	Linker	No linker	Linker	No linker	Linker	No linker
NLuc	372.000	322.000	476.000	372.000	240.000	152.000	278.000	204.000
mBRET	258	240	264	248	97	94	120	118

BRET signals obtained with heterotrimers formed by NLuc-CD40L and YFP-CD40L, in presence or absence of poly-Gly-Ser-linker. The expression of donor fusion proteins was induced for 2 h or 4 h with 2% galactose, comparing two different temperatures.

BRET and luciferase signals were higher in the case of inductions carried out at 20 °C: despite the optimal yeast growth rate is 30 °C, it is possible that the metabolic slowdown due to low temperature makes fusion proteins more stable and less susceptible to degradation. Moreover, YFP expression seems to take advantage of lower temperature for the maturation of the chromophore, and finally influence the stoichiometry of the complex (see below).

Although the levels of expression and energy transfer proved to be higher in the case of four-hour induction rather than 2 h, we opted for "short" induction given the small difference between two conditions and the considerable advantage for the screening system.

We subsequently evaluated BRET signal in dependence of inducer concentration: the trimeric nature of the CD40L complex implies the existence of four different configurations (Fig. 22), of which only two (the heterotrimeric ones) are able to generate a BRET signal. The probability of the four configurations depends on the stoichiometry between NLuc-CD40L and YFP-CD40L, and therefore on inducer-galactose concentration.

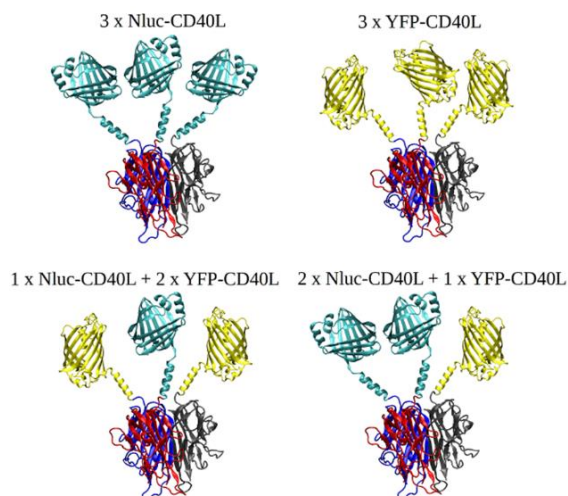


Figure 22. Four possible configurations of CD40L trimeric complex in BRET set-up. Only the two "heterotrimeric" complexes (bottom) can contribute to BRET signal, while the complexes depicted on top cannot give rise to any energy transfer.

The assay showed an opposite correlation between galactose (and subsequent NLuc value) and BRET signal: mBRET signal were stabilized with inducer concentrations higher than 0.01%. We therefore decided to use a galactose concentration of 0.1% in subsequent experiments. This value is a trade-off between sensitivity and reliability of the observed signal (Fig.23).

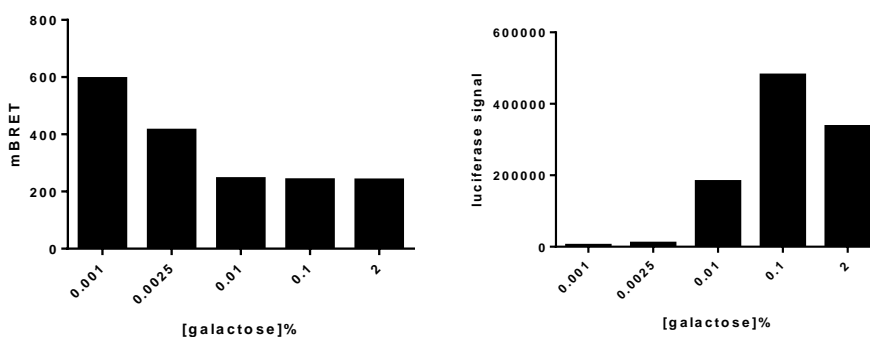


Figure 23. The graphs show the trend of BRET and Luciferase signals in dependence of inducer concentrations.

4.6.3 OPTIMIZATION OF SURFACE YBRET

To study the pentameric protein complex, we have developed a surface-exposed yeast BRET (syBRET), using the *Saccharomyces cerevisiae* EBY100 strain, which had been engineered for yeast display assay. This strain allows the inducible expression of a protein of interest fused to Aga2 (pYD1 vector) and results in the exposure of this protein anchored to the cell wall by two disulphide bonds. The other fusion protein was expressed with a secretory signal peptide at its N-terminal under the constitutive strong promoter *TEF* (p190 vector). As in the case of cytosolic BRET, we have evaluated the expression of NLuc-fusion proteins, monitoring the luciferase signal, obtaining a detectable expression of all fusion proteins, including those containing CD40, probably due to the presence of the protein disulfide isomerase in the endoplasmic reticulum and to the oxidizing extracellular environment. Therefore, both pentameric and trimeric interactions were assayed in syBRET. The expression of the anchored fusion protein was induced with 2% galactose (pYD1 vector) at 20 °C, as suggested for the expression in the yeast display system. As expected, the YFP-CD40L fusion did not lead to a stable pentameric complex, probably due to steric interference with fluorescent protein. The best combination appeared to be the inducible expression of Aga2-NLuc-CD40L anchored to the yeast cell wall and the secretion of receptor fusion protein YFP-CD40. We selected this combination to perform the following assays (Table V).

Table V

pYD1	p190	Construct	mBRET
NLuc-CD40L	YFP-CD40L	heterotrimer	98
YFP-CD40L	NLuc-CD40L	heterotrimer	85
NLuc-CD40L	YFP-CD40	pentamer	96
YFP-CD40	NLuc-CD40L	pentamer	76
NLuc-CD40	YFP-CD40L	pentamer	4

BRET signals obtained with heterotrimeric and pentameric complexes in syBRET. The expression of anchored fusion proteins was induced for 2 h with 2% galactose at 20 °C.

We carried out a donor saturation assay to evaluate the specificity of the BRET signal: NLuc-CD40L was expressed under a constitutive promoter (*TEF*), while different levels of YFP-CD40 expression were tested (Fig.24). The BRET signal increased hyperbolically with the increase concentration of the acceptor, showing that energy transfer is due to a specific interaction. Furthermore, to analyse the contribution of non-specific BRET value, we have verified that the co-expression of the luciferase

fusion protein in the wall (NLuc-CD40L) and secreted YFP only, did not produce any significant BRET signal, confirming the specificity of interaction.

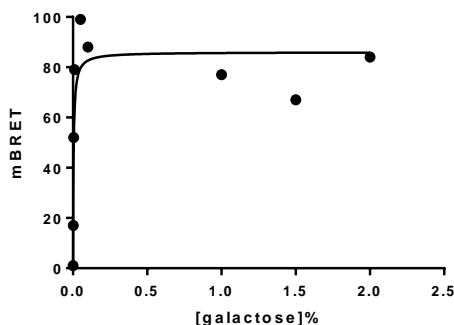


Figure 24. Donor saturation assay for CD40-CD40L interaction in syBRET. The expression of the acceptor fusion protein (YFP-CD40) was induced o/n at 20 °C at different galactose concentrations, while the expression of the donor fusion protein (NLuc- CD40L) was controlled by a constitutive promoter (*TEF* promoter).

While performing the above described experiments, we noticed a leaking level of ectopic expression of the heterologous constructs even before inducer addition. The presence and accumulation of donor fusion protein (NLuc-CD40L) before the induction may represent a problem, since it could reduce the reproducibility of the system, and during the screening the molecules would face a pre-formed complex. In order to avoid ectopic expression, we have tried to silence the galactose promoter, testing different glucose (repressor) concentrations in the pre-induction yeast culture medium. The data obtained showed that the optimal composition of the pre-induction medium was 1.5% raffinose and 0.5% glucose as carbon-sources, which are effectively disposed of in 18 h of yeast growth at 20 °C.

An additional aspect to be considered is that, at variance with the yBRET assay, in the syBRET assay proteins are exposed to the medium and that YFP emission signal is sensitive to pH and to chloride ions. The protocols available in the literature include the use of PBS to dilute luciferase substrate (used in yBRET) due to its high biocompatibility. However, this buffer contains 137 mM sodium chloride, and could therefore not be used in the syBRET assays. We then tested a sodium phosphate buffer with low chloride content, both for dilution of luciferase substrate and as a pH buffer in the induction medium, in order to prevent the acidification of the medium culture caused by cell metabolism and the consequent inhibition of YFP fluorescence. The addition of phosphate buffer 20 mM pH 7.4 in the

induction medium and the use of the same buffer to dilute luciferase substrate proved to improve BRET signal.

Subsequently we evaluated BRET signal in dependence of galactose concentration, obtaining the best expression of NLuc-CD40L at 0.1% galactose (Fig.25)

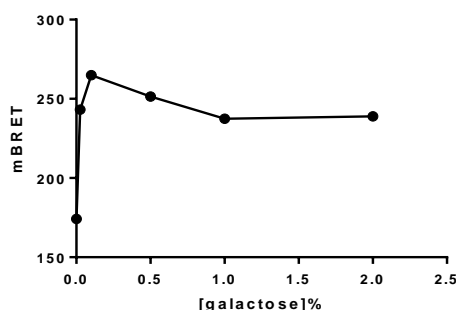


Figure 25. BRET signal evaluated at different galactose concentrations for NLuc-CD40L + YFP-CD40.

Furthermore, we monitored the localization of NLuc-CD40L by measuring the luciferase values derived from the growth medium, the soluble intracellular fraction and the insoluble cell membrane/cell-wall fraction. The results obtained showed that the signals derived from the soluble and insoluble fractions were very similar, indicating an almost equal distribution of intracellular and cell wall-bound fusion protein (Fig.26).

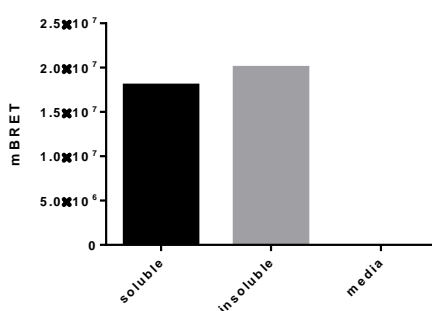


Figure 26. Luciferase signal obtained from different fractions of yeast strain expressing NLuc-CD40L + YFP-CD40.

We also performed a Western-blot on the same fractions to estimate the expression and localization of the receptor fusion protein, which is preceded by a secretory signal peptide (Fig. 27). The results showed that the majority of YFP-CD40 fusion protein accumulated in the insoluble fraction, followed

by the cellular soluble fraction, and that the signal of secreted YFP-CD40 was very low, also considering the difference in sample concentrations.

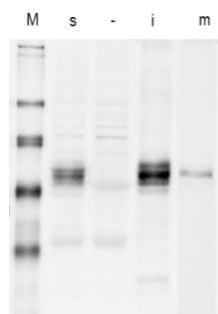


Figure 27. Protein expression evaluated by Western blotting analysis using 40 μ g of cell fractions and 5 μ g of the secreted fraction produced from the syBRET strain expressing NLuc-CD40L + YFP-CD40, and using a polyclonal anti-GFP (antibody #ab290; Abcam). M: marker; s: soluble fraction; -: negative control, yeast expressing NLuc-CD40L alone; i: insoluble fraction; m: yeast medium.

To validate the syBRET assay, we purchased a known inhibitor of CD40-CD40L, Suramin, able to bind the ligand and possibly provoking deoligomerization of the trimer⁷⁸. This compound was tested at 50 μ M displaying inhibitory activity, so we performed an assay to monitor its efficacy at different concentrations (Fig.28).

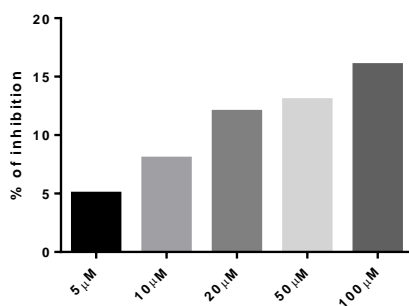


Figure 28. Results of syBRET assay carried out on pentameric complex, in order to test the ability of Suramin to disrupt protein complex at different concentrations.

Suramin showed a dose-dependent behaviour, even if the percentage of inhibition appeared relatively low. However, it must be considered that only a fraction of heterologous proteins was exposed on cell wall, as demonstrated by Western-blot analysis, and that probably the molecule was unable to reach the intracellular fraction of the complex, preventing the complete inhibition of the BRET signal.

4.6.4 SCREENING

We performed a screening using both “heterotrimeric” complex (yBRET) and pentameric complex (syBRET), of two untargeted libraries as well as a PPI inhibitors-enriched compound library, for a total of 6596 compounds of synthetic and natural origin. Molecules were tested at 20 μ M and added to exponentially growing yeast before donor protein induction. The expression was induced by adding 0.1% galactose followed by incubation 2 h at 20 °C, in both assays. Molecules were confirmed at 20 μ M and 10 μ M in the same experimental set-up.

The screening performed on the “heterotrimeric” complex allowed the identification of one hit from the PPI-Australia Compound Library, while the syBRET screening did not lead to detect any molecule capable of inhibiting the formation of pentameric complex.

The hit molecule, D093-0208, was therefore purchased from the public vendor ChemDiv (San Diego, CA, USA), along with five structural analogues; furthermore, we purchased two compounds structurally related to known inhibitors of TNF α trimeric assembling⁷⁹.

The hit molecule, together with five structural analogous and two known inhibitors, were tested at 10 μ M, 20 μ M and 50 μ M in yBRET on trimeric CD40L, but none showed inhibitory activity, neither the hit molecule confirmed its inhibition.

4.7 DISCUSSION

In this study, we have applied the yBRET method to monitor two receptor-ligand interactions involved in immune-modulatory pathway, in order to find small molecules that could overcome the drawbacks associated with immunotherapy.

2B4 is a representative of the major inhibitory receptors overexpressed on exhausted CD8⁺ T cells and the disruption of the interaction between this receptor and its ligand CD48 is effective in reversing T cell functional deficiency in a variety of chronic diseases. Once optimized the yBRET assay, we performed a screening on a PPI inhibitor-enriched library and on other small molecule libraries, which allowed the identification of two classes of potential inhibitors. The methoxy-acrylester-containing molecules, hypothetically active on a cysteine residue located in the interaction interface, did not give any promising results, since they proved to be still active in the interaction inhibition of the targeted cysteine-mutant version. The P300-1755 molecule, instead, exhibited a significant inhibitory activity together with one structural analogue, T266-1682, which showed an IC₅₀ in yBRET assay of 1.33 μ M and 0.67 μ M, respectively. The inhibitory potential of these two hit compounds was also confirmed by an ELISA assay, monitoring a significant percentage of inhibition down to 50-100 μ M. In collaboration with Dr. Carsten Watzl (IfADo, Department of Immunology, Dortmund, Germany), the activity of P300-1755 and T266-1682 was tested on mammalian cell lines, where 2B4 or CD48 were expressed on the surface of NK cells, and the interaction with their soluble, tagged partner was monitored by cytofluorimetry⁵⁷. Preliminary results did not show any inhibitory activity, probably due to an increased bonding affinity of ligand to the receptor when expressed on the cell membrane, in comparison to soluble form, by creating a strikingly periodic zipper-like arrangement, hardly overcome by the molecules, as already observed in the case of the homologous interaction CD28-CD80^{59,80}. The identified molecules will then need to be improved by modifying their structure to achieve activity in the nanomolar range.

The immune-stimulatory interaction CD40-CD40L was particularly challenging to reproduce in yBRET, given the pentameric nature of this protein complex, probably due also to the presence of several disulphide bridges in the receptor. We performed a classic yBRET to reproduce the formation of the homotrimer ligand, and a surface-exposed yeast BRET assay (syBRET) in order to study the pentameric complex. We optimized the condition of trimeric yBRET assay, but the screening performed on small molecule libraries did not identified any potential inhibitor; neither the activity of

known inhibitor was monitored, probably due to a permeability problem of these compounds inside the yeast. More complicated was the optimization and the control of the syBRET, since the BRET signal is likely to come from both inside the yeast cell (e.g. endoplasmic reticulum or Golgi apparatus) and from cell wall-anchored proteins, and that only a small amount of YFP-CD40 is present in the growth medium unbound to Aga2-NLuc-CD40L.

The permeability of the yeast wall appears to be very heterogeneous, and the secretion is influenced by multiple factors such as cell cycle phase, growth phase of the culture, temperature, concentration of nutrients and trace elements, size and chemical-physical properties of the secreted protein, etc.⁸¹. In the case of this system, the pentameric complex exceeds 230 kDa, while the mass of the YFP-CD40 is approximately 47 kDa. It is known that proteins of similar size preceded by a secretion signal peptide (as the invertase encoded by the SUC2 yeast gene) are not secreted in the medium but remain at the extracellular matrix level. It is possible that the YFP-fused receptor also behaves in the same way, and the derived syBRET system could be less sensitive to the action of interaction inhibitors. This hypothesis is in line with the results obtained by testing the known inhibitor Suramin, which allowed to monitor only partial inhibitory activity at higher concentration in comparison with data literature⁷⁸.

Overall these observations led to the following hypotheses: i) even though the donor fusion protein expression is inducible, the 3x(Aga2-NLuc-CD40L) – 2x(YFP-CD40) complex is formed in intracellular organelles (e.g. endoplasmic reticulum and Golgi apparatus) before being exposed to the cell wall; ii) an interaction inhibitor may be able to loosen the pentameric complex, but the released YFP-CD40 protein still remains tightened to the cell wall due to its large molecular mass; iii) the cell membrane of the yeast-display strain EBY100 is not affected by $\Delta erg6$ mutation, therefore it is less permeable to interaction inhibitors.

The use of Suramin allowed to validate the surface-yeast BRET platform even in these not optimized conditions that will need to be improved to perform better during the screening of small-molecule library. Several strategies can be envisaged to increase the permeability of yeast cell membrane/cell wall by using for example nystatin or lyticase, respectively to facilitate the compounds entrance during the screening, and other smaller PPIs with known interaction inhibitors can be used as proof of concept to complete the set-up of this promising surface exposed yBRET.

4.8 MATERIALS AND METHODS

Strains and vectors

Strains

E. coli DH10B™ T1R strain (F- mcrA Δ(mrr-hsdRMS-mcrBC) φ80lacZΔM15 ΔlacX74 recA1 endA1 araD139 Δ(ara,leu)7697 galU galK - rpsL nupG tonA) (Invitrogen); exploited for vector construction.

E. coli BL21+(DE3)TM strain (F-, ompT, hsdSB (rB-, mB-), dcm, gal, λ(DE3), pLysS, Cmr); exploited for protein overexpression (Agilent Technologies).

S. cerevisiae *erg6* yeast strain (BY4742 background: MATa; his3Δ1; leu2Δ 0; met15Δ 0; ura3Δ 0; YML008c::kanMX4) was obtained from Open Biosystems (Huntsville, AL, USA) and employed in the yBRET system.

S. cerevisiae EBY100 yeast strain (MATa AGA1::GAL1 AGA1::URA3 ura352 trp1 leu2delta200 his3delta 00 pep4::HIS3 prb11.Rcan1 GAL) was obtained from Invitrogen and employed in the syBRET system.

Vectors

All sequences used in this study were amplified with PCR and inserted in frame with the donor or the acceptor using *CpoI* restriction enzyme digestion and DNA ligation, using vectors shown in chapter 2 (paragraph 2.2.1). The centromeric vectors p415 (*LEU2*, *GAL1* inducible promoter) and p416 (*URA3*, *GPD* constitutive promoter) were used to express the chimeric proteins⁸². *TRP1* selectable marker gene cannot be employed with *erg6* mutant strain, because *trp1-erg6* double mutant is synthetic lethal. Donor proteins were cloned into p415, and acceptor proteins were cloned into p416. Both C- or N-terminal fusion vectors are available upon request. Vector p190 (*LEU2*, *TEF* constitutive promoter) and p215 (*URA*, *GAL1*) were used to express chimeric proteins in the donor saturation assay. pYD1 (*URA 3*, *GAL1* inducible promoter) is specifically designed to target and display recombinant proteins on the surface of *Saccharomyces cerevisiae*. Displayed proteins can be analyzed for their ability to interact with known or putative ligands. pYD1 uses the α-agglutinin yeast adhesion receptor which consists of two domains Aga1 and Aga2 to display recombinant protein on the surface of *S. cerevisiae*. The gene of interest is cloned into the pYD1 vector in frame with the AGA2 gene. The resulting

construct is transformed into the EBY100 *S. cerevisiae* strain (supplied transformed with Aga1). Aga1 and the Aga2-fusion protein associate within the secretory pathway and are displayed on the cell surface

pGEX was used for the expression of gene in *E. coli* as fusion with *Schistosoma japonicum* GST at the carboxyl terminus.

BRET Calculation and screening analysis protocol

The BRET ratio was calculated by dividing the signal measured at 530 nm by the signal measured at 480 nm. Then, the BRET signal was calculated as the BRET ratio subtracted by the BRET background ratio (obtained when the donor protein was expressed alone) and multiplied by 1000 to express results in milliBRET (mBRET): $\text{BRET} = (\text{BRET ratio} - \text{Background BRET ratio}) \times 1000^{83}$.

The rationale of the assortment takes into account three factors: (i) an interaction inhibition of at least 15% on average, compared to the non-treated plate specific controls. (ii) a percentage of mBRET median lower than 85% compared to the median calculated on the non-treated plate specific controls. (iii) An SSMD statistics considered at least as “weak inhibition” (SSMD represent the ratio of mean to the standard deviation of difference between a test compound and a negative reference group with no specific inhibition/activation effects).

Small molecule libraries

Three libraries are available in our laboratory: *Institut de Chimie des Substances Naturelles* (ICSN), National Cancer Institute (NCI) and PPI Australia Compound Library, which contained compounds of synthetic and natural origin. We screened the other four libraries at the Kinase Inhibitor Specialized Screening facility (KISSf, Station Biologique de Roscoff, France) of Stéphane Bach. Enzo chemical collection is characterized by extracts from terrestrial plants, Prestwick chemical collection by FDA approved compounds, essential chemical compound of Roscoff (ReC3 library) and Marine chemical compound collection (MarC3) include bioinspired molecules from marine organisms. P300-1755 and structural analogues in addition to D093-0208 and related analogues were purchased from ChemDiv (San Diego, USA), while cysteine “reactive” compounds were purchased from CSIRO Institute; Suramin and two known inhibitors of CD40L were purchased from Abcam.

Expression and purification of GST- CD48

The ectodomain sequence of CD48 was cloned in a pGEX vector that joins the N-terminal extremity of the protein to the GST protein, and expressed in BL21 codon plus *E. coli* strain. The best expression condition, in which the protein is most expressed and mainly soluble, has been evaluated as the 16 h induction at 20 °C in Auto Induction Medium. The protein is then extracted from cells and purified through the Glutathione resin low-pressure affinity chromatography. The combined eluted fractions were stored in PBS and glycerol 20%, pH 7 at 800 ng/μL.

ELISA assay

CD48-His tag and 2B4-hlgG1-Fc tag were purchased from ThermoFisher (cat n°10042H02H25 and 10797H08H25), while GST-CD48 tagged protein was recombinantly expressed in BL21 codon plus *E. coli* strain. Protein anchored was diluted at optimal dilution in PBS (CD48-His both 1 μg and 500 ng, GST-CD48 tag at 1 μg, 2B4-hlgG1-Fc at 500 ng, 250 ng and 100 ng) and 100 μl of the solution added into NUNC Maxisorp microtiter plate wells. Following o/n incubation at 4 °C wells were washed one time with 300 μl of PBS and blocked with 400 μl of 2% (w/v) BSA in TBST at RT for 1 h. Plates are then washed two times with wash buffer TBST. 100 μl of different concentrations of the second protein diluted in 0,1% (w/v) BSA in TBST were incubated with compounds (or DMSO) at different concentrations at RT for 1 h. Wells were washed three times with 300 μl of wash buffer, 100 μL of rabbit anti-GST primary antibody (1:2000 in PBS) or mouse anti human IgC (Fc)/HRP (1:500 in 0,5% BSA in TBST) were added, and the plate was incubated at RT for 1 h. After washing, in the case of GST-CD48, HRP-conjugated goat anti-rabbit secondary antibody (1:20000 in PBS) was added to each well and incubated at RT for 1 h. Interactions were detected by the addition of 100 μl of ABTS substrate to each well. The signal was measured, after 30 minutes of incubation at 30 °C, reading absorbance at 415 nm using a microplate reader.

Statistical analysis

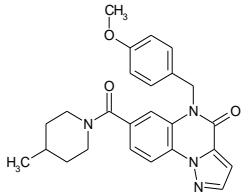
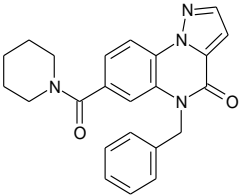
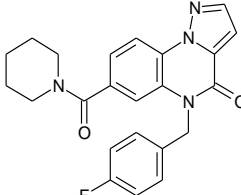
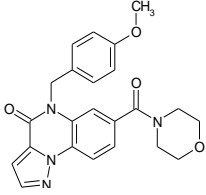
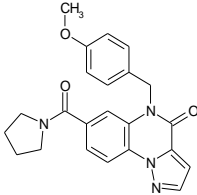
To calculate IC₅₀ for inhibitory activity in ELISA and in *in vitro* transcription, experiments were conducted in triplicate, using at least ten different compound concentrations. Data are analyzed in Prism (GraphPad Software Inc.) using nonlinear regression curve fitting.

Student t test is used to find significant differences when comparing compound inhibitory activities.

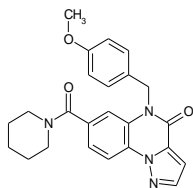
Table VI. List of primers used in this study

Primer name (restriction enzyme)	Sequence (5'-...3')
2B4 Fw (<i>EcoRI/CpoI</i>)	TAAATATAAATGAATTC <u>GGTCCG</u> ATGTGCCAGGGATCAGCTGAC
2B4 Re (<i>XhoI/CpoI</i>)	AATTATTTTACTCGAGCGGACCGATGCGGGGTTTCTCAACTTTATC
2B4 Re (stop codon) (<i>XhoI/CpoI</i>)	AATTATTTTACTCGAGCGGACCGTCAGCGGGGTTTCTCAACTTTATC
2B4 K68-E80-A Fw	TTTCATCACATATTGGCTTGGGCTAATGGCTCTTGCCT
2B4 K68-E80-A Re	AGGCAAAGAGCCATTAGCCCAAGCCAATATGTGATGAAA
CD48 Fw (<i>EcoRI/CpoI</i>)	TAAATATAAATGAATTC <u>GGTCCG</u> ATGCACTTGGTACATATGACCGTGG
CD48 Re (<i>XhoI/CpoI</i>)	AATTATTTTACTCGAGCGGACCGATAGGCTTGGGTACAGGGTCA
CD48 Re (stop codon) (<i>XhoI/CpoI</i>)	AATTATTTTACTCGAGCGGACCGTCAAGGCTTGGGTACAGGGTCA
GST-CD48 Fw (<i>HindIII</i>)	AATTATTTTAAAGCTTAATGTCCCCTATACTAGGTTATTGG
GST-CD48 Re (<i>XhoI</i>)	AATTATTTTACTCGAGTAGGCTTGGGTACAGGGTCAA
CD40 Fw (<i>CpoI</i>)	TAAATATAAACGGTCCGATGCCAGAACCACCCACTGCAT
CD40 Re (stop codon) (<i>CpoI</i>)	AATTATTTTACGGACCGTCAATCCTGGGGACACAGACAA
CD40L Fw (<i>CpoI</i>)	TAAATATAAACGGTCCGATGGGTGATCAGAATCCTCAAATTGC
CD40L Re (stop codon) (<i>CpoI</i>)	AATTATTTTACGGACCGTCAGAGTTTGAGTAAGCCAAAGGAC
NLuc-link 1	AGAACCACCACCACCGCCAGAATGCGTTCGCA
NLuc-link 2	TTATTTTACGGACCGATAGAACCACCACCACAGAACCCACCACCCG
YFP-link 1	ACCAGAACCACCACCACCTTGACAGCTCGTCCATGC
YFP-link 2	TTATTTTACGGACCGATAGAACCACCACCACAGAACCCACCACCACCT
Aga2 signal peptide (<i>BamHI</i>)	TAAATATAAA GGATCC ATGCAGTTACTTCGCTGTTTTTCAATATTTCTGTATTGCTAGCGT

4.9 SUPPLEMENTARY**Table 1.** Structure of hit compounds from PPI-enriched Australia Compound Library (highlighted in bold) and structural analogues.

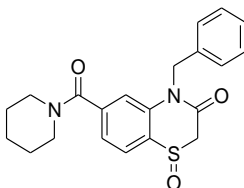
ID compound	Structure	Vendors
P300-1755		ChemDiv
T226-1682		ChemDiv
T226-2126		ChemDiv
T226-2165		ChemDiv
T226-2185		ChemDiv

T226-2186



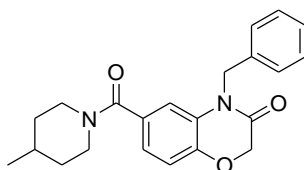
ChemDiv

C531-0681



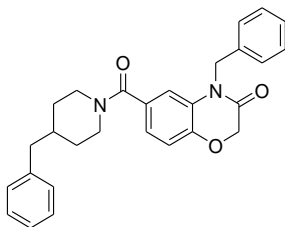
ChemDiv

F119-0048



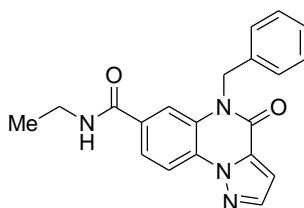
ChemDiv

F119-0088



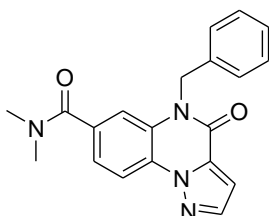
ChemDiv

P300-1431



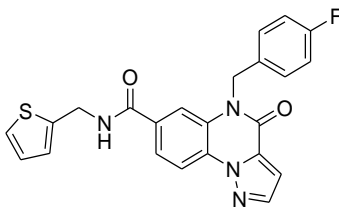
ChemDiv

P300-1543



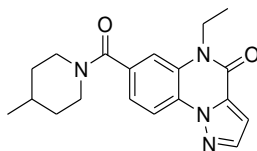
ChemDiv

P300-2104



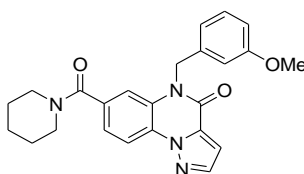
ChemDiv

T226-1213



ChemDiv

T226-2040



ChemDiv

ABBREVIATIONS

APC antigen presenting cells

BCR B cell receptors

BRET Bioluminescence Resonance Energy Transfer

CMV Cytomegalovirus

FADD FAS-associated death domain

GPI Glycosylphosphatidylinositol

GST Glutathione-S-Transferase

HBV hepatitis B virus

HCV hepatitis C virus

HIV Human immunodeficiency virus

IFN- γ interferon- γ

Ig immunoglobulin

IgV immunoglobulin variable region-like

IL-2 Interleukin-2

ITIM immunoreceptor tyrosine-based inhibition motif

ITSM immunoreceptor tyrosine-based switch motif

Jack3 Janus family 3

mAb monoclonal antibody

mBRET milli BRET

MHC Major Histocompatibility Complex

NK cells Natural killer cells

NLuc NanoLuc luciferase

PPI protein-protein interaction

RFP recombinant fusion proteins

RLuc Renilla reniformis luciferase

SAP SLAM-associated protein

SLAM signalling lymphocytic activation molecule

TCR T cell receptor

THD TNF homology domain

TNF tumour necrosis factor

TNFR tumour necrosis factor receptor

TRADD TNFR-associated death domain

TRAF TNF receptor associated factors

WB Western-blot

XHIGM X-linked hyper-IgM syndrome

XLP1 X-linked lymphoproliferative disease 1

yBRET yeast BRET

YFP yellow fluorescent protein

REFERENCES

1. Parkin J, Cohen B. An overview of the immune system. *Lancet*. 2001;357(9270):1777-1789.
2. Chakraborty AK, Weiss A. Insights into the initiation of TCR signaling. *Nat Immunol*. 2014;15(9):798-807.
3. Yao S, Zhu Y, Chen L. Advances in targeting cell surface signalling molecules for immune modulation. *Nat Rev Drug Discov*. 2013;12(2):130-146.
4. Kung P, Goldstein P, Reinherz E, Schlossman S. Monoclonal antibodies defining distinctive human T cell surface antigens. *Science (80-)*. 1979:347-349.
5. Cosimi A, Burton R, Colvin R, et al. Treatment of acute renal allograft rejection with OKT3 monoclonal antibody. *Transplantation*. 1981.
6. Sharpe AH, Freeman GJ. the B7–Cd28 Superfamily. *Nat Rev Immunol*. 2002;2(2):116-126.
7. Fellner c. Ipilimumab (Yervoy) Prolongs Survival In Advanced Melanoma: Serious Side Effects and a Hefty Price Tag May Limit Its Use Therapeutics. *Pharm Ther*. 2012:503-530.
8. Chen L, Flies DB. Molecular mechanisms of T cell co-stimulation and co-inhibition. *Nat Rev Immunol*. 2013;13(4):227-242.
9. Lazar-Molnar E, Yan Q, Cao E, Ramagopal U, Nathenson SG, Almo SC. Crystal structure of the complex between programmed death-1 (PD-1) and its ligand PD-L2. *Proc Natl Acad Sci*. 2008;105(30):10483-10488.
10. Cheng X, Veverka V, Radhakrishnan A, et al. Structure and interactions of the human programmed cell death 1 receptor. *J Biol Chem*. 2013;288(17):11771-11785.
11. Gelaye B, Rondon M, Araya R, Williams MA. Epidemiology of maternal depression, risk factors, and child outcomes in low-income and middle-income countries. *Lancet Psychiatry*. 2016;3(10):973-982.
12. Gangadhar TC, Salama AK. Clinical applications of PD-1-based therapy: A focus on pembrolizumab (MK-3475) in the management of melanoma and other tumor types. *Onco Targets Ther*. 2015;8:929-937.
13. Raedler LA. Opdivo (Nivolumab): Second PD-1 Inhibitor Receives FDA Approval for Unresectable or Metastatic Melanoma. *Am Heal drug benefits*. 2015;8:180-183.
14. Santini F, Rudin C. Atezolizumab for the treatment of non-small cell lung cancer. *Expert Rev Clin Pharmacol*. 2017.
15. Apolo AB, Infante JR, Balmanoukian A, et al. Avelumab, an anti-programmed death-ligand 1 antibody, in patients with refractory metastatic urothelial carcinoma: Results from a multicenter, Phase Ib study. *J Clin Oncol*. 2017;35(19).
16. Massard C, Gordon MS, Sharma S, et al. Safety and efficacy of durvalumab (MEDI4736), an anti-programmed cell death ligand-1 immune checkpoint inhibitor, in patients with advanced urothelial bladder cancer. *J Clin Oncol*. 2016;34(26):3119-3125.
17. Tangye SG, Phillips JH, Lanier LL. The CD2-subset of the Ig superfamily of cell surface molecules: receptor-ligand pairs expressed by NK cells and other immune cells. *Semin Immunol*. 2000;12:149-157.

18. Veillette A. SLAM-family receptors: immune regulators with or without SAP-family adaptors. *Cold Spring Harb Perspect Biol.* 2010;2(3):1-15.
19. Chamian F, Lowes MA, Lin SL, et al. Alefacept reduces infiltrating T cells, activated dendritic cells, and inflammatory genes in psoriasis vulgaris. *PNAS.* 2005;102(6):2075-2080.
20. Gokhale A, Kanthala S, Latendresse J, Taneja V, Satyanarayanajois S. Immunosuppression by co-stimulatory molecules: Inhibition of CD2-CD48/CD58 interaction by peptides from CD2 to suppress progression of collagen-induced arthritis in mice. *Chem Biol Drug Des.* 2013;82(1):106-118.
21. Engel P, Eck MJ, Terhorst C. The SAP and SLAM families in immune responses and X-linked lymphoproliferative disease. *Nat Rev Immunol.* 2003;3(10):813-821.
22. Aggarwal BB. Signalling pathways of the TNF superfamily: a double-edged sword. *Nat Rev Immunol.* 2003;3(9):745-756.
23. Bremer E. Targeting of the tumor necrosis factor receptor superfamily for cancer immunotherapy. *ISRN Oncol.* 2013;2013:371854.
24. Sedger LM, McDermott MF. TNF and TNF-receptors: From mediators of cell death and inflammation to therapeutic giants - past, present and future. *Cytokine Growth Factor Rev.* 2014;25(4):453-472.
25. MacEwan DJ. TNF ligands and receptors - a matter of life and death. *Br J Pharmacol.* 2002;135(4):855-875.
26. Hehlhans T, Pfeffer K. intriguing biology of the tumour necrosis factor/tumour necrosis factor receptor superfamily: Players, rules and the games. *Immunology.* 2005;115(1):1-20.
27. Feldman AM, Combes A, Wagner D, et al. The role of tumor necrosis factor in the pathophysiology of heart failure. *J Am Coll Cardiol.* 2000;35(3):537-544.
28. Thomas PS. Tumour necrosis factor- α : The role of this multifunctional cytokine in asthma. *Immunol Cell Biol.* 2001;79(2):132-140.
29. Spooner CE, Markowitz NP, Saravolatz LD. The role of tumor necrosis factor in sepsis. *Clin Immunol Immunopathol.* 1992;62:11-17.
30. McCauley ME, Grush KA. Alzheimer's Disease: Exploring the Role of Inflammation and Implications for Treatment. *Int J Alzheimers Dis.* 2015:1-10.
31. Balkwill F. Tumour necrosis factor and cancer. *Nat Rev Cancer.* 2009;9(5):361-371.
32. Aringer M, Smolen JS. The role of tumor necrosis factor-alpha in systemic lupus erythematosus. *Arthritis Res Ther.* 2008;10(1):202.
33. de Vos S, Forero-Torres A, Ansell SM, et al. A phase II study of dacetuzumab (SGN-40) in patients with relapsed diffuse large B-cell lymphoma (DLBCL) and correlative analyses of patient-specific factors. *J Hematol Oncol.* 2014;7(1):44.
34. Wherry EJ, Kurachi M. Molecular and cellular insights into T cell exhaustion. *Nat Rev Immunol.* 2015;15(8):486-499.
35. Wherry EJ, Ha S-J, Kaech SM, et al. Molecular signature of CD8⁺ T cell exhaustion during chronic viral infection. *Immunity.* 2007;27(4):670-684.
36. Yi JS, Cox M a, Zajac AJ. T-cell exhaustion: characteristics, causes and conversion.

- Immunology*. 2010;129(4):474-481. doi:10.1111/j.1365-2567.2010.03255.x.
37. Wherry EJ. T cell exhaustion. *Nat Immunol*. 2011;131(6):492-499.
 38. Crawford A, Wherry EJ. The diversity of costimulatory and inhibitory receptor pathways and the regulation of antiviral T cell responses. *Curr Opin Immunol*. 2009;21(2):179–186.
 39. Blackburn SD, Shin H, Haining WN, et al. Coregulation of CD8+ T cell exhaustion during chronic viral infection by multiple inhibitory receptors. *Nat Immunol*. 2009;10(1):29-37.
 40. Odorizzi PM, Wherry EJ. Inhibitory receptors on lymphocytes: insights from infections. *J Immunol*. 2012;188(7):2957-2965. doi:10.4049/jimmunol.1100038.
 41. Barber D, Wherry E, Masopust D, et al. Restoring function in exhausted CD8 T cells during chronic viral infection. *Nature*. 2006;9:682-687.
 42. Nguyen L, Ohashi P. Clinical blockade of PD1 and LAG3--potential mechanisms of action. *Nat Rev Immunol*. 2015;15:45-56.
 43. McNerney ME, Lee KM, Kumar V. 2B4 (CD244) is a non-MHC binding receptor with multiple functions on natural killer cells and CD8 + T cells. *Mol Immunol*. 2005;42(4 SPEC. ISS.):489-494.
 44. Boles KS, Stepp SE, Bennett M, Kumar V, Mathew P a. 2B4 (CD244) and CS1: novel members of the CD2 subset of the immunoglobulin superfamily molecules expressed on natural killer cells and other leukocytes. *Immunol Rev*. 2001;181(August 2015):234-249.
 45. Lee K-M, McNerney ME, Stepp SE, et al. 2B4 acts as a non-major histocompatibility complex binding inhibitory receptor on mouse natural killer cells. *J Exp Med*. 2004;199(9):1245-1254.
 46. Vaidya S V., Stepp SE, McNerney ME, et al. Targeted disruption of the 2B4 gene in mice reveals an in vivo role of 2B4 (CD244) in the rejection of B16 melanoma cells. *J Immunol*. 2005;174(2):800-807.
 47. Sivori S, Falco M, Marcenaro E, et al. Early expression of triggering receptors and regulatory role of 2B4 in human natural killer cell precursors undergoing in vitro differentiation. *Proc Natl Acad Sci*. 2002;99(7):4526-4531.
 48. Eissmann P, Beauchamp L, Wooters J, et al. Molecular basis for positive and negative signaling by the natural killer cell. *Blood*. 2012;105(12):4722-4729.
 49. Meazza R, Falco M, Marcenaro S, et al. Inhibitory 2B4 contributes to NK cell education and immunological derangements in XLP1 patients. *Eur J Immunol*. 2017;47(6):1051-1061.
 50. Meazza R, Tuberosa C, Cetica V, et al. XLP1 inhibitory effect by 2B4 does not affect DNAM-1 and NKG2D activating pathways in NK cells. *Eur J Immunol*. 2014;44(5):1526-1534.
 51. Hislop AD, Palendira U, Leese AM, et al. lymphoproliferative disease is restricted to SLAM family – positive B-cell targets Impaired Epstein-Barr virus – specific CD8 α T-cell function in X-linked lymphoproliferative disease is restricted to SLAM family – positive B-cell targets. *Immunology*. 2012;116(17):3249-3257.
 52. Colonna M. Fine-tuning NK cell responses: it's a family affair. *Nat Immunol*. 2005;6:1-2.
 53. Chlewicki LK, Velikovskiy CA, Balakrishnan V, Mariuzza RA, Kumar V. Molecular Basis of the Dual Functions of 2B4 (CD244). *J Immunol*. 2008;180(12):8159-8167.

54. Velikovskiy CA, Deng L, Chlewicki KL, Fernández MM, Kumar V, Mariuzza RA. Structure of Natural Killer Receptor 2B4 Bound to CD48 Reveals Basis for Heterophilic Recognition in Signaling Lymphocyte Activation Molecule Family. *Immunity*. 2007;27(4):572-584.
55. Mathew SO, Kumaresan PR, Lee K, et al. Mutational Analysis of the Human 2B4 (CD244)/CD48 Interaction: Lys 68 and Glu 70 in the V Domain of 2B4 Are Critical for CD48 Binding and Functional Activation of NK Cells. *J Immunol*. 2005;4:1005-1013.
56. Margraf-schönfeld S, Böhm C, Watzl C. Glycosylation Affects Ligand Binding and Function of the Activating Natural Killer Cell Receptor 2B4 (CD244) Protein. *J Biol Chem*. 2011;24142-24149.
57. Claus M, Wingert S, Watzl C. Modulation of natural killer cell functions by interactions between 2B4 and CD48 in cis and in trans. *Open Biol*. 2016;6(5).
58. Labbé CM, Laconde G, Kuenemann MA, Villoutreix BO, Sperandio O. IPPI-DB: A manually curated and interactive database of small non-peptide inhibitors of protein-protein interactions. *Drug Discov Today*. 2013;18(19-20):958-968.
59. Green NJ, Xiang J, Chen J, et al. Structure-activity studies of a series of dipyrzolo[3,4-b:3',4'-d]pyridin-3-ones binding to the immune regulatory protein B7.1. *Bioorganic Med Chem*. 2003;11(13):2991-3013.
60. Huxley P, Sutton DH, Debnam P, et al. High-affinity small molecule inhibitors of T cell costimulation: Compounds for immunotherapy. *Chem Biol*. 2004;11(12):1651-1658.
61. Uvebrant K, Da Graca Thrige D, Rosen A, et al. Discovery of Selective Small-Molecule CD80 Inhibitors. *J Biomol Screen*. 2007;12(4):464-472.
62. Freedman JE. CD40-CD40L and Platelet Function: Beyond Hemostasis. *Circ Res*. 2003;944-947.
63. Young LS, Eliopoulos AG, Gallagher NJ, Dawson CW. CD40 and epithelial cells: Across the great divide. *Immunol Today*. 1998;19(11):502-506.
64. Elgueta R, Benson MJ, Vries VC De, Noelle RJ. Molecular mechanism and function of CD40 /CD40L engagement in the immune system. *Immunol Rev*. 2009;229:152-172.
65. Gavins FNE, Li G, Russell J, Perretti M, Granger DN. Microvascular Thrombosis and CD40/CD40L Signalling. *J Thromb Haemost*. 2011;9:574-581.
66. Grewal IS, Flavell RA. CD40 and CD154 in Cell Mediated Immunity. *Annu Rev Immunol*. 1998;16:111-135.
67. Notarangelo LD, Hayward AR. X-linked immunodeficiency with hyper-IgM (XHIM). *Clin Exp Immunol*. 2000;120(3):399-405.
68. Ciferska H, Horak P, Hermanova Z, et al. The levels of sCD30 and of sCD40L in a group of patients with systemic lupus erythematosus and their diagnostic value. *Clin Rheumatol*. 2007;26(5):723-728.
69. Goules A, Tzioufas AG, Manousakis MN, Kirou KA, Crow MK, Routsias JG. Elevated levels of soluble CD40 ligand (sCD40L) in serum of patients with systemic autoimmune diseases. *J Autoimmun*. 2006;26(3):165-171.
70. Ludwiczek O, Kaser A, Tilg H. Plasma levels of soluble CD40 ligand are elevated in

- inflammatory bowel diseases. *Int J Colorectal Dis.* 2003;18(2):142-147.
71. Heeschen C, Dimmeler S, Hamm CW, et al. Soluble CD40 Ligand in Acute Coronary Syndromes. *N Engl J Med.* 2003;348:1104-1111.
 72. MacDonald KP, Nishioka Y, Lipsky PE, Thomas R. Functional CD40 ligand is expressed by T cells in rheumatoid arthritis. *J Clin Invest.* 1997;100(9):2404-2414.
 73. Sawada-Hase N, Kiyohara T, Miyagawa J, et al. An increased number of CD40-high monocytes in patients with Crohn's disease. *Am J Gastroenterol.* 2000;95(6):1516-1523.
 74. Desai-Mehta A, Lu L, Ramsey-Goldman R, Datta SK. Hyperexpression of CD40 ligand by B and T cells in human lupus and its role in pathogenic autoantibody production. *J Clin Invest.* 1996;97(9):2063-2073.
 75. Kitagawa M, Mitsui H, Nakamura H, et al. Differential regulation of rheumatoid synovial cell interleukin-12 production by tumor necrosis factor alpha and CD40 signals. *Arthritis Rheum.* 1999;42(9):1917-1926.
 76. Heath AW. Antibodies to murine CD40 stimulate normal B-lymphocytes but inhibit proliferation of B-lymphoma cells. *Cell Immunol.* 1993;152:468-480.
 77. An HJ, Kim YJ, Song DH, et al. Crystallographic and mutational analysis of the CD40-CD154 complex and its implications for receptor activation. *J Biol Chem.* 2011;286(13):11226-11235.
 78. Margolles-Clark E, Jacques-Silva M, Ganesan L, et al. Suramin inhibits the CD40-CD154 costimulatory interaction: A possible mechanism for immunosuppressive effects. *Biochem Pharmacol.* 2009;77(7):1236-1245.
 79. Silvian L, Friedman J, Strauch K, et al. Small Molecule Inhibition of the TNF Family Cytokine CD40 Ligand Through a Subunit Fracture Mechanism. *ACS Chem Biol.* 2011;6(6):363-647.
 80. Erbe D V, Wang S, Xing Y, Tobin JF. Small Molecule Ligands Define a Binding Site on the Immune Regulatory Protein B7.1. *J Biol Chem.* 2002;277:7363-7368.
 81. Klis FM, Mol P, Hellingwerf K, Brul S. Dynamics of cell wall structure in *Saccharomyces cerevisiae*. *FEMS Microbiol Rev.* 2002;26:239-256.
 82. Mumberg D, Muller R, Funk M. Yeast vectors for the controlled expression of heterologous proteins in different genetic backgrounds. *Gene.* 1995;156:119-122.
 83. Corbel C, Sartini S, Levati E, et al. Screening for Protein-Protein Interaction Inhibitors Using a Bioluminescence Resonance Energy Transfer (BRET)-Based Assay in Yeast. *SLAS Discov.* 2017;22(6).

